# A COMPARISON OF THE REACTIVITY OF DIFFERENT SYNTHETIC CALCIUM CARBONATE MINERALS WITH ARSENIC OXYANIONS

A thesis

Submitted to the College of Graduate Studies and Research

In Partial Fulfillment of the Requirements

For the Degree of

**Master of Science**

in the

Department of Soil Science

University of Saskatchewan

Saskatoon, Saskatchewan, Canada

by

Abhishek Mandal

## PERMISSION TO USE

In presenting this thesis in partial fulfillment of the requirements for a postgraduate degree from the University of Saskatchewan, I agree that the Libraries of this University may make it freely available for inspection. I further agree that permission for copying of this thesis in any manner, in whole or in part, for scholarly purposes may be granted by the professor or professors who supervised my thesis work or, in their absence, by the Head of the Department or the Dean of the College in which my thesis work was done. It is understood that any copying or publication or use of this thesis or parts thereof for financial gain shall not be allowed without my written permission. It is also understood that due recognition shall be given to me and to the University of Saskatchewan in any scholarly use which may be made of any material in my thesis.

Requests for permission to copy or to make other use of material in this thesis in whole or part should be addressed to:

Head of the Department of Soil Science
University of Saskatchewan
Saskatoon, Saskatchewan
Canada, S7N 5A8

## ABSTRACT

This study was conducted to determine how the structure and surface chemistry of bulk $CaCO_3$ differs from that of nanometer-sized $CaCO_3$ and then to determine rate, extent and mechanisms of As adsorption on various synthetic $CaCO_3$ materials. Additionally, we sought to devise a chemical $CaCO_3$ precipitate that approximates biogenic $CaCO_3$. The bulk $CaCO_3$ precipitation was performed by using a solution that was highly oversaturated so that large $CaCO_3$ precipitates rapidly form. Two different methods were employed for the synthesis of nanometer size $CaCO_3$ i) an *in situ* deposition technique and ii) an interfacial reaction (water in oil emulsion). Mineral characterization of all $CaCO_3$ precipitates was done with Nitrogen Porosimetry (Brunauer Emmett Teller method), particle size analysis, X-ray diffraction and Fourier Transform Infrared/ Fourier Transform Raman spectroscopy. The principal objective of the research was to assess the overall reactivity of As(III) and As(V) with different synthetic $CaCO_3$ minerals. This was accomplished by i) running adsorption isotherms (varying As concentration), ii) measuring pH envelopes (varying pH at a fixed concentration) and iii) kinetic experiments (varying reaction time). Also, electrophoretic mobility experiments were performed in the presence of As(III) and As(V), and these studies revealed that As(III) forms stronger inner-sphere complexes with $CaCO_3$ than As(V). Also, it was found that nanometer-sized $CaCO_3$ prepared via deposition formed stronger inner-sphere complexes with As oxyanions ($q = 5.26\ \mu mol/m^2$) compared to either nano-sized $CaCO_3$ from interfacial reactions ($q = 4.51\ \mu mol/m^2$) or bulk $CaCO_3$ ($q = 4.39\ \mu mol/m^2$).

The PEG-based nano $CaCO_3$ prepared by an *in-situ* deposition technique presents a novel and readily available synthesis route that can be used as proxy for the biogenic $CaCO_3$ known to be present in many different environmental conditions. The results of this study suggest that $CaCO_3$ can be used as a sorbent for As in groundwater.

## ACKNOWLEDGEMENTS

I dedicate this Master's Thesis to my most beloved mother Mrs. Sudebi Mandal to whom this dissertation may have no significant importance. The completion of this thesis would be impossible without the support and encouragement of many special people, to whom I extend my deepest gratitude. First of all, I would like to take the time to thank my supervisor Dr. Derek Peak, the source of inspiration for his guidance and advice throughout my thesis.

I would like extend my thanks to committee members, Dr. D.W. Anderson, Dr. P.M. Huang, Dr. S. Siciliano and Dr. M.F. Paige (Dept. of Chemistry) for their recommendations and suggestions. I would also like to acknowledge and thank the other members of the Department of Soil Science for their expertise and guidance throughout my graduate work.

I owe a great debt of thanks to the participants in this study who were gracious enough to share their time, experiences, and expertise with me. Their insights and reflections provided the valuable information critical to the success of my study.

Most importantly, I would like to express my deepest appreciation to Sarker Tarek Mahmud (Ph.D. student) to whom I am indebted for his timely help and support. A special thanks to my father for his support in my educational pursuits, no matter the cost and personal sacrifice. I am highly indebted to him for his unconditional love, encouragement and motivation during my hardship. Finally, I would like to thank the office staff for their support and friendship and everyone in the Department of Soil Science for providing congenial atmosphere needed to pursue research. This project was funded by an NSERC Special Research Opportunity grant.

## TABLE OF CONTENTS

## LIST OF TABLES

## LIST OF FIGURES

## LIST OF ACRONYMS AND ABBREVIATIONS

| | |
|---|---|
| AAS | Atomic Absorption Spectroscopy |
| AFS | Atomic Fluorescence Spectroscopy |
| BET | Brunauer Emmett and Teller |
| CCA | Chromated Copper Arsenate |
| Eh | Redox Potential |
| EM | Electrophoretic Mobility |
| EXAFS | Extended X-Ray Absorption Fine Structure |
| FT-IR | Fourier Transform Infrared Spectroscopy |
| FT-RS | Fourier Transform Raman Spectroscopy |
| FWHM | Full Width at Half Maximum |
| pe | Negative logarithm of the activity of the electrons |
| PEG | Polyethylene Glycol |
| PSA | Particle Size Analyzer |
| PZC | Point of Zero Charge |
| SEAR | South East Asian Region |
| WHO | World Health Organization |
| XRD | X-Ray Diffraction |
| ZP | Zeta Potential |

# 1.0 INTRODUCTION

Arsenic is one of the most toxic elements in the environment, and has thus been of great interest in soil science and geochemistry studies (Smedley and Kinniburgh, 2002; Nickson *et al*., 1998). In particular, naturally occurring arsenic contamination in groundwater in the Ganges delta plain has received significant attention (Smedley and Kinniburgh, 2002; Nickson *et al.*, 1998). To prevent water borne disease, Bangladesh shifted its drinking water supply from surface to groundwater. The groundwater contained substantial arsenic, and has led to widespread arsenic poisoning in that region. It is clear that there is a pressing need to find some inexpensive and effective remediation techniques for arsenic removal from groundwater.

Arsenic affinity for iron oxides is well established and often considered a sink for As in natural systems, but in Bangladesh arsenic sorbed on iron oxides is a source rather than a sink for arsenic. In fact, arsenic release into groundwater of Bangladesh occurs due to microbial reduction of iron oxide (Ahmed *et al.*, 2004; Akai et al., 2004; Anawar *et al.*, 2002; 2003). This microbial reduction process is mediated by bacteria -arsenic associated iron oxide on the mineral surface in this region is reduced by the carbon rich indigenous bacteria originated from the natural peat deposits. Thus, iron oxide immobilization of arsenic is not a practical remediation technique in many aquifers. However, bacterial precipitation and incorporation of other elements into $CaCO_3$ in groundwater is another possibility (Fujita *et al.*, 2000; Fujita *et al.*, 2004). Most natural bacteria found in groundwater can mediate $CaCO_3$ precipitation via urease enzyme, so ureolytic $CaCO_3$ precipitation might be viable in many areas at risk for arsenic contamination. However, the affinity of $CaCO_3$ phases for arsenic and their long-term stability are not well-known.

# 2.0 LITERATURE REVIEW

## 2.1 Biogeochemistry of Arsenic:

Arsenic (Z = 33), is ubiquitous in the earth's crust, and many of its forms are extremely toxic (Vaughan, 2006; Alam *et al.*, 2002). Arsenic can exist in four valence states: -3, 0, +3 and +5. Arsenic does not often occur in its elemental state and is far more common in sulfides and sulfo salts such as arsenopyrite (FeAsS) , orpiment ($As_2S_3$) , realgar (AsS), enargite (CuAsS), iollingite and tennanite (Alam *et al.*, 2002; Smith *et al.*, 2005) Arsenic occurs naturally in about 245 minerals, (James and Paul, 1999) which when subjected to weathering processes can release soluble arsenic into natural waters (Smith *et al.*, 2005). Under mildly reducing conditions, arsenite [As(III)] is the dominant form; arsenate [As (V)] is generally the stable form in oxygenated environments. Elemental arsenic is not soluble in water. Other arsenic salts exhibit a wide range of solubilities depending on pH and the ionic environment (Driehaus *et al.*, 1995).

Other sources of large scale arsenic contamination include mining wastes and old orchards where As was used as a pesticide and dissolution of naturally occurring minerals. The mobility of arsenic in a groundwater system is mediated by the geochemistry and interaction of arsenic with other minerals such as oxides and sulphides (Stollenwerk, 2003). The mechanism of arsenic sorption in oxide mineral surfaces occurs via inner-sphere complex formation (Stollenwerk, 2003; Plant *et al.*, 2004) which is controlled by pH and redox potential (Eh). Rodriguez *et al.* (2004) reported that increase of Eh or oxidation of the groundwater system can result in arsenic contamination from sulphide minerals. The release of arsenic from sulphide oxidation dramatically decreases the pH in the solution which in turns increases the solubility of arsenic. As a result, release of arsenic from oxidized sulphide minerals due to mining activities has resulted in high concentration of arsenic in surface water, groundwater and soil vegetation.

In addition to polluting the aquatic system, arsenic contamination can also create serious environmental effects upon soil. Soil pedogenesis plays an important role in As

contamination of soil as the main origin of As is the parent material from which the soil is derived. As in surface soils is due to a combination of geological, hydrological and soil-forming biogeochemical processes (Kabata-Pendias and Adriano, 1995). Under typical soil-forming conditions, the lithology of the parent rock materials, volcanic activity, weathering history, transport, sorption, biological activity and precipitation all influence the nature of As in soils (Kabata-Pendias and Adriano, 1995). Arsenate is also the prevalent form in well-aerated soils where oxidizing conditions prevail and generally predominates over As(III) (Pongratz, 1998; Smith *et al.*, 1998a; Turpeinen *et al.*, 1999; 2002). However, in water-saturated soils and soils with significant organic matter or waste, As(III) dominates in these reducing conditions (Smith et al., 1998a). Arsenite, is known to be more toxic and mobile than arsenate but the relative proportion of these two species varies depending on a number of factors, including As sources, soil solution chemistry (pH and redox conditions), solid composition, adsorption and desorption, and biological transformations, volatilization, and cycling of As in soil (Panstar-Kallio and Manninen, 1997; Stronach *et al.*, 1997; Sadiq, 1997). Until the late 1950s, lead arsenate-based pesticide was extensively used to control agricultural pests in fruit orchards. Application of arsenate pesticides has caused soil levels to be a concern as both these metals can be toxic at high concentrations in soils. Arsenic from this historic pesticide use is less likely to impact groundwater. Another source of arsenic in soil is the current use of chromated copper arsenate (CCA); an inorganic waterborne wood preservative developed in 1933 to protect wood from bacterial, fungal and insect attack has been widely used throughout the world since then. There are three waterborne formulations designated as CCA types A, B and C depending on the relative proportions of metals present (Balasoiu *et al.*, 2001) In North America, the most widely used formulation of CCA is type C, containing (w/w) 47.5% $CrO_3$, 18.5% CuO, and 34% $As_2O_5$ (Cooper, 1994). The long-term use of CCA results in the leaching of these components, and arsenic due to its toxicity and higher mobility in soils relative to chromium and copper poses more risk (Dobran and Zagury, 2006; Zagury *et al.*, 2003; Stilwell and Gorny, 1997; Andersen *et al.*, 1996). Thus, soils contaminated by arsenic can be found near CCA-treated domestic wood structures, wood impregnating plants and also at sites where accidental spillage of CCA occur (Zagury *et al.*, 2003).

## 2.2 Global regions with arsenic ground water issues

As the world population continues to increase, arsenic contamination in drinking water has become a major public health issue globally (Nordstrom, 2002). Revised estimates from the World Health Organization for 1990 indicate that 22% of the world's population consumes drinking water unfit for consumption (Nriagu *et al.*, 1990). Arsenic contamination is widespread and found in scattered geographical areas in United States and Canada as well as in many other countries of Latin America such as Mexico, Chile, and Argentina. The sources of As are naturally-occurring as well as anthropogenic (Smedley and Kinniburgh, 2002; Matschullat, 2000; Nriagu, 1990; Nordstrom, 2002; Kabata-Pendias and Adriano, 1995). Arsenic contamination in the groundwater in countries like Bangladesh and India (West Bengal) has reached a very alarming level especially in the Bengal Delta plain and requires immediate attention (Ng *et al.*, 2003).
Groundwater is a source of drinking water in many parts of the world, in particular the South East Asia Region (SEAR) Countries where arsenic in groundwater is often elevated from natural sources (Ng *et al.*, 2003). In Vietnam, the aquifers under large deltas of the Mekong and Red Rivers are widely exploited for water consumption. In the Red River delta, As concentration up to 3050 μg/L in groundwater have been reported and, therefore, the potential health risk to the population is large (Berg *et al.*, 2001). One Southeast Asia nation that mines tin, Thailand, has accumulated large waste piles from tin mining that contain arsenopyrites with high As concentrations and have been shown to contaminate local soil and groundwater via leaching (Williams, 1997). As a result, arsenic concentrations up to 5000 μg/L have been detected in shallow groundwaters overlying quaternary alluvial sediments in this region (Williams *et al.*, 1996). In Eastern Europe, groundwater from alluvial sediments in the southern part of the Great Hungarian Plain of Hungary and neighboring Romania has As concentrations above 50 μg/L (Smedley and Kinniburgh, 2002). Arsenic in groundwater is a problem in many Mexican regions, La Comarca Lagunera, San Luis Potosi, Salamanca, Andocutin, Zimapán and others (Parga *et al.*, 2005). Arsenic contamination has been found in well water from several communities ranging from 240 to 1000 μg/L. This region has substrata rich in As and minerals dissolving naturally from weathered rocks and soils results in As in groundwater and well water (Parga *et al.*, 2005). There are number of regions in North

America which have soils which are enriched with As levels greater than 8–10 mg/kg, but most of the continent has solid state As less than 5 mg/kg (Grosz *et al.*, 2004). However, in the continental United States, half of the drinking water comes from groundwater, and reports suggest that about 2.5 million people in United States might be supplied with water with As levels more than 25 μg/L (Rasul *et al.*, 2002).

**Table 2.1** Population at risk around the world due to the As contamination in groundwater.

| Country/ region | Population at risk | Concentration (µg/L) | Environmental Conditions | References |
|---|---|---|---|---|
| Bangladesh | 30,000,000 | <1 to 2,500 | Natural; alluvial/deltaic sediments with high phosphate, organics | Ng *et al.*, 2003; Nordstrom, 2002; |
| India (West Bengal) | 6,000,000 | <10 to 3,200 | Same as Bangladesh | Ng *et al.*, 2003; Nordstrom, 2002; |
| Vietnam | >1,000,000 | 1 to 3,050 | Natural; alluvial sediments | Nordstrom 2002; Berg *et al.*, 2001 |
| Thailand | 15,000 | 1 to >5,000 | Anthropogenic; mining | Nordstrom, 2002 |
| Mexico | 400,000 | 8 to 620 | Natural and anthropogenic; volcanic sediments, mining | Nordstrom, 2002 |
| Chile | 400,000 | 100 to 1,000 | Natural and anthropogenic; volcanogenic sediments; closed basin lakes, thermal springs, mining. | Nordstrom 2002; Smedley and Kinniburgh, 2002; Sancha and Castro, 2001; Ng *et al.*, 2003 |
| Argentina | 2,000,000 | 100-1000 | Natural; loess and volcanic rocks, thermal springs; high alkalinity | Nordstrom 2002; Sancha and Castro, 2001; Ng *et al.*, 2003 |
| Hungary, Romania | 400,000 | <2 to 176 | Natural; alluvial sediments; organics | Nordstrom 2002; Smedley and Kinniburgh, 2002 |
| Ghana | <100,000 | <1 to 175 | Natural and anthropogenic; gold mining | Nordstrom, 2002 |
| USA/Canada | – | 10-48,000 | Natural and anthropogenic; mining, pesticides, $As_2O_3$ stockpiles, thermal springs, alluvial, various rocks. | Nordstrom, 2002; Smedley and kinniburgh, 2002; Welch *et al.*, 1988 |

### 2.2.1 Bengal delta plain, Bangladesh

Measured As concentration in the Bengal delta plain generally ranges from 30 to 750 μg/L but levels may reach up to 1000 μg/L in some locations. This is far above the limit set for drinking in Bangladesh (50 μg/L) or the 10 μg/L that is recommended by the World Health Organization (Sengupta, 2003; Dhar *et al.*, 1997). A group of scientists has observed that groundwater arsenic levels in 52 districts in Bangladesh have already crossed the maximum tolerable limit of 50 μg/L, as determined by the Department of Environment in Bangladesh (Karim, 2000). As a consequence, serious health problems are experienced by the people in this region since long-time exposure to arsenic from drinking arsenic-contaminated water causes cancer of skin, lungs, urinary bladder, liver and kidneys (Roy and Saha, 2002).

The Bengal delta plain is one of the largest deltas in the world and is divided into Ganges delta, the Brahmaputra flood plain the Meghna flood plain and the Sylhet basin (Karim, 2000). The first three are interconnected by arsenic rich sediments. Over the last two decades in Bengal, untreated tube well water was heavily promoted and developed as a seemingly safe and environmentally acceptable alternative to untreated surface water (Dhar *et al.*, 1997; Mallick and Rajagopal, 1996). In the 1980's, scientists began finding evidence of arsenic contamination in wells. The origin of the arsenic pollution is geologic - the arsenic is released to groundwater under naturally occurring aquifer conditions.

The groundwater arsenic problem in Bangladesh is due to the combination of three factors: i) The aquifer sediment in this region is rich in arsenic ii) The mobilization process of As happens via release of As to groundwater from the arsenic-rich sediments and iii) The transport of As generally occurs when arsenic is discharged to the natural groundwater circulation.

The potential mechanism by which arsenic is released into groundwater in this aquifer has been a subject of intense debate. The As contamination in Bangladesh has drawn the attention of many research groups and different hypotheses on possible mechanisms of

As mobilization have been proposed. There are several possible pathways which could explain the contamination of arsenic in Bengal basin.

(1) Pyrite and arsenopyrite present in aquifer sediments are oxidized by atmospheric oxygen present due to the lowering of the water table caused via excessive groundwater abstraction (Saunders *et al.*, 1997; Mallick and Rajagopal, 1996).

(2) Reductive dissolution of ferric-oxyhydroxide that contains sorbed As and releases the As oxyanions into alluvial aquifers (Acharyya, 2002).

(3) Mobilization of sorbed arsenic by phosphate generated from excessive use of fertilizers (Harvey *et al.*, 2002).

(4) Carbonate precipitation via microbial metabolism.

(5) Changes in the As sorption capacity of ferric hydroxides.

**[1] Sulfide oxidation hypothesis:**

The As affected area of Bangladesh contains sediment rich in arsenopyrite (FeAsS) and covers almost the entire alluvial region of the River Ganges. This hypothesis proposes that due to the lower water tables, $O_2$ entering the aquifer leads to the oxidation of arsenopyrite and the release of As(III) in the vadose zone as shown in the equation below (Adriano, 2001; Mahimaraja *et al.*, 2005). The dissolution of these As-bearing minerals depends on the availability of $O_2$ and the rate of oxidation of sulfide. The As(III) released can be partially oxidized to As(V) via microbial mediated reactions (Mahimaraja *et al.*, 2005).

$$FeAsS + 13Fe^{3+} + 8H_2O \rightarrow 14\ Fe^{2+} + SO_4^{2-} + 13H^{+} + H_3AsO_4 \quad \text{.....(2.2.1)}$$

Harvey et al. (2002) found a negative correlation between As and $SO_4^{2-}$ and concluded that As cannot be directly mobilized from sulphide minerals. However, it is possible that surface-deposited sulphide minerals are oxidized and dissolved by liberating arsenic.

**[2] The Fe oxyhydroxides reduction hypothesis:**

This hypothesis was first proposed by Nickson et al. (2000) and was later supported by others (Fazal *et al.*, 2001a; Zheng *et al.*, 2004; Horneman *et al.*, 2004, Hossain, 2006). It

states that origin of arsenic-rich groundwater is due to microbially-mediated reductive dissolution of Fe(III) oxy-hydroxides. The arsenic-rich groundwater is mostly confined to the alluvial aquifers, without being flushed from the Ganges delta (Hossain, 2006). Under oxidizing conditions, arsenic is assumed to be present in alluvial sediments of sand grains coated with iron hydroxide. The reduction of arsenic–rich iron oxyhydroxides is enhanced by the deposition of sedimentary organic matter leading to microbial dissolution of FeOOH. The microbial reduction of FeOOH results in the solubilization of arsenic in groundwater shown in equation below (Mahimaraja *et al.*, 2005).

$$8\ \text{FeOOH-As (sorbed)} + CH_3COOH + 14\ H_2CO_3 \rightarrow 8\ Fe^{2+} + \text{As (dissolved)} + 16\ HCO_3^- + 12\ H_2O \quad \text{……..(2.2.2)}$$

**[3] Competitive exchange of phosphate from fertilizer:**

This hypothesis is based on the release of arsenic ions sorbed to aquifer minerals by competitive exchange with phosphate ions that migrate into aquifers due to excessive application of fertilizer to surface soil (Acharyya *et al.*, 1999). The migration of phosphate due to the surface-application of fertilizers to the deeper aquifers is unlikely because of the low mobility of phosphate in tropical soils (Bose and Sharma, 2002). Experiments performed by Ravensoft *et al.* (2004) indicated that only 2 μg/L of As would be desorbed by 5 μg/L phosphorus concentration in groundwater. Hence, the quantities of phosphate required for explaining the subsurface mobilization of arsenic is not likely to reach the deep aquifers.

**[4] Carbonate precipitation:**

Arsenic in ground water and the reducing geochemical condition of subsurface aquifer correlate well with both bicarbonate and dissolved organic carbon (DOC) concentrations. Anawar *et al.* (2003) reported that the dominant process of arsenic release in the Ganges-Meghna (GM) delta is bacterially-mediated mineralization of organic matter (including localized peat layer) and the reductive dissolution of Fe and Mn oxyhydroxide. The mobilization of arsenic in the Ganges delta region was attributed

to substantial leaching of arsenic from sediments containing $NaHCO_3$ and of high pH values.

**[5] Sorptive capacity of ferric hydroxides:**

Appolo et al. (2002) reported that sorption of carbonate at common soil and groundwater concentrations decrease the sorption ability of ferrihydrite. Sediments with high concentration of sorbed As are deposited on surface water with low carbonate concentrations. This As-rich sediment is subsequently exposed to groundwater with a high dissolved carbonate content and As is displaced from the sediment by carbonate and mobilized into groundwater.

### 2.3. Aqueous Arsenic Speciation:

Arsenic in the aquatic environment follows complex chemistry and depends on a number of factors including pH and redox potential. Redox potential (Patrick *et al.* 1996) is defined as the voltage potential with respect to the standard hydrogen electrode (SHE) as calculated by the Nernst equation as follows.

$$Eh = E° - \frac{RT}{nF} ln \frac{(Red)}{(Ox)} + \frac{mRT}{nF} lnH^+ \quad \text{(2.3.1)}$$

Where *Eh* is redox potential, $E^o$ is the standard half-reaction reduction potential, *F* is the Farady constant, *n* is the number of electrons exchanged, *m* is the number of protons exchanged and the activities of the oxidized and reduced species are in parenthesis.

The chemical speciation of arsenic is essential to predict the environmental impacts of arsenic and its transformations with time (Mariner *et al.*, 1996; Manning and Martens, 1997; Hug *et al.*, 2001). Speciation of dissolved arsenic determines the extent of reaction with solid phases and the mobility of arsenic in groundwater (Ferguson and Gavis, 1972). Inorganic dissolved arsenic is present as an oxyanion either as arsenate [As(V)] or in the arsenite [As(III)] form. The solubility of these species is governed by a number of factors including pH, other ions present and the adsorbing surfaces. Depending on the *Eh* conditions prevalent in groundwater both arsenate and arsenite can form protonated oxyanions in aqueous solution and therefore their degree of protonation is dependent on the pH. (See Figure 2.1)

**i) Aqueous As(V) speciation**

Arsenate [As(V)] exists in oxidizing conditions whereas reducing conditions favor the formation of arsenite [As(III)]. In oxidizing environments in groundwater, i.e., Eh 0.4 to 1.3V, arsenate exists as $H_2AsO_4^-$ at pH values of 2.2-6.9 and as $HAsO_4^{2-}$ between pH 6.9-11.5. Completely dissociated arsenate ion ($AsO_4^{3-}$) is not commonly found in groundwater bodies as the pH value does not exceed 11.5 (Stollenwerk, 2003). Under oxidizing conditions, As(III) oxidizes to As(V) in water equilibrated with atmospheric oxygen, but the reaction half life (the time when the expected value of the number of entities that have decayed is equal to half the original number) is very slow ranging from 1-3 years (Stollenwerk, 2003). However, this oxidation of As(III) to As(V) is rapid when groundwater is brought to the surface (Yan *et al.*, 2000).

**ii) Aqueous As (III) speciation**

In reducing conditions i.e., Eh of 0 to -0.8V, arsenite exists predominantly as $H_3AsO_3$ below pH 9.2 and as $H_2AsO_3^-$ between pH 9.2-12 (Ferguson and Gavis, 1972).The differences in charge are responsible for the adsorption and desorption reactions between these different arsenic species and solid-phase surfaces in aquifers.

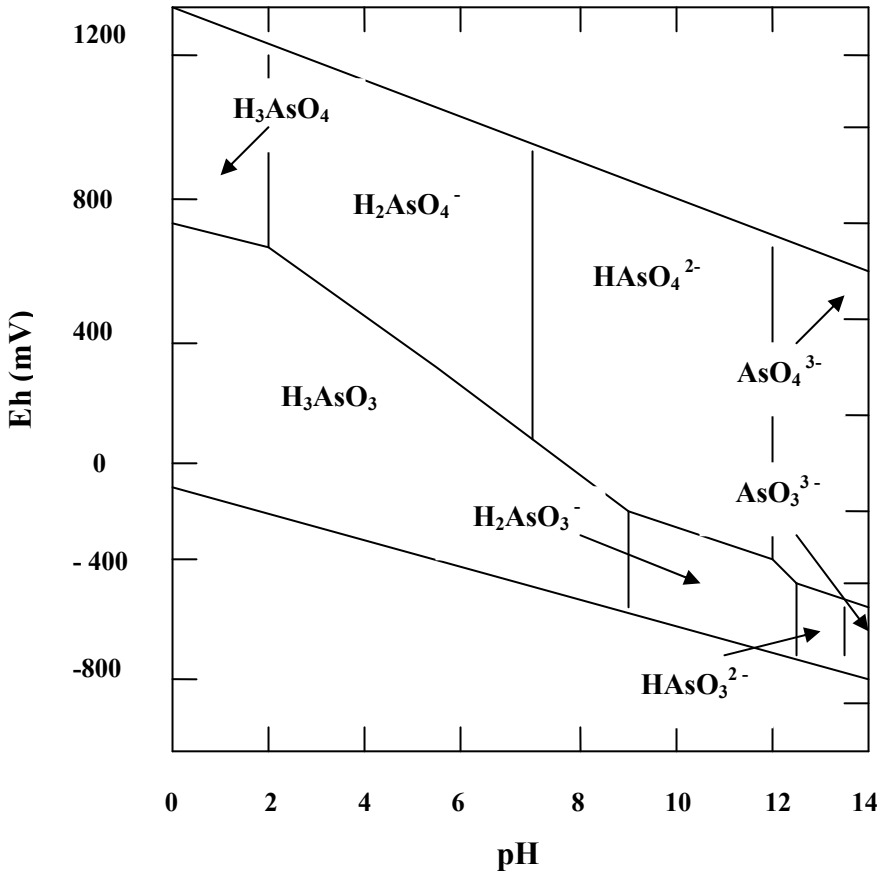


**Figure 2.1** Eh-pH diagram for aqueous As species in the As-$O_2$-$H_2O$ system at 25°C and 1bar total pressure (adapted from Smedley and Kinniburgh, 2002).

**Table 2.2** Equilibrium constant (K) at 25°C used in the calculation of aqueous As (V) speciation and solid-phase saturation state reported by Alexandratos *et al.* (2007).

| Reaction | log K | Reference* |
|---|---|---|
| $HAsO_4^{2-} = AsO_4^{3-} + H^+$ | -11.50 | [1] |
| $H_2AsO_4^- = HAsO_4^{2-} + H^+$ | -6.96 | [1] |
| $H_3AsO_4^0 = H_2AsO_4^- + H^+$ | -2.24 | [1] |
| $CaAsO_4^- = Ca^{2+} + AsO_4^{3-}$ | -4.36 | [2] |
| $CaHAsO_4^0 = Ca^{2+} + HAsO_4^{2-}$ | -2.66 | [2] |
| $CaH_2AsO_4^+ = Ca^{2+} + H_2AsO_4^-$ | -1.30 | [2] |
| $Ca_4(OH)_2(AsO_4)_2(H_2O)_{4\,(s)} = 4\,Ca^{2+} + 2\,AsO_4^{3-} + 2\,OH^- + 4H_2O$ | -29.20 | [2] |
| $Ca_5(AsO_4)_3(OH)_{(s)} = 5\,Ca^{2+} + 3\,AsO_4^{3-} + OH^-$ | -38.04 | [2] |
| $Ca_5(AsO_4)_3(OH)_{(s)} = 5\,Ca^{2+} + 3\,AsO_4^{3-} + OH^-$ | -39.60 | [2] |
| $Ca_3(AsO_4)_2(H_2O)_{4\,(s)} = 3\,Ca^{2+} + 2\,AsO_4^{3-} + 4H_2O$ | -21.00 | [2] |
| $CaHAsO_4(H_2O)_{(s)} = Ca^{2+} + HAsO_4^{2-} + H_2O$ | -4.79 | [2] |

**Table 2.3** Equilibrium constant (K) at 25°C of aqueous As(III) speciation and solid-phase saturation state (Ross *et al.*, 2006; Bothe and Brown, 1999).

| Reaction | log K | Reference* |
|---|---|---|
| $H_3AsO_3 = H_2AsO_3^- + H^+$ | -9.17 | [1] |
| $H_3AsO_3 = H_2AsO_3^- + H^+$ | -9.32 | [3] |
| $H_2AsO_3^- = HAsO_3^{2-} + H^+$ | -14.10 | [1] |
| $H_2AsO_3^- = HAsO_3^{2-} + H^+$ | -12.10 | [3] |
| $HAsO_3^{2-} = AsO_3^{3-} + H^+$ | -15.00 | [1] |
| $HAsO_3^{2-} = AsO_3^{3-} + H^+$ | -13.41 | [3] |
| $H_3AsO_3^0 + CaCO_3 + Ca^{2+} = CaCO_{3(s)} + CaHAsO_3 + 2H^+$ | -4.82 | [3] |

* [1] Bothe and Brown, 1999 [2] Myneni *et al.*, 1997 [3] Ross *et al.*, 2006

## 2.4. Sorption

Arsenic mobility in the aquifer is controlled by two sets of processes: i) Sorption (adsorption and desorption) ii) Solid phase precipitation and dissolution reactions. The formation of Ca, Mn and Pb arsenates has been reported in the literature, but the sorption onto mineral surfaces more typically provides the natural control for metals and arsenic in natural systems (Dzombak and Morel, 1990; Sadiq, 1990). Changes in pH, presence of competing ions and redox reactions are responsible for arsenic adsorption /desorption reactions.

There are two accepted mechanisms for the adsorption of arsenic onto variable-charge mineral surfaces: outer-sphere surface complexation and inner-sphere surface complexation. Outer-sphere surface complexation is a non-specific mode of adsorption formed via electrostatic interactions and contains more than one water molecule between the adsorbate and the adsorbent functional groups (Arai *et al.*, 2001; Goldberg and Johnston, 2001). Outer-sphere complexes with anions such as sulphate or selenate are common and are very sensitive to ionic strength (I) (Stollenwerk, 2003). In contrast, inner-sphere surface complexation is specific adsorption via ligand exchange reactions with surface functional groups, and no water molecules are present between the surface functional groups and the adsorbate ions (Sposito, 1989). Due to the stronger adsorption of ions to the mineral surface, inner-sphere complexes (covalent or ionic) have stronger bonds than outer-sphere complexes (electrostatic coulombic interaction) (Arai *et al.*, 2001; Goldberg and Johnston, 2001). Arsenic adsorbs to mineral surfaces by ligand exchange with $-OH^-$ and $H_2O$ functional groups and forms inner-sphere complexes (Stollenwerk, 2003; Sposito and Goldberg, 1984).

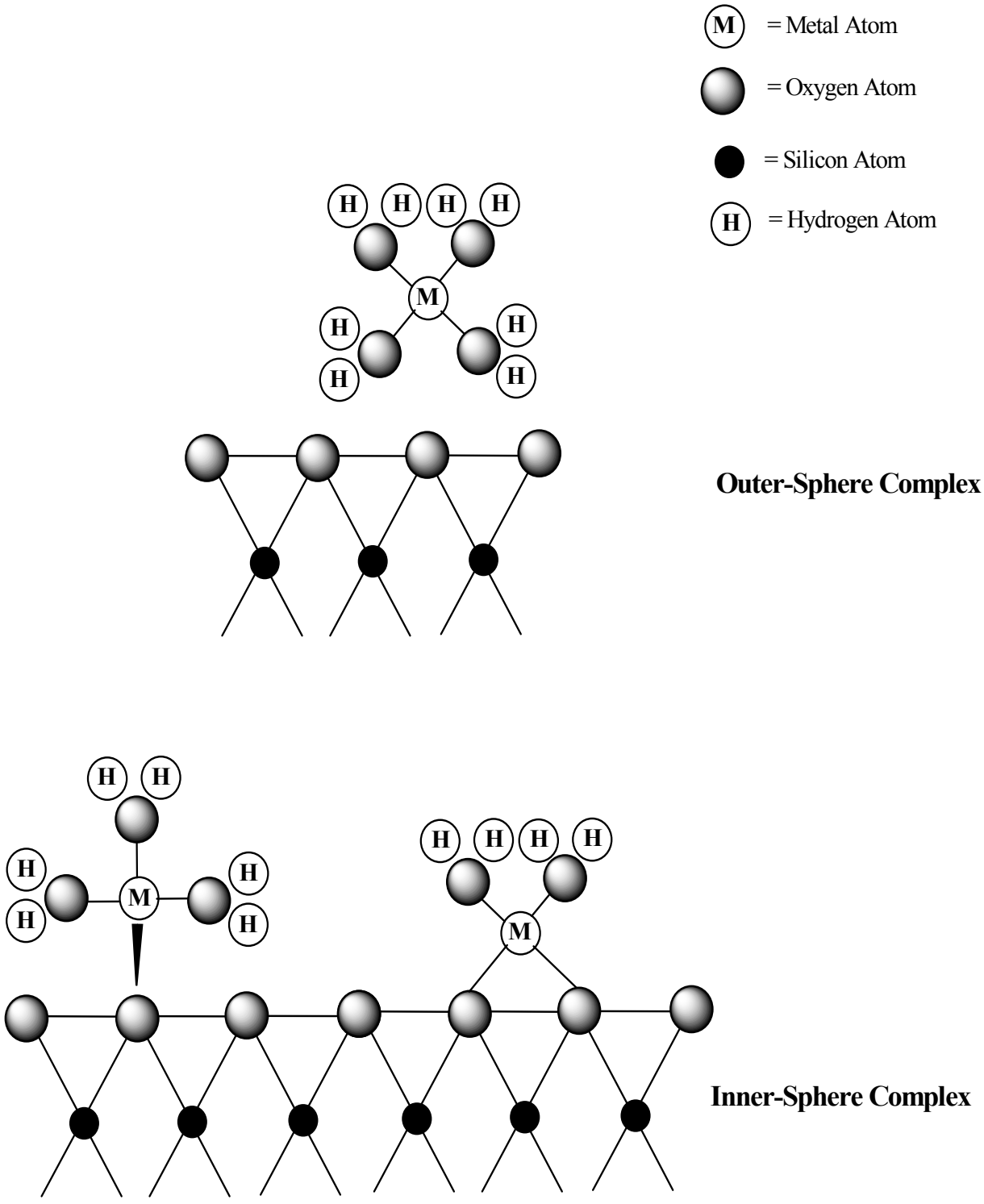


**Figure 2.2** Schematic diagram of adsorption mechanisms: Inner- and outer- sphere complexation (adapted from Foster, 2003).

Arsenate and arsenite adsorb to surfaces of a variety of aquifer materials. Among them, the metal oxides of iron (Fe), aluminum (Al), and manganese (Mn) because of their chemistry, abundance and ability to coat other particles are considered to be potentially the most important source/sink for As in aquifer sediments. When exposed to water, the metal ions on the oxide surface coordinate with OH groups (Hingston *et al.*, 1972) and surface charge then develops due to binding or release of OH groups depending on pH. The presence of surface functional groups ($>S\text{-}OH_2^+$, $>S\text{-}OH^+$ and $>S\text{-}O^-$) affects the adsorption properties of oxides (Sposito and Goldberg, 1984). Sorption reactions between arsenate and iron-oxide surfaces are particularly important reactions as iron oxides are ubiquitous in the natural environment and sorb strongly at acidic and near neutral pH (Waychunas *et al*., 1993; Dzombak and Morel, 1990). However, Fuller and Davis (1989) showed that desorption of arsenate from iron oxide surface is favored as pH values become alkaline. The arsenate adsorption to iron-oxide surfaces is pH dependent as there is net surface change from positive to negative values with the increase of pH (Dzombak and Morel, 1990).

The adsorption reaction of arsenite with iron oxides appears to generally be weaker than arsenate adsorption on iron oxide under typical environmental pH (Dzombak and Morel, 1990). Unfortunately, arsenate and arsenite sorption reactions with other common surfaces are less well characterized, and since adsorption is pH dependent, changes in groundwater pH may promote the adsorption or desorption of arsenic on these surfaces (Manning and Goldberg, 1997a). Redox reactions can also affect the aqueous arsenic concentrations as they have an effect on both arsenic speciation and also on the adsorption and desorption (Manning and Goldberg, 1997a). Manning and Goldberg (1997a) concluded that redox reactions involving either aqueous or adsorbed arsenic can affect arsenic mobility. The presence of competing ions can also affect the arsenic adsorption as they can compete with arsenate and arsenite for the sorption sites (Manning and Goldberg, 1996a).

Due to its similarities to Fe(III), the Al oxide minerals are structurally close to Fe oxides and show same type of pH dependence as observed with iron oxides. Additionally, Al(III) cations have the same charge and similar coordination numbers as Fe(III).

However, the As adsorption capacities of aluminum oxides are significantly lower than iron oxides. It has been shown that amorphous $Al(OH)_3$ adsorbed more As(V) per gram than crystalline $Al_2O_3$ and gibbsite, which indicates that crystallinity and surface area of Al oxides and hydroxides are important for As adsorption (Anderson *et al.*, 1976; Hingston *et al.*, 1972). Manning and Goldberg (1996b) compared the adsorption of As(V) by goethite and gibbsite at pH 5-9 with an identical initial concentration of either solid and aqueous As(V). They found that gibbsite adsorbed about 17% less As(V) than goethite. Thus, the number of reactive surface sites may not be indicated by surface area alone. In contrast to As(V), substantially lower adsorption of As(III) by hydrous Al oxides than iron oxides has been noted. (Arai *et al.,* 2001; Manning and Goldberg, 1997a) Both inner-sphere and outer-sphere As(III) complexes have been observed on aluminum oxides.

Aluminosilicate clay minerals are also known to adsorb arsenic in natural systems. These clay minerals are composed of alternating layers of Si and Al oxide. The OH groups of silica sheets are not typically considered reactive with As, but the OH groups associated with Al ions exposed at the edges of clay particles can accept protons and complex with anionic species of As (Davis and Kent, 1990). Thus, properties that control adsorption of arsenic by Al oxide minerals also apply to clay minerals. It has been shown that As(V) adsorbs to a greater extent than As(III) with clay minerals, with maximum As(V) adsorption at pH 7 (Goldberg and Glaubig, 1988b; Manning and Goldberg, 1997a; Lin and Puls, 2000). Also, it was observed that at pH values > 7 the adsorption levels of both As(V) and As(III) become more comparable (Lin and Puls, 2000; Frost and Griffin, 1977). The surface area of montmorillonite is 2.5 times greater than kaolinite and was found to adsorb about twice as much As(III) and As(V) as kaolinite (Frost and Griffin, 1977). This result suggests that surface area could play a significant role in adsorption of As by clay minerals. Halloysite adsorbed As(V) to a greater extent than kaolinite, illite, and montmorillonite (Lin and Puls, 2000). The behavior supports the above mentioned observation as highly disordered halloysite has much larger surface area than many other clay minerals. However, surface area is not always a good indicator of As(V) adsorption by clay minerals as higher As(V)

adsorption by kaolinite compared to illite and montmorilonite (which both have much higher total surface area) has been documented (Manning and Goldberg, 1996a).

Mn oxides can accept electrons and are often associated with the oxidation of As(III) to As(V) in soils and sediments. Manganese oxides in natural systems have poor crystallinity and show mixed oxidation states (McKenzie, 1981). Differences in mineral crystallinity have a significant effect on As adsorption, since poorly crystalline minerals have faster oxidation rates than more organized minerals. For example, the high surface area Mn oxide cryptomelane showed higher adsorption of As(V) and As(III) compared to lower surface area pyrolusite. The most common Mn oxide is the birnessite group formed from weathering processes, and As(V) adsorption to this mineral is negligible as birnessite has a net negative surface charge at pH values common in groundwater. The energy needed to displace a functional group from the negatively charged birnessite surface is not provided by the negatively charged species, $H_2AsO_4^-$ at pH 4-7. However, at pH 7, the neutral charge on $H_3AsO_3$ results in a lower energy barrier to exchange with surface functional groups and so As(III) was adsorbed by birnessite (Oscarson *et al.*, 1983).

Carbonate minerals could also be important in controlling the aqueous concentrations of As, especially at higher pH values. Arsenic adsorption by limestone and calcite has been documented (Cheng *et al.*, 1999; Bothe and Brown, 1999; Maeda *et al.*, 1992; Ohki *et al.*, 1996). Limestone has been used specifically as an adsorption medium for arsenic in drinking water and it was found that crushed and sieved limestone grains enhanced As removal (Maeda *et al.*, 1992; Ohki *et al.*, 1996). Phase transformation of $CaCO_3$ polymorphs has been studied by Peric *et al.* (1996). However, no reports are available on the stability of the arsenite and arsenate complexes with $CaCO_3$. Sorption of As(III) on calcite as a function of concentration, pH and time has been reported (Ross *et al.*, 2006). Thus, $CaCO_3$ could be one of the important sorbents for arsenic removal in groundwater.

## 2.5 Calcium carbonate

### 2.5.1. Mineralogy and stability:

Calcium carbonate is among the most extensively researched biominerals (Xu *et al.*, 2004). A notable feature of $CaCO_3$ is its tendency to exist in different polymorphic forms (Chakraborty *et al.*, 1996). The temperature-pressure phase diagram (in Figure 2.3) indicates calcite as the thermodynamically stable form at ambient conditions (Wray and Daniel, 1952; White, 1997) while aragonite predominates at high pressure (Bottcher and Wyllie, 1968; Johnaness and Puhan, 1971). Aragonite does form in high pressure rocks, but also forms metastably under low pressure near-surface conditions. As well as forming the shells of some marine invertebrates, aragonite also forms in hot-spring and cave deposits, and may also be directly precipitated from warm sea water (Bottcher and Wyllie, 1968; Johnaness and Puhan, 1971). Vaterite has a density of 2.65g/cm$^3$ and due to this low density, it is metastable with respect to the other two polymorphs and is not common in natural environments (Carlson, 1983). As biogenic minerals, calcite and aragonite are the more stable forms. However, in synthetic phase, vaterite exists in high temperature precipitation of calcium carbonate when the formation of calcite and aragonite is chemically inhibited (Nancollas and Swada, 1982). Vaterite is hexagonal with a structure analogous to the high temperature modification of $YbBO_3$, where the Ca and C atoms occupy the alternating planes parallel to (0001) and planar $CO_3$ groups stand perpendicular to (0001) (Leeuw and Parker, 1998). In calcite, Ca atoms have a face-centered distribution on this rhombohedron, and the triangular $CO_3$ groups lie at the centre of each edge. (See Figure 2.4) This results in layers of $CO_3$ groups lying normal to the c axis of calcite, with layers of Ca atoms lying between them (Leeuw and Parker, 1998).

Aragonite also contains layers of alternating triangular $CO_3$ groups and Ca atoms, but they are arranged differently from calcite. The layers lie perpendicular to the c axis of the orthorhombic unit cell. Hence, aragonite has an orthorhombic symmetry **(**2/m 2/m 2/m**)** instead of calcite's trigonal ($\bar{3}$ 2/m) symmetry (De Villiers, 1971; Leeuw and Parker, 1998).The relationship between calcium carbonate precipitation temperature and the coordination number of calcium in the polymorph has been reported (Vecht and Ireland, 2000; Kahmi, 1963). Calcite with six-fold coordination of calcium was the

predominant phase at temperatures below 15°C whereas eight coordinate calcium was found in vaterite synthesized from 25 to 60°C. The stabilization of the structure is probably due to an increase in the effective radii of the calcium atoms caused by thermal vibrations. Above 60°C aragonite having coordination to nine oxygen atoms becomes the stable phase (Kahmi, 1963).

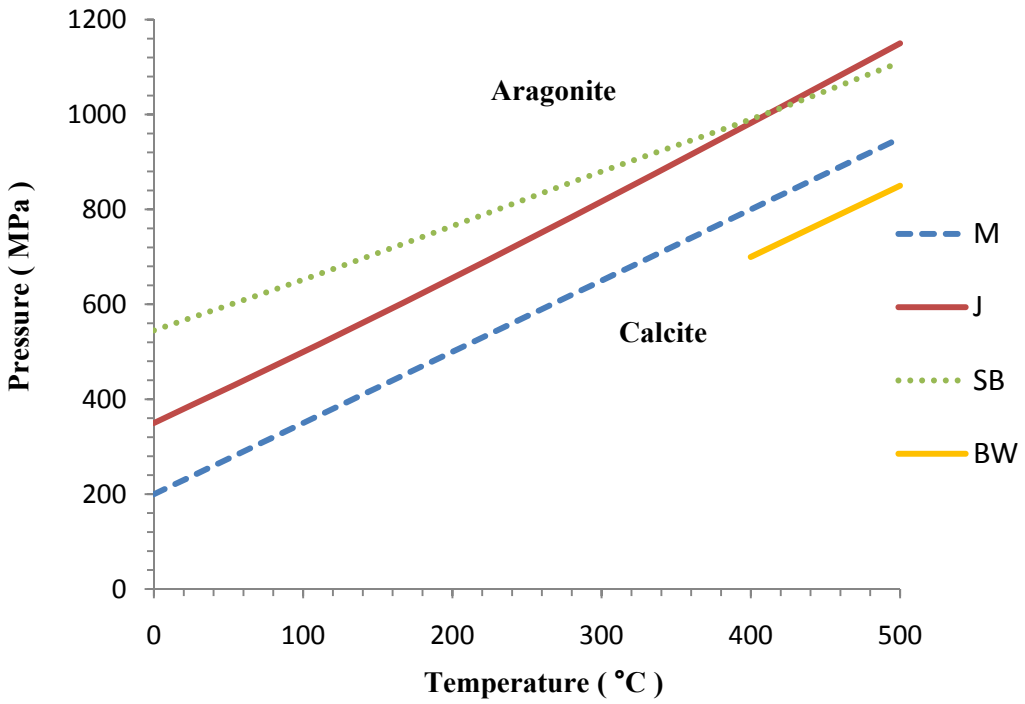


**Figure 2.3** The temperature-pressure dependent calcite-aragonite stability diagram. (Adapted from White, 1997) *M*: (MacDonald, 1956); *J*: (Jamieson, 1953); *SB*: (Simmons and Bell, 1963); *BW*: (Boettcher and Wyllie, 1968).

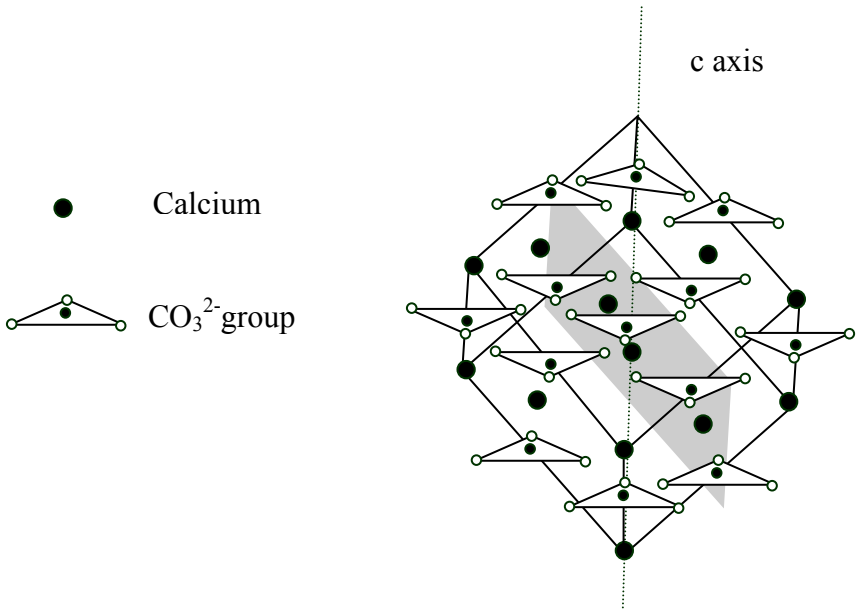


**Figure 2.4:** Crystal lattice of calcite with (0001) plane.

The process of aragonite-calcite transformation and the reverse transformation of calcite to aragonite have received considerable attention because of their geological importance and also as a model for other complex reactions (Carlson, 1983). Brar and Schloessin (1979, 1981) studied the aragonite-calcite transformation process under the conditions from 14 to 25 kbar at 300-600 ºC on single crystals and polycrystalline samples of calcite. The results indicated an activation energy of 67kJ/mol at 17 kbar and found that the rate for polycrystalline samples decreased with the square root of grain size. Gammage and Glasson (1976) have demonstrated that grinding leads to aragonite formation from calcite at room temperature, indicating that calcite-aragonite transformation can occur outside the aragonite stability field (Gammage and Glasson, 1976). When a mineral forms outside its stability field, it means that the growth occurs under non-equilibrium conditions, and that there is some kinetic reason for its formation. Petrographic observations and data on bulk transformation kinetics indicate that the solid state transformation of aragonite to calcite proceeds by thermally activated growth of heterogeneous topotactic nuclei at constant linear rates (Carlson, 1983). The driving mechanisms behind the aragonite dissolution and calcite precipitation are either the equilibration of water and carbonate mineral (water controlled) or the differing solubility of calcite and aragonite (mineral controlled) (James and Choquette, 1984; Budd, 1988).Water exerts a strong catalytic effect, and instead of the mechanism involving Ca-O bond destruction and reformation, the hydrous reaction substitutes a sequence of mechanisms with lower activation energies: dissolution, transport, and precipitation (Carlson, 1983). The greater solubility of aragonite compared to calcite is a result of the mineral-controlled mechanism (Budd, 1988).

The above discussion centers on abiotic $CaCO_3$ formation and synthesis, however biological ureolytic hydrolysis presents another viable method for $CaCO_3$ production since most bacteria possess the urease enzyme (Hammes *et al.*, 2003; Stocks-Fischer *et al.*, 1999; Hammes *et al.*, 2003). Bacterial ureolysis occurs when the coordination of urea and water at the active catalytic site of the urease enzyme results in a transient activated complex, which accelerates the rate of the reaction $10^{14}$ relative to uncatalyzed urea hydrolysis (Jarbi, 1995).

### 2.5.2. $CaCO_3$ importance in aquifers

Calcite is a common mineral phase found in groundwater zones (Zachara *et al.*, 1993). In calcareous groundwater, all metal concentrations are influenced by metal carbonate solubility. $CaCO_3$ acts as buffer for groundwater pH and its precipitation/dissolution behavior influences the groundwater composition (Plummer, 1977; Morin *et al.*, 1988; Langmuir, 1971; Zachara *et al.*, 1993). Although $CaCO_3$ present in limestone and calcareous sediments show appreciable surface area, its importance as a sorbent for metal ions and oxyanions in groundwater is not well known.

Studies by Oscarson *et al.* (1983) showed that there was no adsorption of As(III) by $CaCO_3$ at pH 7. However, Cheng *et al.* (1999) inferred using x-ray standing wave diffraction that solution of As (III) when allowed to react with calcite was removed from the solution and occupied the carbonate sites on the calcite surface. Goldberg and Glaubig (1988b) observed an increase of As(V) adsorption of 0.7 mM/kg at pH 6 to a maximum of 2mM/kg at pH 11. This suggests that at higher pH values, carbonate minerals may be important in controlling the aqueous concentration of As and might play a vital role in adsorption of As in carbonate buffered groundwater system.

### 2.5.3. Potential reactions with arsenic oxyanions

Much research has been done on the surface potential of $CaCO_3$ (Siffert and Fimbel, 1984; Cicerone *et al.*, 1992; Fuerstenau *et al.*, 1992; Vodovic, 2001). According to Somasundaran and Agar (1967) the surface ions $Ca^{2+}$ and $CO_3^{2-}$ can be hydrolyzed as follows:

$$CO_3^{2-} + H_2O \leftrightarrow HCO_3^- + OH^- \quad \text{..... (2.5.1)}$$

$$HCO_3^- + H_2O \leftrightarrow CO_2 + H_2O + OH^- \quad \text{..... (2.5.2)}$$

$$Ca^{2+} + OH^- \leftrightarrow Ca(OH)^+ \quad \text{..... (2.5.3)}$$

$$Ca(OH)^+ + OH^- = Ca(OH)_2\,(aq) \quad \text{..... (2.5.4)}$$

At low pH, equations 2.5.1 and 2.5.2 proceed to the right direction whereas equations 2.5.3 and 2.5.4 proceed in the opposite direction. At high pH the reverse trend follows (Moulin and Roques, 2003; Somasundaran and Agar, 1967; Foxall *et al.*, 1979).

It is possible to draw some inferences on possible adsorption mechanisms that might result in the observed changes in zeta potential in the presence of arsenite and arsenate. While the exact mechanisms are not known for $CaCO_3$/As complexation, it is clear that the overall surface charge becomes more negative in the presence of arsenic oxyanions. Complexes consistent with the data are compiled below in Table 2.4. The likely complexes are based on the composition of solution speciation, surface charge and surface constraints (site density, sterics, and electrostatics).

**Table 2.4** Hypothetical arsenate and arsenite complexes at different pH value with $CaCO_3$.

**Low pH**

$Ca^{2+} + H_3AsO_3 \longrightarrow (CaH_2AsO_3)^+ + H^+$ 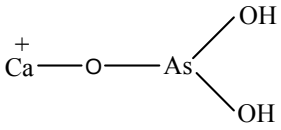 (1)

$Ca^{2+} + H_3AsO_3 \longrightarrow CaHAsO_3 + 2H^+$ 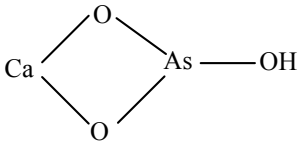 (2)

$Ca^{2+} + H_2AsO_4^- \longrightarrow CaHAsO_4 + H^+$ 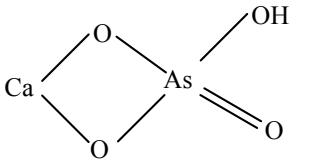 (3)

**Neutral pH**

$Ca(OH)^+ + H_2AsO_3^- \longrightarrow CaO_2AsOH + H_2O$ 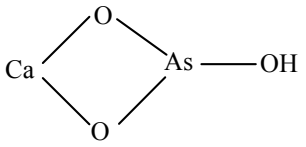 (4)

$Ca(OH)^+ + H_3AsO_3 \longrightarrow CaO_2AsOH + H_2O + H^+$ 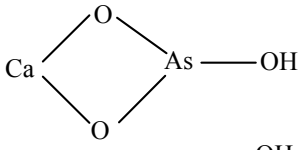 (5)

$Ca(OH)^+ + HAsO_4^{2-} \longrightarrow CaO_2AsO(OH) + OH^-$ 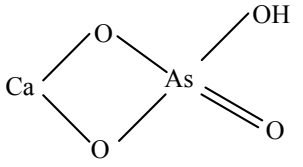 (6)

$Ca(OH)^+ + H_2AsO_4^- \longrightarrow CaO_2AsO(OH) + H_2O$ 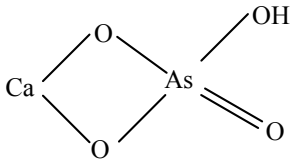 (7)

**High pH**

$Ca(OH)_2 + HAsO_3^{2-} \longrightarrow CaO_2AsOH + H_2O + OH^-$ 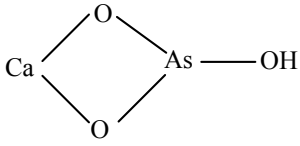 (8)

$Ca(OH)_2 + HAsO_4^{2-} \longrightarrow CaO_2AsO(OH) + 2\,OH^-$ 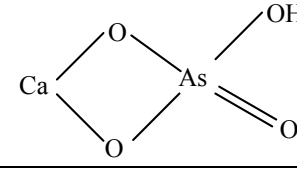 (9)

Arsenite and arsenate could combine with $Ca^{2+}$ ion to form monodentate complex at low pH as indicated by equation1and bidentate mononuclear complex indicated by equations 2 and 3. The increase in the release of $H^+$ ions results in the decrease of surface charge. At higher pH values, arsenate and arsenite are expected to potentially form bidentate mononuclear complexes as shown by the equations 8 and 9. Equations 4-7 represent the formation of bidentate mononuclear complexes for arsenite and arsenate, respectively, at neutral pH. The result of these type of complexation would be an increase in surface charge due to the net release of $OH^-$ ions in case of arsenate and decrease in surface charge in the case of arsenite due to the release of $H^+$ ions at neutral pH.

Formation of monodentate complexes at low pH and bidentate complexes at pH 9.2 has been reported in the case of arsenite and arsenate adsorption on ferrihydrite (Jain *et al.*, 1999; Waychunas *et al.*, 1993). $Pb^{2+}$ forms monodentate complexes with calcite at lower concentrations (Rouff *et al.*, 2004). EXAFS study on rare-earth element (REE) coordination in calcite reveal that bidentate mononuclear complex formation cannot be excluded (Elzinga *et al.*, 2002). Oxygens in $CO_3^{2-}$ group are coordinated to Ca via monodentate linkages in the calcite structure. A seven fold coordination is possible when a $CO_3^{2-}$ group has bidentate linkage (Elzinga *et al.*, 2002). This can be achieved by twisting or rotation of the $CO_3^{2-}$ group. Another possibility is the addition of oxygen ligands, either as OH or $H_2O$ retained from the adsorbing cation's hydration shell. The OH provides charge compensation when the $CO_3^{2-}$ ligands are left unchanged (Elzinga *et al.*, 2002). However, no spectroscopic work on the detailed mechanistic assessment of adsorption of arsenite and arsenate on to calcite surface has been reported in the literature. For metal oxides, Arai *et al.* (2004) reported the formation of bidentate binuclear complexes of As(III) and As(V) at aluminium oxide/water interface, but this bonding mode on calcite is unlikely due to steric constraints caused by calcium-calcium repulsions.

## 3.0 HYPOTHESES AND OBJECTIVES:

The goal of this project is to examine the structure and surface properties of synthetic $CaCO_3$ minerals and then to investigate the suitability of these $CaCO_3$ materials for the remediation of As(III) and As(V).

The hypotheses are as follows:

[1] $CaCO_3$ particle size and preparation method will significantly affect its surface chemistry and reactivity with arsenic oxyanions.

[2] Synthesis of $CaCO_3$ nanoparticles can be accomplished abiotically to produce products similar to the biomineralization process.

The specific objectives are to i) devise a chemical $CaCO_3$ precipitation that approximates biogenic $CaCO_3$ ii) determine rate, extent and mechanism of arsenic adsorption by synthetic $CaCO_3$, and relate mineral structure/properties back to the observed arsenic sorption.

### 3.1 How does particle size and preparation method affect $CaCO_3$ reactivity with arsenic oxyanions?

Among the $CaCO_3$ polymorphs, calcite is the most thermodynamically stable. However, particle size is one of the factors that can invert the thermodynamic stability (Navrotsky, 2004). At the nanoscale, there can be crossovers and other metastable phases can exist. The nucleus of the metastable phases will have lower activation barrier and there is a possibility of lower free energy compared to the bulk phases (See Figure 3.1). Biogenic $CaCO_3$ is formed under conditions that contain a variety of metabolites and a myriad of Ca-ligand reactions could possibly influence the particle size.

According to the classical nucleation theory, the barrier of the growing particle is the net outcome of the competition of positive surface energy and negative bulk free energy change which are dependent on the particle radius (Navrotsky, 2004). The role of surfactants as templates in the synthesis of $CaCO_3$ has been studied extensively (Donners *et al.*, 2002). In the present investigation, we have used simple polyethylene glycol (PEG) for the preparation of nanometer-sized $CaCO_3$ materials. The motive for this is to devise a chemical $CaCO_3$ precipitation that mimics biogenic $CaCO_3$ prepared

via ureolytic bacterial $CaCO_3$ precipitation. Nanoparticle precursors may play a vital role in biomineralization by providing alternative mechanisms for crystal growth. Since the differences in the enthalpy and free energies are small among metastable phases of $CaCO_3$, they "offer controlled thermodynamic and mechanistic pathways" (Navrotsky, 2004). Some PEGs form micelles in aqueous solution, and these micelles perform the role of solubilizers. Therefore, it may be possible that the calcium in $CaCO_3$ is subdivided in PEG micelles and as a result has reduced particle size.

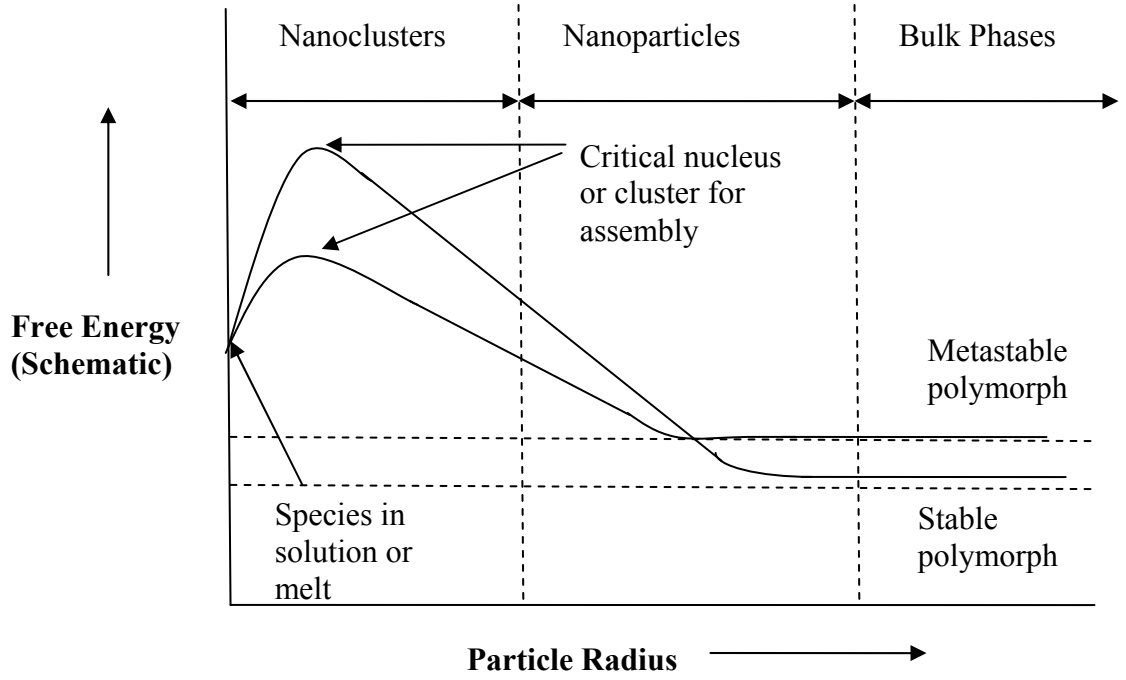


**Figure 3.1** Schematic representation of particle size effects on the critical nucleus and the activation energy (Adamson, 1990).

### 3.2 Which of these synthesis methods simulates biogenic $CaCO_3$?

There has been considerable effort in recent years (Dujardin and Mann, 2002; Aizenberg 2004) to understand the biomineralization process (Gotliv *et al.*, 2003; Dickinson and McGrath, 2004). Most bacteria possess the urease enzyme and so ureolytic hydrolysis presents a method for biotic $CaCO_3$ production (Hammes *et al.*, 2003; Stocks-Fischer *et al.*, 1999). The essence of urea hydrolysis in terms of $CaCO_3$ precipitation can be described as follows (Hammes *et al.*, 2003). Intracellular cleavage of urea by urease produces one mole of carbamate and one mole of ammonia (see equation 3.2.4). Spontaneous hydrolysis of carbamate produces an additional mole of ammonia and one mole of carbonic acid (see equation 3.2.5). The resulting carbonic acid equilibrates with water according to equation 3.2.2, and the ammonia will hydrolyze to yield two moles of ammonium ion and two moles of hydroxide ions (see equation 3.2.6).

$CO_2 + H_2O \leftrightarrow H_2CO_{3\,(aq)}$ …… (3.2.1)

$H_2CO_3 \leftrightarrow HCO_3^- + H^+ \leftrightarrow CO_3^{2-}{}_{(aq)} + H^+$ ….(3.2.2)

$CO_3^{2-} + Ca^{2+} \rightarrow CaCO_{3\,(s)}$ .....(3.2.3)

$CO(NH_2)_2 + H_2O \rightarrow NH_{3(g)} + H_2NCOOH$ …...(3.2.4)

$H_2NCOOH + H_2O \rightarrow NH_3 + H_2CO_{3\,(aq)}$ …. (3.2.5)

$2NH_3 + 2H_2O \leftrightarrow 2NH_4^+{}_{(aq)} + 2OH^-$ …. (3.2.6)

Combining all the above equations from equation (3.2.4) to equation (3.2.6),

$CO(NH_2)_2 + 2H_2O \rightarrow 2NH_4^+ + CO_3^{2-}{}_{(aq)}$ ……...(3.2.7)

The formation of two moles of hydroxide ion according to equation (3.2.6) increases the pH and hence shifts the equilibrium in equation (3.2.2) in the forward direction. The overall process, the combination of equation (3.2.4) to (3.2.6), is the hydrolysis of urea to yield ammonium ion and carbonate ion according to equation (3.2.7). The resulting carbonate ions then precipitate as $CaCO_3$ in the presence of soluble calcium cations (Stocks-Fischer *et al.*, 1999).

In $CaCO_3$ precipitation, a nucleation site is a pre-requisite for the initiation of crystal formation (Hammes *et al.*, 2003; Stocks-Fischer *et al.*, 1999). Abiotic $CaCO_3$

precipitation occurs on suspended particles in water whereas biotic $CaCO_3$ precipitation utilizes bacteria as nucleation sites (Warren *et al.*, 2001). Bacterial surfaces possess a variety of reactive sites (Small *et al.*, 1998) in the form of surface functional groups (e.g., carboxyl, phosphoryl, amino and hydroxyl groups) that are associated with structural polymers in cell walls and various other cellular materials (Warren and Ferris, 1998). The exact type and number of reactive sites are species dependent. Bacteria provide appropriate surfaces for heterogeneous nucleation and can act as nucleation templates that reduce the activation energy required for precipitation to occur (Warren and Ferris, 1998; Warren *et al.*, 2001).

Deng *et al.* (2005) speculated that the soluble acidic proteins in moluscan shells, an invertebrate producing $CaCO_3$, are involved in controlling mineral formation. These soluble acidic proteins can function as nucleators of mineral formation or as modulators of mineral growth. For such a process to occur, the non-covalent interaction and cooperation between soluble macromolecules play important roles by providing chemical microenvironments for the deposition of minerals. Researchers have mimicked this biomineralization process using organic additives or templates to facilitate the formation of molecular aggregates by non-covalent interaction (Aizenberg 1997; Kato 2000; Kato *et al.*, 2002; Colfen, 2003; Han and Aizenberg, 2003; Sugawara *et al.*, 2003; Pomogailo and Kestelman, 2005).

Inspired by the biomineralization process, we have prepared $CaCO_3$ namoparticles following two different synthetic strategies:

**i) *in situ* deposition.** Nanometer-sized $CaCO_3$ was prepared through dissolving a complex of $CaCl_2$ and Poly ethelyne glycol (PEG) polymer and adding stoichiometric amount of $K_2CO_3$. The crystal morphology and the nanoparticle size distribution depend on the precursor concentrations: nanoparticle size decreases with the PEG polymer concentration. This relationship is due to the strong interactions in the system. The polymer matrix can undergo considerable chemical reactions leading to partial chain destruction and cross linking as well as changes corresponding to thermal destruction (Pomogailo and Kestelman, 2005). Since phase growth is restricted to only certain

crystalline phases, the resulting nanoparticle exhibits more controlled shape and morphology.

**ii) interfacial precipitation method.** Nano-sized $CaCO_3$ was synthesized by *in situ* mixing of balanced micellar solutions of $CaCl_2$ and $K_2CO_3$ with Tween 80 surfactant. They form a polynuclear colloidal complex formed in w/o emulsion consisting of calcium salts, Tween 80, -(Ca-$Cl_2$)- segments and bound water 3-4 nm size (Pomogailo and Kestelman, 2005). To create a homogenous dispersion of colloidal micelles, the emulsion is stirred to homogenize it, poured into aqueous $K_2CO_3$, and the resulting $CaCO_3$ precipitate is separated by centrifugation. These complex micelles may function as templates and provide a microenvironment in which the nucleation and growth of $CaCO_3$ occur. This process demonstrates the importance of noncovalent interaction and cooperation among the additives for the preparation of inorganic crystal lattice. They coordinate with each other and their cooperative function in this aggregate contributes strongly to the final polymorph and morphology of $CaCO_3$ that is produced. Accordingly, the major requirement in this surfactant-mediated precipitation appears to be the selection of multiple components that are able to construct well defined aggregates and provide an appropriate chemical environment for crystallization.

# 4.0 METHODOLOGY

## 4.2 Mineral synthesis

### 4.2.1 Bulk $CaCO_3$ synthesis

The bulk $CaCO_3$ precipitation was performed by using a solution that was highly oversaturated (based on Ion Activity Product) so that large $CaCO_3$ precipitates rapidly form. For these experiments, 250 mL of 0.1M $Ca(NO_3)_2.4H_2O$ and $Na_2CO_3$ solutions were prepared. Equal volumes of both solution ($Ca(NO_3)_2.4H_2O$ and $Na_2CO_3$) were added to maintain 1:1 mole ratio. To produce a precipitate, the pH was adjusted to 7.5 by addition of 1mL of $HNO_3$. The precipitated $CaCO_3$ was then centrifuged for 10 minutes at 4000 revolutions per minute (rpm). After centrifugation the $CaCO_3$ precipitate was oven-dried for 24 hours at 60 ºC and the % yield was found to be 92%.

### 4.2.2 Nano $CaCO_3$ synthesis

**Method 1)**

An *in situ* deposition technique was employed for the synthesis of nanometer-sized calcium carbonate (Mishra *et al.*, 2004). $CaCl_2.2H_2O$ (2.92g by weight) was mixed in 200 mL of milliQ water. PEG (240.00 g by weight) was diluted by mixing 200 mL of milliQ water and heating mildly for proper mixing (Fig. 4.1 a). The calcium:PEG complex was prepared in 1:2 molar ratio. The contents were mixed and digested for 12 hours. A solution of $K_2CO_3$ was prepared by mixing 2.80g in 200 mL of milliQ water and added slowly into the PEG digest and reacted overnight. The resulting precipitate was filtered and dried at 40ºC. This method produced 1.61g of $CaCO_3$ and the % yield was calculated to be 87%.

**Method 2)**

A second nanometer-sized $CaCO_3$ was also synthesized by following the interfacial precipitation procedure used by Yohta Mori *et al.* (2005). Preparation of this nano $CaCO_3$ was based on an interfacial reaction (water in oil emulsion) (Fig. 4.1 b). 1M $CaCl_2$ solution was prepared and added to 5% mass/mass solution of toluene and Tween

80 in a volume ratio of 7:3 respectively. The contents were stirred with a homogenizer for 2 minutes and then immediately poured into 1M solution of $K_2CO_3$. The precipitate formed was centrifuged for 5 minutes and the liquid phase was decanted. Repeated washings with deionized water and acetone were performed to completely remove residual toluene. Finally, the precipitate was dried for 12 hours at room temperature and 88% yield of the precipitate was obtained.

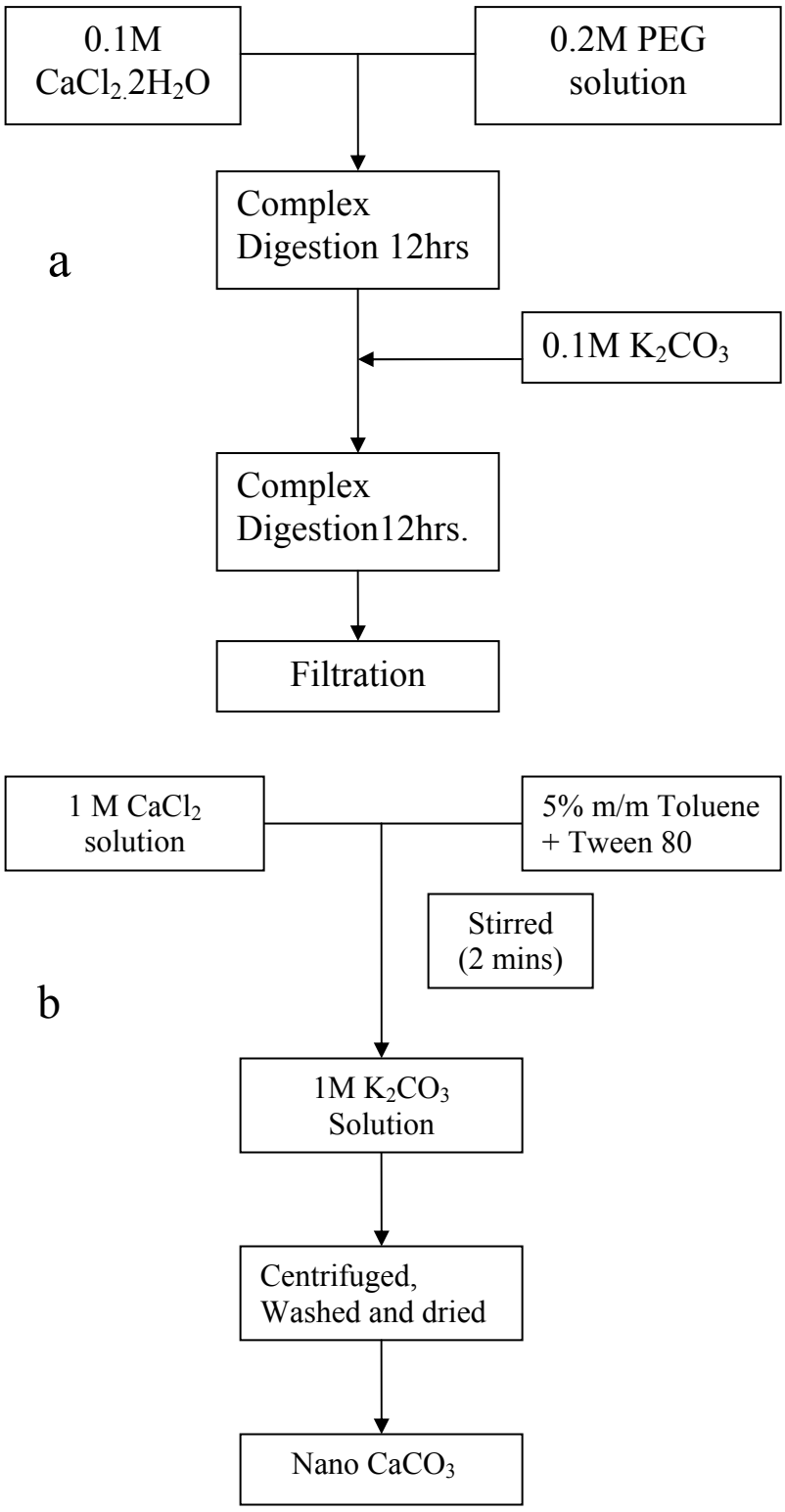


**Figure 4.1** a) Nano $CaCO_3$ (*in situ* deposition method) synthesis technique using PEG and b) Nano $CaCO_3$ (interfacial method) prepared by an interfacial reaction (W/O emulsion).

### 4.3. Mineral Characterization:

#### 4.3.1 BET - Specific surface area measurement

A simple model of physisorption is the basis of Brunauer Emmett and Teller (BET) theory (Brunauer *et al.*, 1938). The adsorption of gases on the surface of an adsorbent is not via monolayer formation at high pressures and low temperatures. Instead, as the pressure of the gas reaches saturation, vapour pressure of the liquefied adsorbent multilayer formation is enhanced. This can be modeled via the BET equation and the volume of a gas required for a monolayer to form can be calculated. This volume can then be used to calculate an external surface area for the particles. The specific surface area of laboratory synthesized $CaCO_3$ was determined using $N_2$ BET (Quantachrome Autosorb-1 instrument).

#### 4.3.2. Particle Size Analyzer:

The particle size distribution of all synthesized $CaCO_3$ was analyzed with a Horiba LA 950 particle size analyzer. This instrument uses the principle of Mie scattering (Fraunhofer diffraction). For particles larger than the wavelength of light, the light scatters from the edge of the particle at an angle dependent on the size of the particle. Larger particles scatter light at relatively smaller angles compared to smaller particles. By observing the intensity of light scattered at different angles, the relative amount of different sized particles is determined. The procedure involved is as follows: The instrument's Nalgene container was filled with distilled water, and the instrument was powered on. The software controlling the instrument (LA-950 for Windows) was started followed by feeding, rinsing, circulation and agitation prior to de-bubble. Finally, 1g of $CaCO_3$ was added to the distilled water and stirred until it was fully dispersed in the solution. The sample was pipetted into the machine, sonified and auto diluted using standard analysis routines, and then the particle size analysis was performed.

#### 4.3.3 Fourier Transform Infra Red Spectroscopy (FT-IR) and Fourier Transform Raman Spectroscopy (FT-RS):

The characterization of different polymorphs of mineral samples was performed via FT-IR (EQUINOX 55, Bruker) and FT-RS (FRA-106/S FT-Raman, Bruker, Karlsruhe,

Germany).FT-IR analysis was conducted on pressed disks. IR grade potassium bromide (KBr) was dried in an oven overnight (110°C) to remove water. Reference (pure KBr) and sample discs were prepared with either 200 mg KBr or 198 mg KBr + 2mg $CaCO_3$. All samples were mixed and ground as finely as possible with an agate mortar and pestle. The samples were stored in the desiccator to preclude $H_2O$. The ground powders were then placed in the pellet die and sealed with plunger and O-ring. A pressure of 10 tons of force (hydraulic press) was applied for at least 15 minutes with the press also under vacuum. The pellets were analyzed by FT-IR (EQUINOX 55, Bruker) using a DTGS detector over the spectral range 4000-400 $cm^{-1}$ at $4cm^{-1}$ resolution.

The infrared technique may not be conclusive due to overlapping bands if all three polymorphs are simultaneously present (Table 4.1). Apart from broadness of inorganic adsorption bands, the other challenge of FT-IR technique is that sample preparation (grinding and pelleting) can convert vaterite and aragonite to the more stable form calcite (Kontoyannis and Vagenas, 2001). Raman spectroscopy yields complimentary information, similar to IR spectroscopy. So, FT-RS may also prove useful for the characterization of $CaCO_3$ samples. Raman spectroscopy uses a monochromatic laser at $10^{11}$ nm wavelength and the photons excite the sample whereas IR spectroscopy utilizes infrared radiation to determine the structure of various organic and inorganic compounds. Both IR and Raman spectroscopy are important in the identification of simple molecules as the exclusion rule indicates that if the molecule has a centre of inversion, then it cannot be both Raman and IR active, making both techniques extremely complementary (Shriver *et al.*, 1994).

In the case of mixture of different polymorphs of $CaCO_3$, the characteristic Raman peaks at 750 $cm^{-1}$ for vaterite, 711 $cm^{-1}$ for calcite and $705cm^{-1}$ for aragonite may overlap with each other and may not prove to be conclusive. Also, due to extensive overlap between the three polymorphs, the stronger and more highly resolved bands at 1085 $cm^{-1}$ are unable to be used in the case of the mixed systems. Hence, peaks at all of the vibrational modes are used to distinguish and characterize the sample that contains different polymorphs of $CaCO_3$ (Dickinson and McGrath, 2001).

**Table 4.1** Vibrational frequencies ($cm^{-1}$) of $CaCO_3$ polymorphs.

| **Modes** | **Aragonite** | | **Vaterite** | | **Calcite** | |
|---|---|---|---|---|---|---|
| | **IR** [¶] | **Raman** [#] | **IR** [†] | **Raman** [#] | **IR** | **Raman** [‡] |
| $\nu_1$ | 1085 | 1087 | 1085<br>1070 | 1090<br>1066 | | 1086 |
| $\nu_2$ | 875<br>870 | | 870 | 845 | 876 [¶] | |
| $\nu_3$ | 1490 | 1466 [(¶)] | 1490<br>1420 | 1466<br>1416 | 1444 | 1434 |
| $\nu_4$ | 712<br>699 | 703 | 750 | 752<br>713 | 724 | 712 |
| **Lattice Modes** | | 287 [*]<br>276<br>263<br>250<br>217<br>193<br>183<br>155 | | 325<br>300<br>267 | | 284 |

* Couture, 1947; # Griffith, 1969; [†] Santo and Matsuda, 1969; [¶] Huang and Kerr, 1960; [‡] Gabrielli *et al.,* 2000

### 4.3.4 X-Ray Diffraction (XRD):

The mineral phases present in the $CaCO_3$ samples was also determined with Rigaku X-ray diffractometer, using Cu Kα radiation. Also, from the full width at half maximum (FWHM) of the peaks the particle size of the $CaCO_3$ samples was estimated using Scherrer's formula (Pathak *et al.*, 2003) given below:

Particle Size d (Å) = $K \times \lambda / \Delta 2\theta \cos\theta$ …….(4.1)

Where K = order of the refection, λ = 1.54 Å and θ = angle of diffraction.

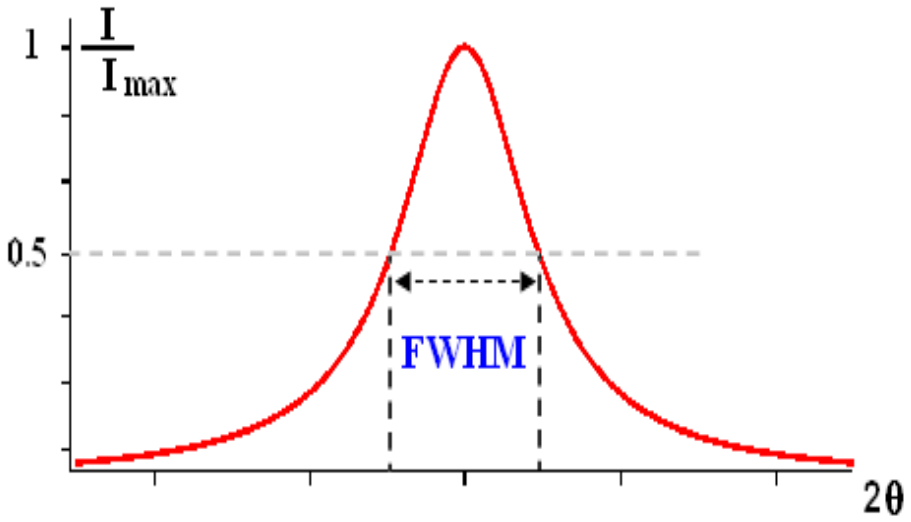


**Figure 4.2** Calculation of particle size by full width at half maximum (FWHM) of XRD peaks.

### 4.4 Macroscopic studies

#### 4.4.1 Arsenic quantitative analysis via Atomic Fluorescence Spectrometry (AFS)

AFS arsenic quantification used the following method: To 9 mL of each sample, 6 mL of HCl, 4.5 mL of milliQ water and 0.4mL of KI are added and allowed to react for 30 minutes. Standards with concentration of 0, 5, 10, 20 and 40 μg/L As(V) are separately prepared and then the samples and standards are analyzed by AFS(Millennium Excalibur, PSA Analytical Ltd.). The mean detection limits (MDL) was 0.74 μg/L, and 90.15% of arsenate was recovered when 48.75 μg/L of arsenate was spiked and 79.75% was recovered in the case of arsenite. The analyses were performed in triplicate. The coefficient of variation of the three replicates was 0.369 and the standard error was 0.095.

#### 4.4.2 Adsorption isotherms

Stock solutions of 2 mM of As(III) and As(V) were prepared by dissolving fresh reagent grade salts in deionized water. A stock solution of 0.002 M $NaNO_3$ was prepared to maintain the ionic strength of 0.01M in the system. Adsorption isotherms were produced by varying the As(III) /As(V) concentration. The solution pH was adjusted using 0.01M NaOH or HCl to the desired pH value. The procedure involved in the preparation of samples is described in Tables 4.2 and 4.3 respectively. The samples were reacted for 24 hours with continuous mixing using a rotary shaker. The supernatant solution was then filtered through 0.45μm membrane filter with a disposable syringe. For nano-sized $CaCO_3$, a 0.1μm membrane filter was used.

*Co-precipitation of As(III) and As(V) with $CaCO_3$.*

For these experiments, 0.04 g of Ca $(NO_3)_2.4H_2O$ was added to 5mL water followed by As(III). Different volumes of arsenic were added to obtain the desired concentration range. For the values refer to the Table 4.2 above. The pH was adjusted to 5.6 with the addition of 1 mL of $HNO_3$ and then 0.0265 g of $Na_2CO_3$ was added to precipitate $CaCO_3$. 5mL of $NaNO_3$ was added to maintain constant ionic strength for all samples. Approximately 1 mL of $HNO_3$ was added to adjust the pH to 7.5. The volume of the water was adjusted to maintain the 25 mL total volume. These samples were then reacted for 24 hours and then centrifuged. The supernatant obtained was filtered and

**Table 4.2** Preparation of samples with different concentrations of As(III) added to $CaCO_3$.

| **Weight of $CaCO_3$ ( g )** | **Volume of $NaNO_3$ ( mL )** | **Concentration of As(III) ( µM )** | **Volume of As(III) ( mL )** | **Volume of $H_2O$ added ( mL )** | **Total Volume ( mL )** |
|---|---|---|---|---|---|
| 0.025 | 5 | 0 | 0 | 25 | 25 |
| | | 1 | 0.013 | 24.99 | |
| | | 5 | 0.063 | 24.93 | |
| | | 25 | 0.31 | 24.69 | |
| | | 100 | 1.25 | 23.75 | |
| | | 250 | 3.13 | 21.87 | |
| | | 500 | 6.25 | 18.75 | |
| | | 1000 | 12.50 | 12.50 | |

**Table 4.3** Preparation of samples with different concentrations of As(V) added to $CaCO_3$.

| **Weight of $CaCO_3$ ( g )** | **Volume of $NaNO_3$ ( mL )** | **Concentration of As(V) ( µM )** | **Volume of As(V) ( mL )** | **Volume of $H_2O$ added ( mL )** | **Total Volume ( mL )** |
|---|---|---|---|---|---|
| 0.025 | 5 | 0 | 0 | 25 | 25 |
| | | 1 | 0.013 | 24.99 | |
| | | 5 | 0.063 | 24.93 | |
| | | 25 | 0.31 | 24.69 | |
| | | 100 | 1.25 | 23.75 | |
| | | 250 | 3.13 | 21.87 | |
| | | 500 | 6.25 | 18.75 | |
| | | 1000 | 12.50 | 12.50 | |

15mL was collected and stored for later analysis via AFS. A similar procedure was followed for the co-precipitation of As (V).

### 4.4.2 Adsorption envelopes

The effect of pH on the adsorption of arsenate and arsenite on $CaCO_3$ was evaluated within the pH range of 7.5-9.5 at fixed 500 μM arsenic concentration. 0.02 g of $CaCO_3$ was weighed and added to a 200 mL volumetric flask. From the As stock solution, 7.5 mL was pipetted to the volumetric flask along with 2 mL of 1M $NaNO_3$ to obtain an ionic strength of 0.01M. The solution was transferred to a beaker and constantly stirred with a magnetic stir bar. The pH was adjusted stepwise by addition of 0.01M $HNO_3$ using a Metrohm 716 titrator, and 1mL of suspension was collected for each pH value and transferred into 15 mL centrifuge tubes. These samples were spun for 24 hours on a rotary shaker. The sorption of arsenate on $CaCO_3$ was determined via AFS after filtration of these reacted samples.

### 4.4.3 Kinetics experiment (Adsorption as function of time)

Pre-equilibration of $CaCO_3$ (1g/L) in 0.01 M $NaNO_3$ solution at desired pH was done using a pH stat titrator and 0.01M $HNO_3$ to stabilize the suspension pH constant. The titrator maintained suspension pH at 9.5± 0.05 throughout the experiment. After this pre-equilibration period, the pH electrode was recalibrated and the desired arsenate or arsenite concentration was spiked into the vessel. Then, 1 mL of sample is collected when pH returns to the set point and then additional samples were drawn at regular intervals of time. Time was recorded with a stop watch. The kinetic study was carried out over a period of 168 hours. This experiment was run with the reaction vessel open to the atmosphere throughout the reaction.

### 4.4.4 Electrophoretic mobility:

The electrophoretic mobility of $CaCO_3$ at 500 μM As(III) and As(V) concentrations as a function of pH was measured to determine the point of zero charge (PZC), which is the unique pH at which the net surface charge is zero. The point of zero charge of our $CaCO_3$ solids was determined via electrophoretic mobility (EM) using a Zeta Sizer Nano-ZS instrument. The pH was adjusted between 5 and 12 by dropwise addition of either 0.1M HCl or NaOH with the instrument's pH titrator. The EM experiments were performed in triplicate.

# 5.0 RESULTS

## 5.1 Characterization of $CaCO_3$

### 5.1.1 BET Analysis:

The external surface area of the bulk $CaCO_3$ was measured by Multi point BET (with five points) $N_2$ method and found out to be 4.68 $m^2/g$. For nano $CaCO_3$ synthesized using methods 1 (*in situ* deposition with PEG) and 2 (interfacial reaction in w/o emulsion), resulted in an external surface area of 20.41$m^2/g$ and 14.59 $m^2/g$, respectively.

### 5.1.2 $CaCO_3$ particle size distribution:

The bulk $CaCO_3$ particles ranged from 0.3-100 μm in size, with an average particle size of 19.9 μm. This is in contrast with the nano-sized precipitates, which had particle size ranging from 0.09-20 μm with the majority of the particles less than 100 nm (*in situ* deposition method) versus 0.06-37 μm with most of the particles less than 200 nm (interfacial method).

### 5.1.3 FT-RS Spectroscopy

The peaks at 1087, 703, 223 and 155 $cm^{-1}$ indicate the presence of aragonite. The peak at 287 $cm^{-1}$ indicates the presence of calcite whereas the peaks at 300 and 325 $cm^{-1}$ indicate the presence of vaterite. FT-RS concludes that the bulk $CaCO_3$ is comprised of only calcite whereas nano $CaCO_3$ (*in situ* deposition method) is a mixture of calcite and aragonite and nano (interfacial method) is a mixture of calcite and vaterite.

### 5.1.4 FT-IR Spectroscopy

The solid line in Figure 5.3 represents the peaks of bulk $CaCO_3$ and the dotted lines indicate that of nano $CaCO_3$ prepared with the two different methods. The peaks at 872, 1444 and 724 $cm^{-1}$ indicate that the bulk $CaCO_3$ is made up of calcite whereas the peaks at 1449, 1083, 875, 853,712 and 701$cm^{-1}$ indicate that PEG based $CaCO_3$ is a mixture of calcite and aragonite. The interfacially-produced $CaCO_3$ showed peaks at 1087, 872, 850, 745, 721$cm^{-1}$ indicating that it is a mixture of vaterite and calcite. Additionally, FT-IR spectroscopy of PEG was performed to determine if PEG is present in nano $CaCO_3$ (*in situ* deposition method) and has affected the $CaCO_3$ structure (See Figure 5.4). The solid line represents the peaks of PEG and the dotted line indicates that of nano $CaCO_3$

(*in situ* deposition method). FT-IR spectroscopy of PEG confirmed the peaks from 1050-1150 $cm^{-1}$ as stretching of ether (C-O-C) groups with the maximum peak at 1150 $cm^{-1}$. Also, characteristic alkyl ($R\text{-}CH_2$) stretching modes from $\nu$ = 2850-3000 $cm^{-1}$ and hydroxyl group contribution at $\nu$ = 3200-3600 $cm^{-1}$ were observed (Mansur *et al.*, 2004). The characteristic peaks of PEG were not found to be present in the $CaCO_3$ sample. The solid line (in Figure 5.5) represents the peaks of Tween 80 and the dotted line indicates that of the nano $CaCO_3$ produced using this surfactant. The absorption band at 951 $cm^{-1}$ indicates the presence of polyoxyethylene ($\nu_s$ C-O-C). The band at 1240 $cm^{-1}$ confirms the presence of ester and the bands at 1447 $cm^{-1}$ and 1345 $cm^{-1}$ are due to the presence of alkyl groups respectively (Zhang *et al.*, 2006). These characteristic bands were absent in our nano $CaCO_3$ prepared using Tween 80, therefore no detectable contamination was present.

### **5.1.5**. **X-Ray Diffraction:**

The peaks at 2θ values of 30º, 40º, 47º and 49º indicate that the bulk $CaCO_3$ is comprised of calcite. The PEG based nano $CaCO_3$ contains mixture of aragonite and calcite: peaks at 2θ values of 27º and 28º indicate aragonite whereas 2θ values of 30º indicate calcite. In the surfactant-based interfacial method, the strong peak at 2θ = 30º shows the presence of calcite, and the peaks at 2θ values of 24º, 44º, 50º and 55º indicate vaterite. This result shows that while bulk $CaCO_3$ is composed of calcite, PEG based nano $CaCO_3$ is a mixture of aragonite and calcite and surfactant based nano $CaCO_3$ contains calcite and vaterite.

XRD was also used to determine the particle size of the bulk and nano $CaCO_3$. The nano-size of $CaCO_3$ particles was confirmed by XRD scans with Scherrer's formula. The particle sizes of the bulk $CaCO_3$ was found to be 3.47 μm whereas the particle size of the nano $CaCO_3$ (method 1 and 2) were found to be 31.33 nm and 37.68 nm respectively. The particle size distribution of nano $CaCO_3$ was measured with Scherrer's formula and it was ± 5% of the particle sizes observed in particle size analysis.

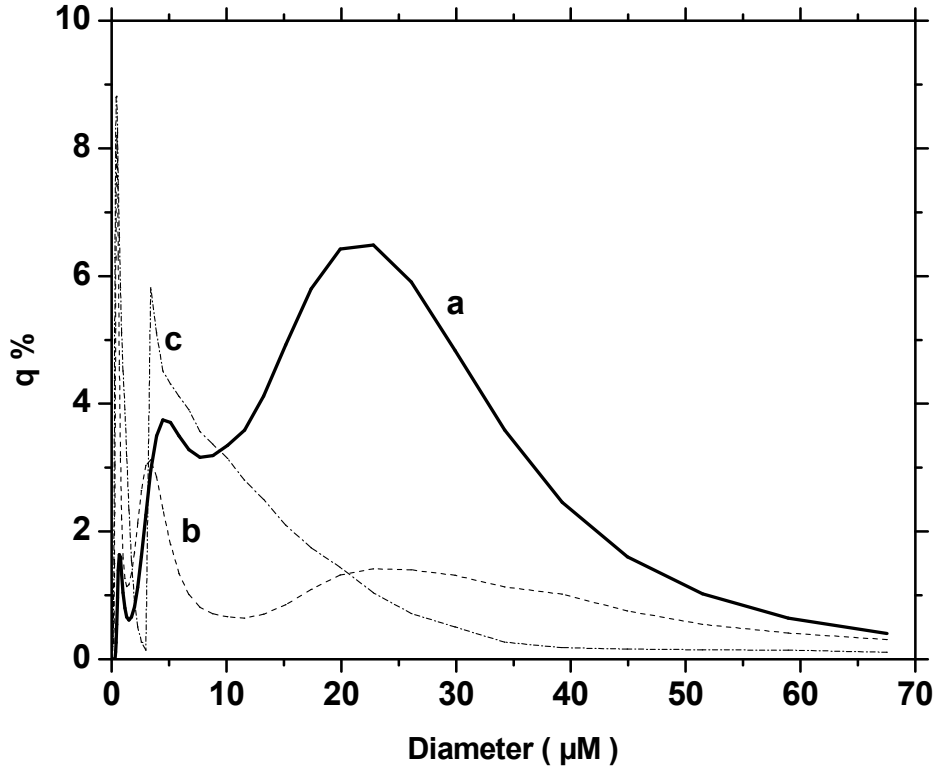


**Figure 5.1** Particle size distribution of **a)** bulk **b)** nano $CaCO_3$ (*in situ* deposition method) and **c)** nano $CaCO_3$ (interfacial method).

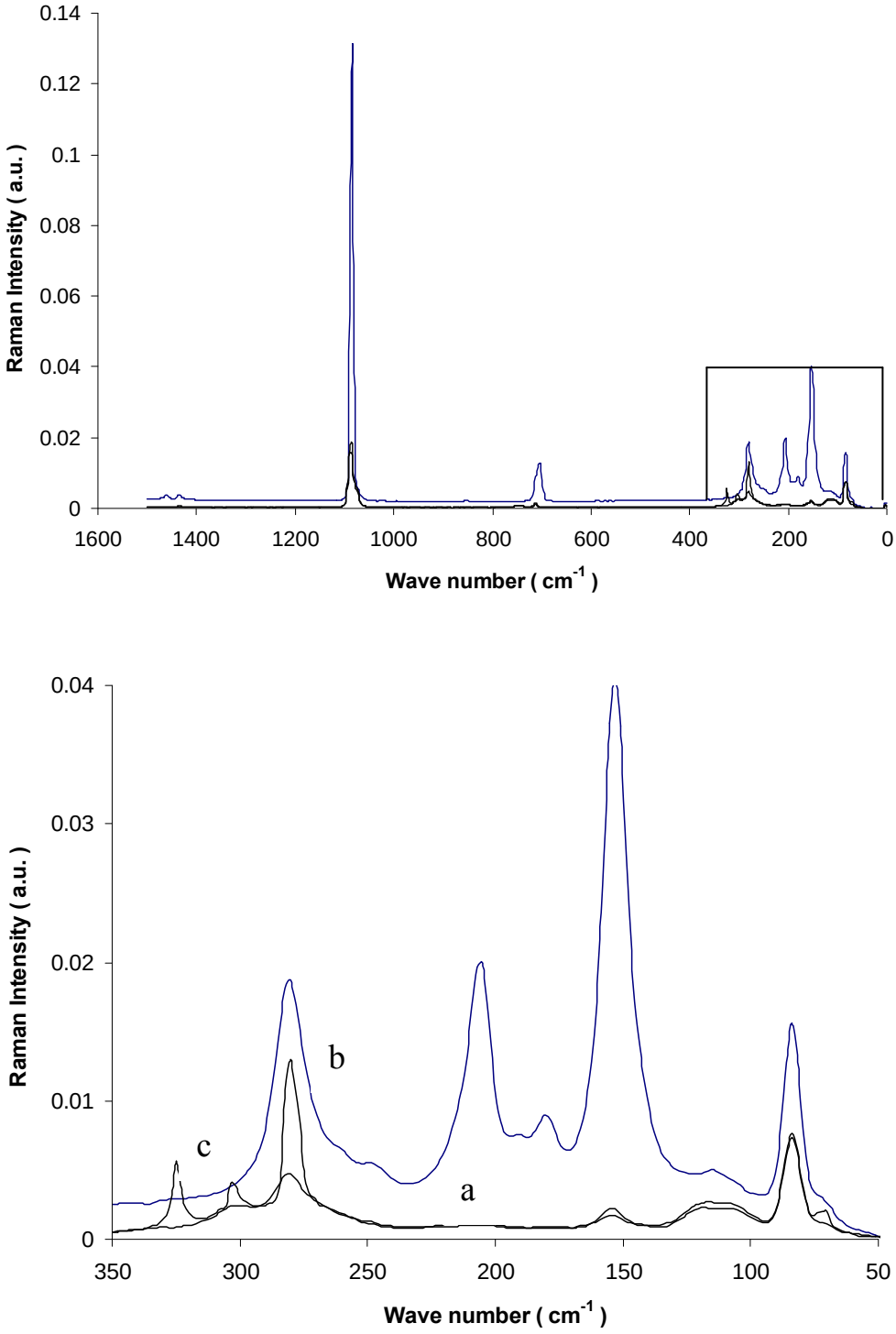


**Figure 5.2** FT-RS spectrum of **a)** bulk and **b)** nano (*in situ* deposition method) and c) nano (interfacial method) $CaCO_3$.

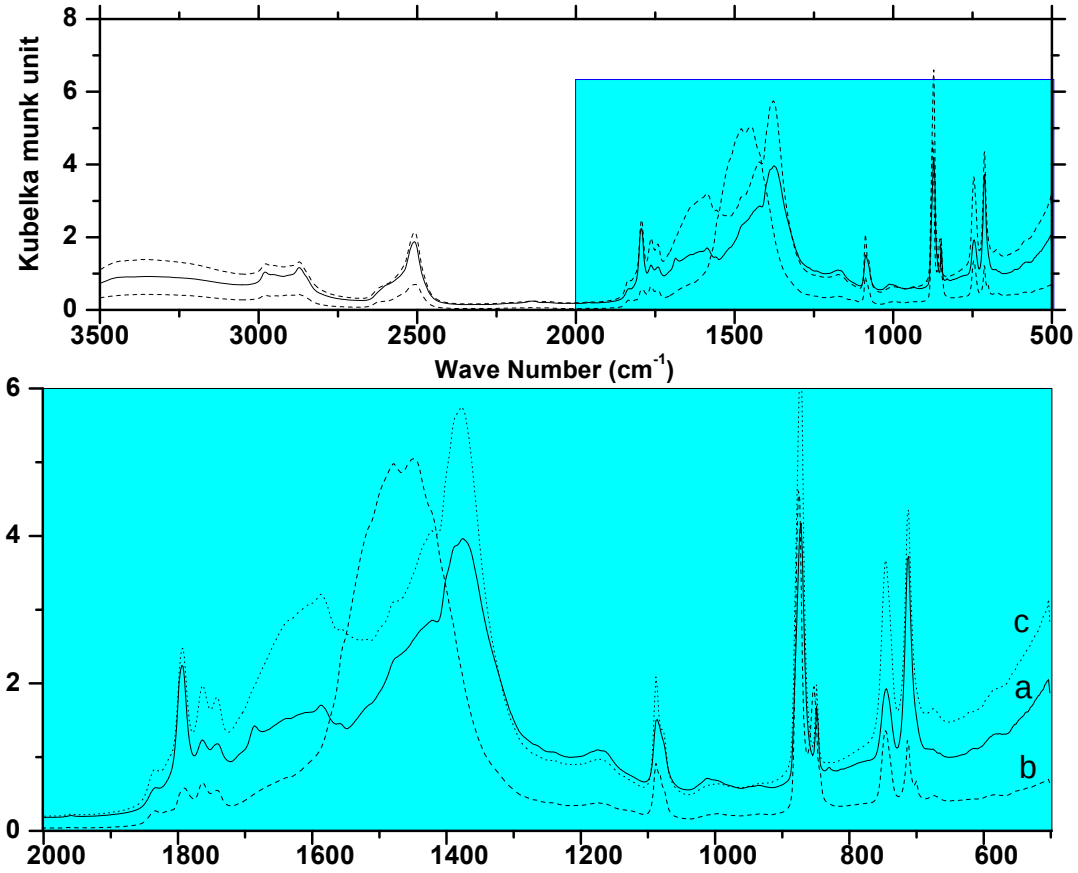


**Figure 5.3** FT-IR spectrum of **a)** bulk **b)** nano (*in situ* deposition method) and **c)** nano (interfacial method) $CaCO_3$. The lower graph is an expansion of the shaded region in the upper graph.

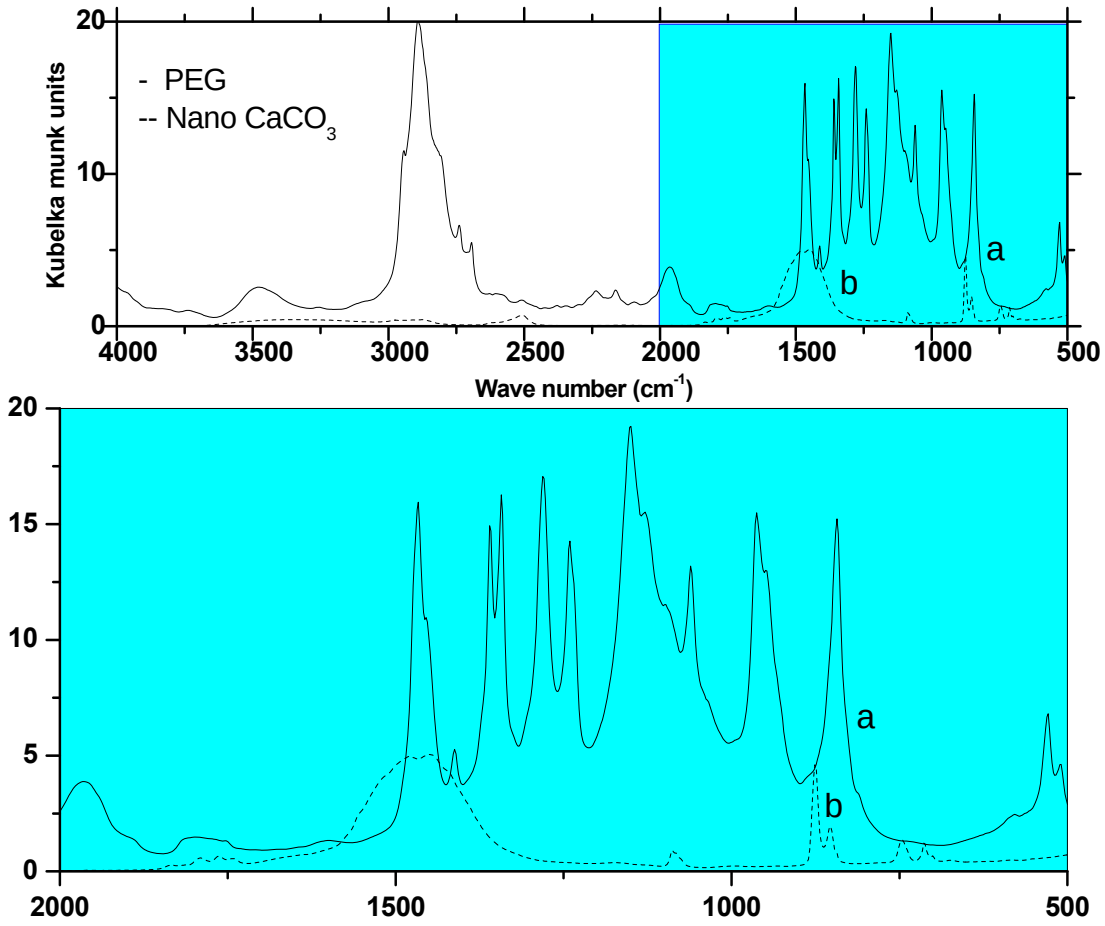


**Figure 5.4** FT-IR spectrum of **a)** PEG and **b)** nano $CaCO_3$ (*in situ* deposition method). The lower graph is an expansion of the shaded region in the upper graph.

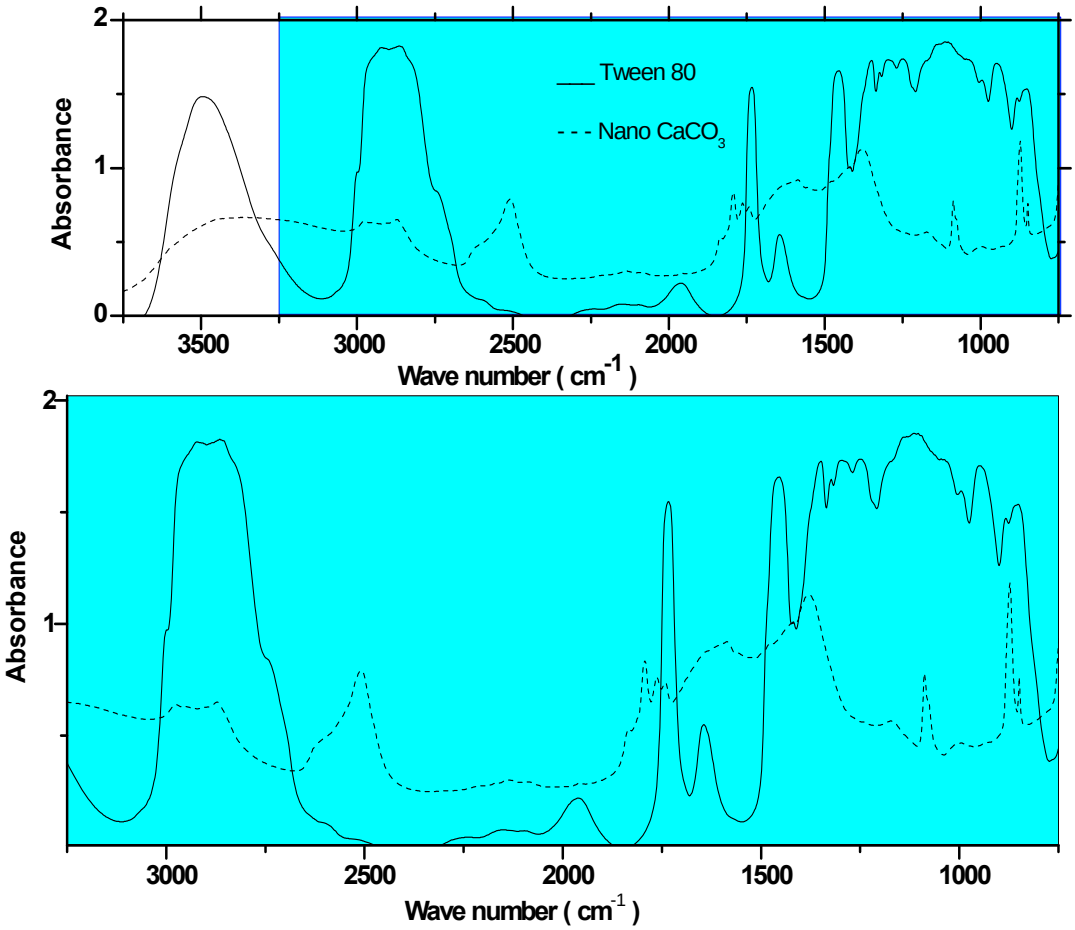


**Figure 5.5** FT-IR spectrum of **a)** Tween 80 and **b)** nano $CaCO_3$ (interfacial method). The lower graph is an expansion of the shaded region in the upper graph.

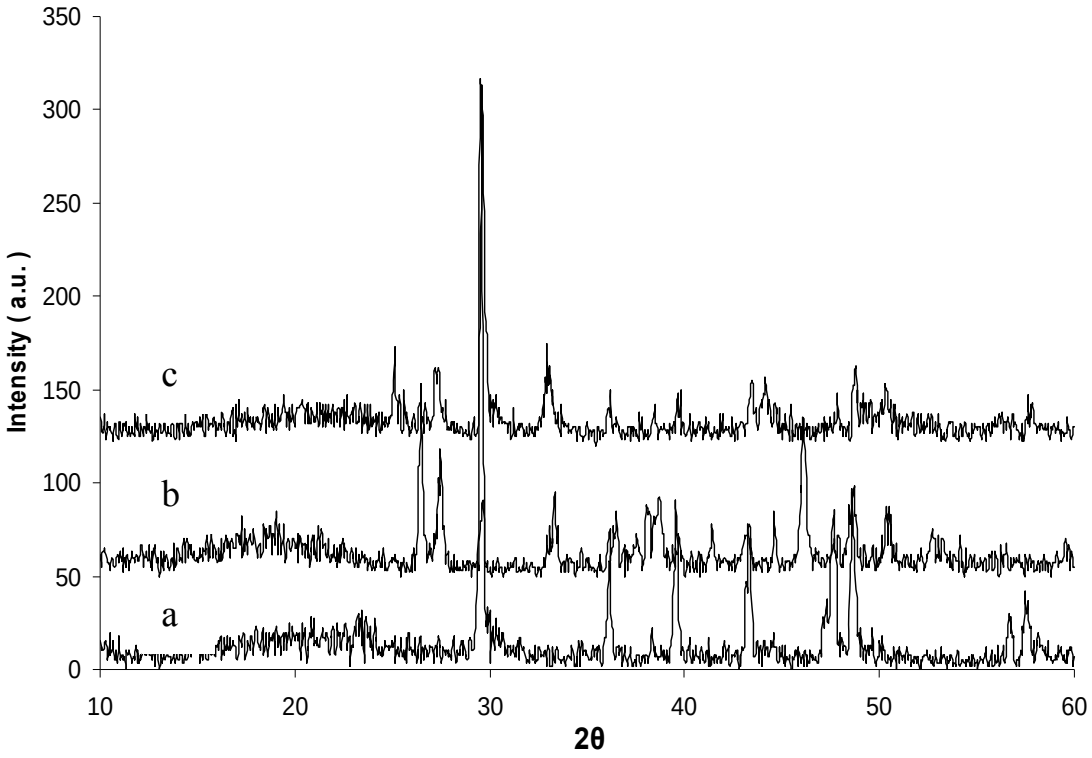


**Figure 5.6** XRD peaks of **a)** bulk $CaCO_3$ **b)** nano (*in situ* deposition) and **c)** nano (Interfacial method) $CaCO_3$.

**Table 5.1** Particle size calculation from the FWHM of XRD peaks.

| $CaCO_3$ | d value | Particle size (nm) |
|---|---|---|
| Nano (*in situ* deposition method) | 3.37<br>3.02 | 31 |
| Nano (interfacial method) | 3.0<br>1.87 | 37 |
| Bulk | 3.02 | 3473 |

## 5.2 Macroscopic studies:

The principal objective of my research was to assess the overall reactivity of arsenic species with $CaCO_3$. This can be accomplished by three different ways i) running adsorption isotherms (varying As concentration), ii) pH envelopes (varying pH at a fixed concentration) and iii) kinetic experiments (varying reaction time). Arsenic concentration in solution was monitored with Atomic Absorption Spectroscopy (AAS) or Atomic Fluorescence Spectroscopy (AFS), depending upon concentration. Arsenic adsorption studies are purely descriptions of macroscopic data and they do not definitively prove a reaction mechanism. Instead, mechanisms should ideally be ascertained from direct molecular investigations, i.e., with the aid of spectroscopic techniques.

### 5.2.1 Adsorption isotherm experiments

A comparison of arsenic adsorption and co-precipitation as a function of [As] at pH 7.5 was the first experiment performed.

#### 5.2.1.1 Adsorption isotherm at 0.01 M ionic strength and pH 7.5 with either co-precipitation or adsorption of As(III) /As(V).

It can be inferred that there is a significant increase in As(V) removal by co-precipitation whereas a smaller difference was observed in As(III) adsorption with respect to co-precipitation (Figs. 5.7 and 5.8). At pH 7.5, the adsorption of As(V) on bulk $CaCO_3$ ($q_{max}$ = 3.79μmol/$m^2$) was lower than As(III) adsorption ($q_{max}$ = 4.38 μmol/$m^2$) whereas co-precipitation results at pH 7.5 indicated higher $q_{max}$ values of 42.19 μmol/$m^2$ for As(V) compared to 18.5 μmol/$m^2$ for As(III) co-precipitation with $CaCO_3$.

Next, adsorption of arsenate and arsenite on to bulk and nano sized $CaCO_3$ were performed over a range of pH (7.5-10). In groundwater aquifers, the pH should lie within this range and so it was chosen for the experimental design. (Fig. 5.9-5.14)

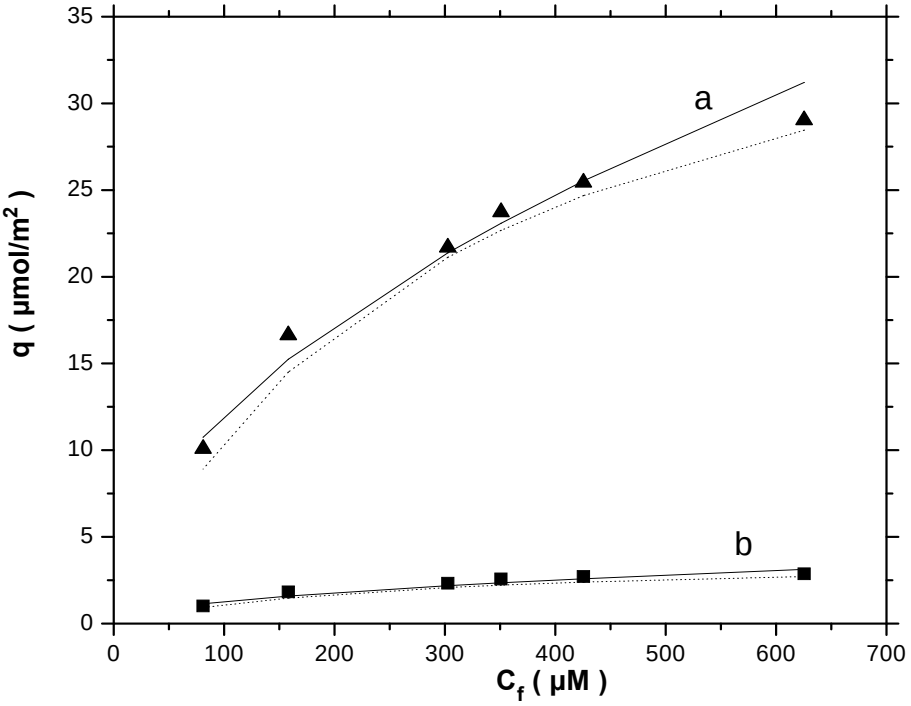


**Figure 5.7** **a)** Co-precipitation of As(V) and **b)** Adsorption of As(V) with bulk $CaCO_3$ at pH 7.5. Solid lines represent Freundlich fitting and broken lines indicate Langmuir fitting.

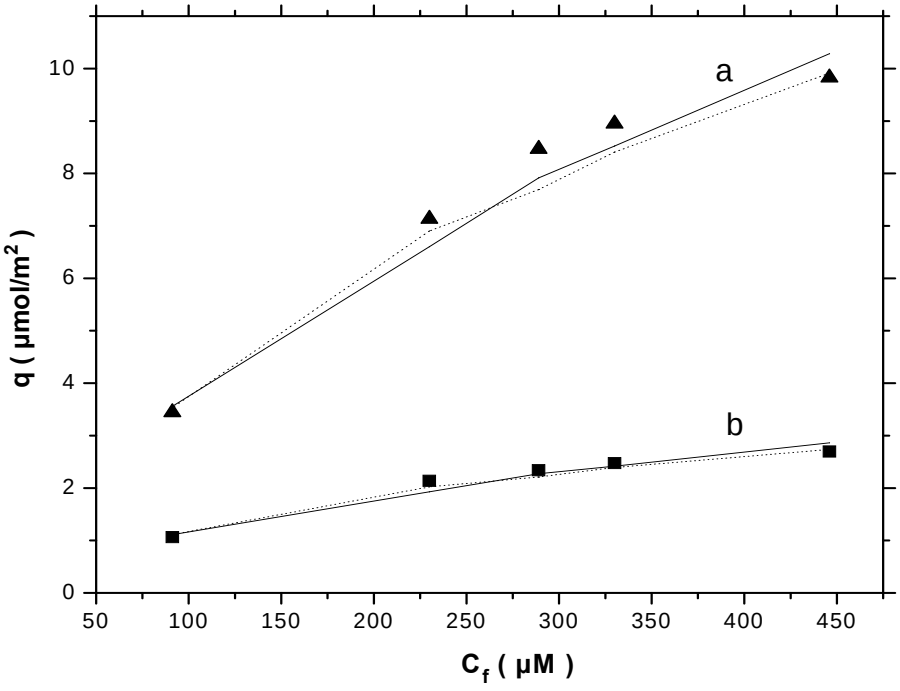


**Figure 5.8** **a)** Co-precipitation of As(III) and **b)** Adsorption of As(III) with bulk $CaCO_3$ at pH 7.5.Solid lines represent Freundlich fitting and broken lines indicate Langmuir fitting.

**Table 5.2** Adsorption isotherm parameters for arsenic i) adsorption and ii) co-precipitation on bulk $CaCO_3$ at pH 7.5.

| As | Adsorption | | | Co-precipitation | | |
|---|---|---|---|---|---|---|
| | Linear regression parameter ($R^2$) | | *$q_{max}$ (µmol/$m^2$) | Linear regression parameter ($R^2$) | | *$q_{max}$ (µmol/$m^2$) |
| | *L | *F | | *L | *F | |
| As(V) | 0.99 | 0.96 | 3.79 | 0.99 | 0.98 | 4.38 |
| As (III) | 0.98 | 0.97 | 42.19 | 0.97 | 0.96 | 18.5 |

*Note: $\mathbf{q_{max}}$ – Maximum adsorption capacity, **L** – Langmuir, **F** – Freundlich

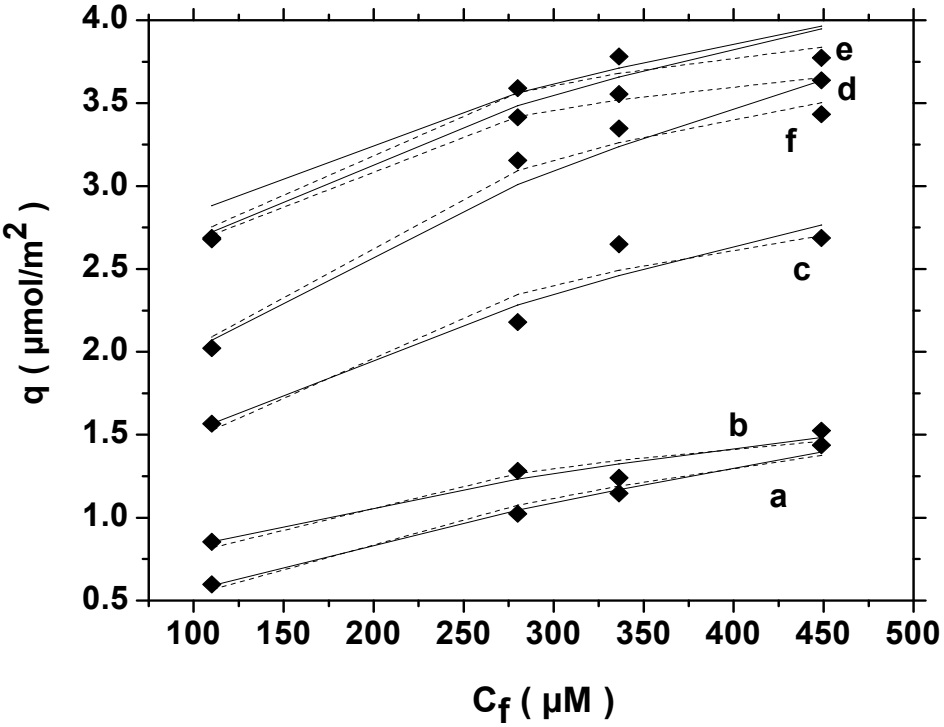


**Figure 5.9** Adsorption of As(V) on bulk $CaCO_3$ at pH **a)** 7.5 **b)** 8.0 **c)** 8.5 **d)** 9.0 **e)** 9.5 **f)** 10.0

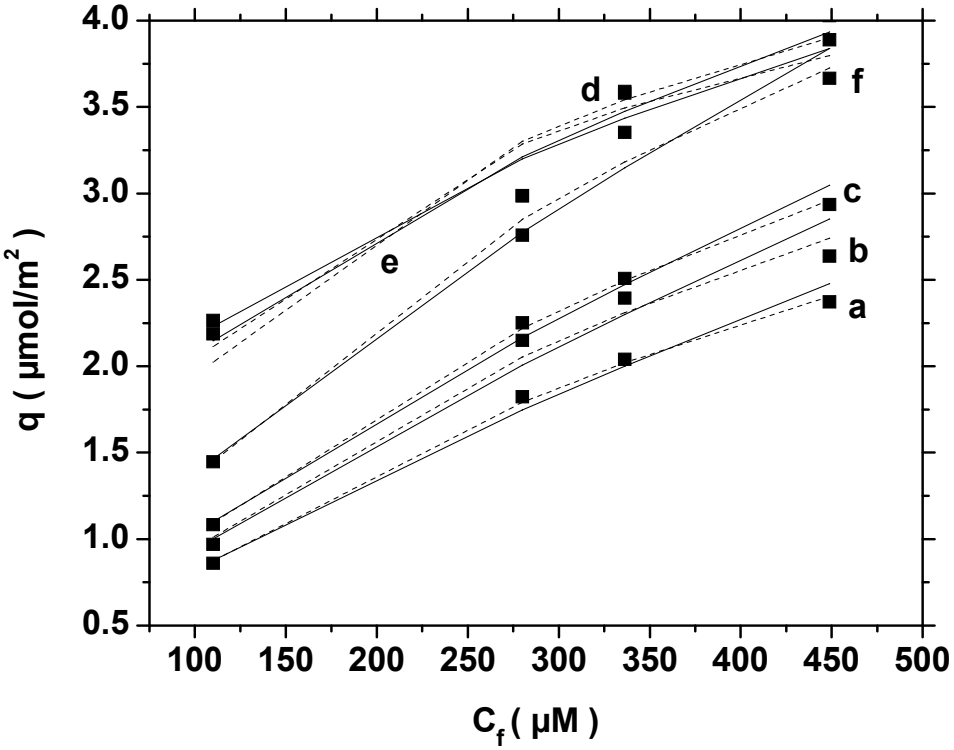


**Figure 5.10** Adsorption of As(III) on bulk $CaCO_3$ at pH **a)** 7.5 **b)** 8.0 **c)** 8.5 **d)** 9.0 **e)** 9.5 **f)** 10.0.

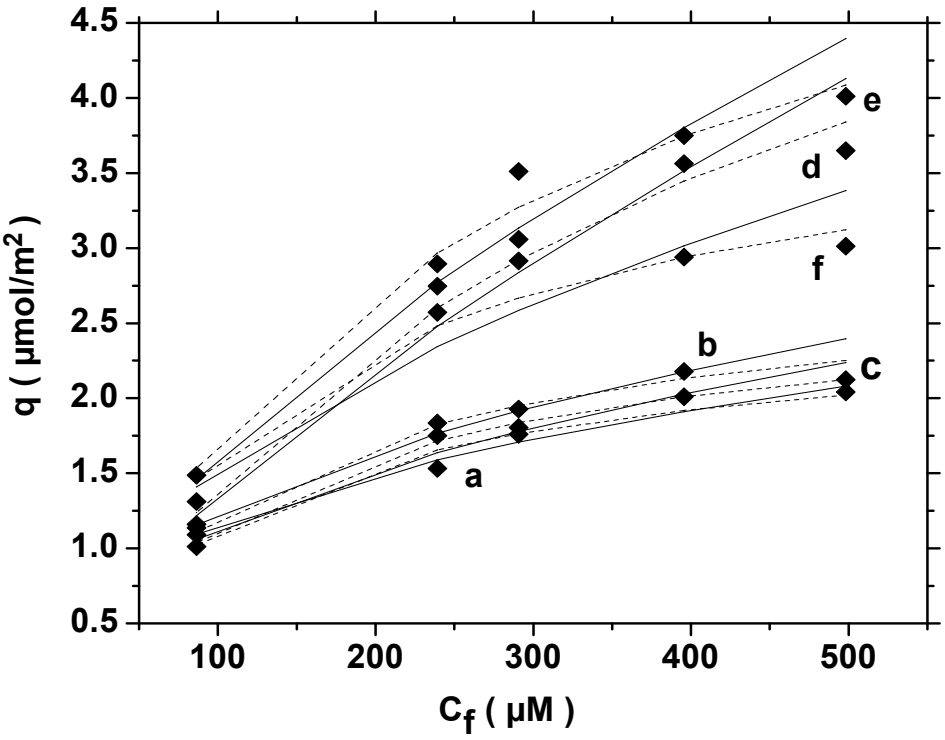


**Figure 5.11** Adsorption of As(V) on nano $CaCO_3$ (*in situ* deposition method) at pH **a)** 7.5 **b)** 8.0 **c)** 8.5 **d)** 9.0 **e)** 9.5 **f)** 10.0

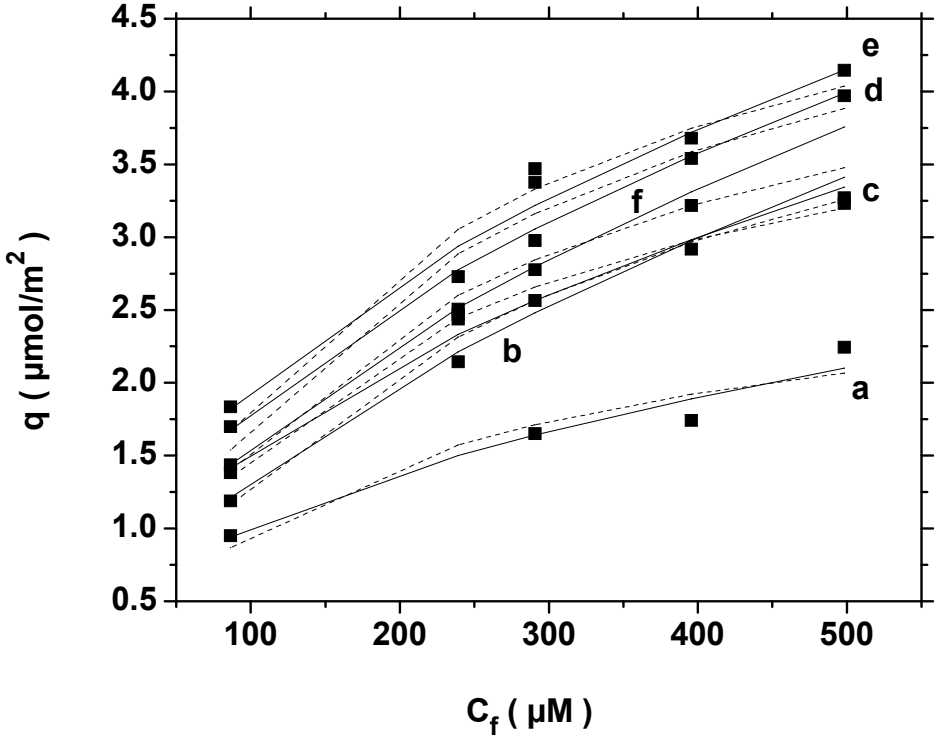


**Figure 5.12** Adsorption of As(III) on nano $CaCO_3$ (*in situ* deposition method) at pH **a)** 7.5 **b)** 8.0 **c)** 8.5 **d)** 9.0 **e)** 9.5 **f)** 10.0

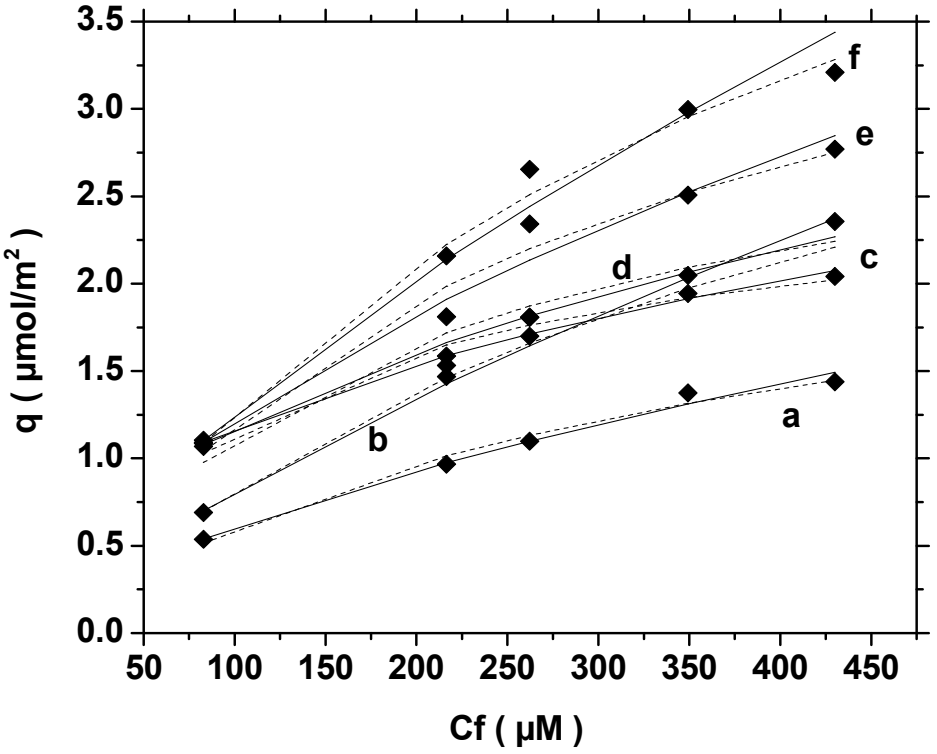


**Figure 5.13** Adsorption of As(V) on nano $CaCO_3$ (interfacial method) at pH **a)** 7.5 **b)** 8.0 **c)** 8.5 **d)** 9.0 **e)** 9.5 **f)** 10.0

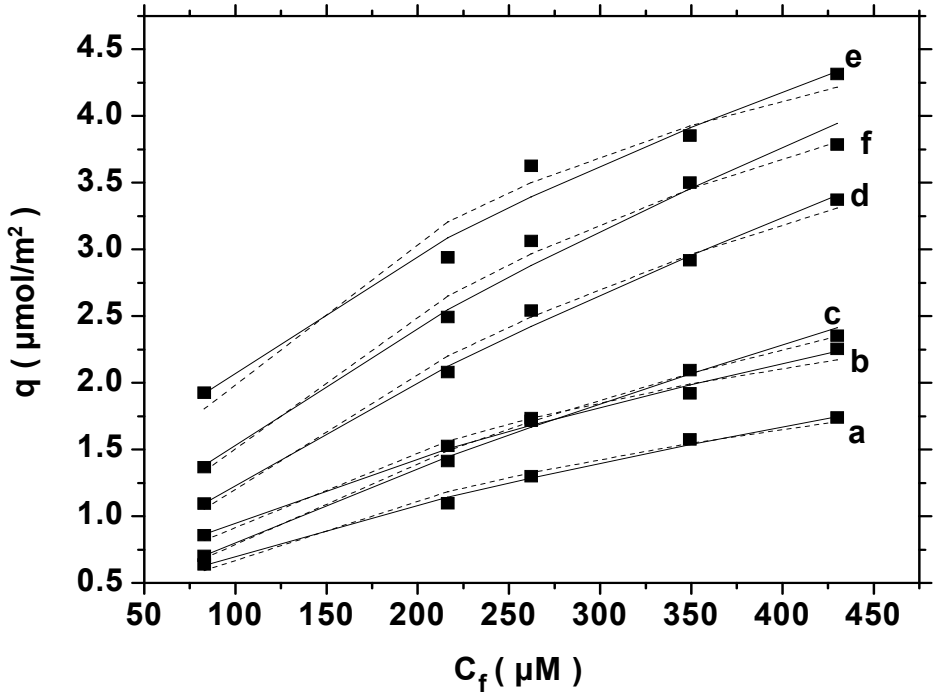


**Figure 5.14** Adsorption of As(III) on nano $CaCO_3$ (interfacial method) at pH **a)** 7.5 **b)** 8.0 **c)** 8.5 **d)** 9.0 **e)** 9.5 **f)** 10.0

**Table 5.3** Adsorption isotherm parameters for As(V) adsorption on i) bulk and ii) nano $CaCO_3$ at different pH.

| pH | Bulk $CaCO_3$ | | | Nano $CaCO_3$ | | | | | |
|---|---|---|---|---|---|---|---|---|---|
| | | | | From method 1 | | | From method 2 | | |
| | Linear regression parameter ($R^2$) | | *$q_{max}$ ($\mu mol/m^2$) | Linear regression parameter ($R^2$) | | *$q_{max}$ ($\mu mol/m^2$) | Linear regression parameter ($R^2$) | | *$q_{max}$ ($\mu mol/m^2$) |
| | *L | *F | | *L | *F | | *L | *F | |
| 7.5 | 0.94 | 0.99 | 2.58 | 0.98 | 0.97 | 2.87 | 0.97 | 0.99 | 2.54 |
| 8.0 | 0.95 | 0.96 | 1.96 | 0.98 | 0.99 | 2.54 | 0.98 | 0.97 | 2.62 |
| 8.5 | 0.97 | 0.96 | 3.60 | 0.99 | 0.95 | 2.71 | 0.98 | 0.99 | 3.24 |
| 9.0 | 0.99 | 0.98 | 4.13 | 0.94 | 0.96 | 4.85 | 0.95 | 0.98 | 4.56 |
| 9.5 | 0.99 | 0.95 | 4.39 | 0.98 | 0.97 | 5.26 | 0.95 | 0.98 | 4.51 |
| 10.0 | 0.99 | 0.96 | 4.48 | 0.97 | 0.92 | 4.90 | 0.97 | 0.98 | 6.34 |

**Table 5.4** Adsorption isotherm parameters for As(III) adsorption on i) bulk and ii) nano $CaCO_3$ at different pH.

| pH | Bulk $CaCO_3$ | | | Nano $CaCO_3$ | | | | | |
|---|---|---|---|---|---|---|---|---|---|
| | | | | From method 1 | | | From method 2 | | |
| | Linear regression parameter ($R^2$) | | *$q_{max}$ ($\mu mol/m^2$) | Linear regression parameter ($R^2$) | | *$q_{max}$ ($\mu mol/m^2$) | Linear regression parameter ($R^2$) | | *$q_{max}$ ($\mu mol/m^2$) |
| | *L | *F | | *L | *F | | *L | *F | |
| 7.5 | 0.99 | 0.99 | 2.66 | 0.92 | 0.97 | 2.91 | 0.95 | 0.99 | 3.09 |
| 8.0 | 0.93 | 0.98 | 3.58 | 0.96 | 0.98 | 5.04 | 0.96 | 0.99 | 5.13 |
| 8.5 | 0.99 | 0.99 | 5.12 | 0.97 | 0.99 | 5.22 | 0.98 | 0.99 | 5.61 |
| 9.0 | 0.96 | 0.96 | 6.62 | 0.93 | 0.96 | 5.70 | 0.97 | 0.99 | 6.77 |
| 9.5 | 0.95 | 0.97 | 5.57 | 0.96 | 0.97 | 5.74 | 0.98 | 0.98 | 6.99 |
| 10.0 | 0.96 | 0.98 | 5.59 | 0.99 | 0.98 | 5.48 | 0.98 | 0.99 | 6.11 |

*Note: $\mathbf{q_{max}}$ – Maximum adsorption capacity, **L** – Langmuir, **F** – Freundlich

All adsorption data were fitted with Langmuir and Freundlich isotherm equations,

$q = q_{max} K_L C / 1 + K_L C$ ……..(5.2.1)

$q = K_F C^{1/n}$ ……..(5.2.2)

where $q_{max}$ (μmol/$m^2$) is the maximum adsorption capacity, $q$ (μmol/$m^2$) is the amount of adsorbed As, C (μM) is the equilibrium solute (As) concentration, $K_F$ and $n$ are the Freundlich constants, and $K_L$ is the Langmuir constant. Using the Langmuir equation (5.2.1), the surface-area based Langmuir parameter ($q_{max}$, μmol/$m^2$) has been calculated and is shown in tables 5.3 and 5.4. The maximum adsorption capacities of As(V) is smaller compared to As(III) on $CaCO_3$. The reduction in As(V) adsorption compared to that of As(III) at high pH values (>pH 8) is attributable to the electrostatic repulsion of the negatively charged As(V) species by the negatively charged surface sites. With respect to the effect of $CaCO_3$ size, both As(III) and As(V) had slightly higher affinities for nano-sized particles compared to the bulk as indicated by the larger surface area normalized $q_{max}$ values for nano-sized particles. The surface area normalized As(III) and As(V) adsorption capacities ($q_{max}$, μmol/$m^2$) were very similar for 100 and 200 nm $CaCO_3$ particles (nano1 and nano2), but each shows an increase in $q_{max}$ with increasing pH.

### 5.2.2. pH Envelope Experiments (Adsorption as a function of pH)

The graphs shown below (See Figs. 5.15-5.17) indicate that adsorption of arsenite decreases at pH above 9.0 and there is an increase in adsorption of arsenate on to $CaCO_3$ with increase in pH. Overall the sorption of arsenite is greater than arsenate in the pH range 7.5-9.5. At high pH values, lower adsorption of arsenate compared to arsenite is possibly due to an increased repulsion between more negatively charged arsenate species and negatively charged surface sites. The arsenite species possess less negative charge character when compared to arsenate species at same pH value and so they exhibit less repulsion.

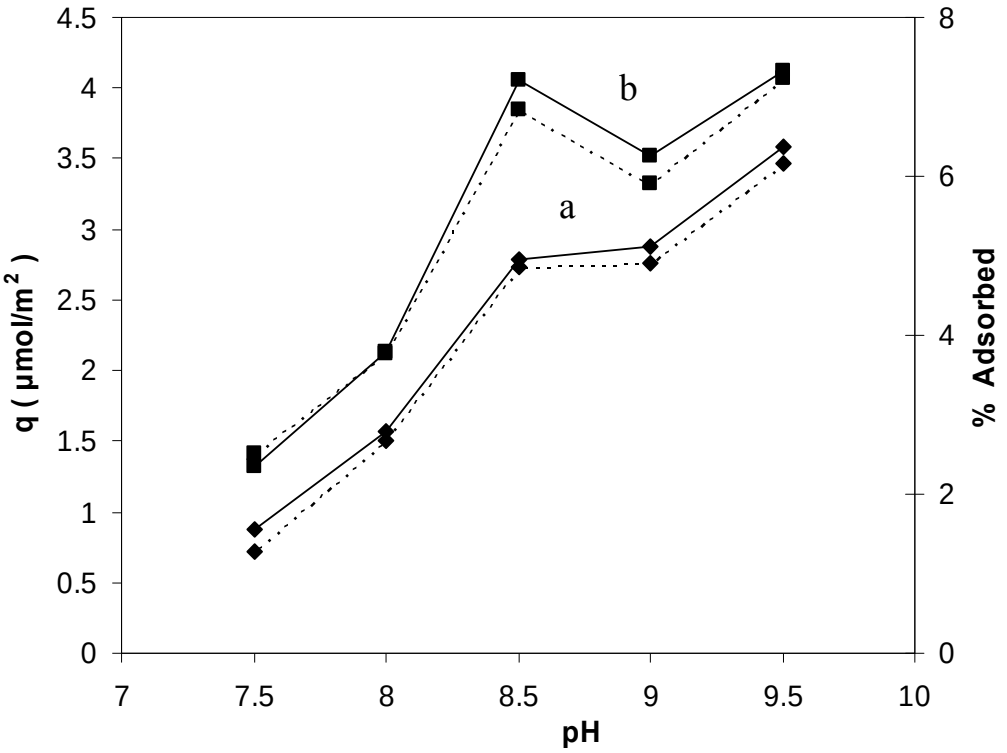


**Figure 5.15** **a)** Adsorption of As(V) and **b)** As(III) on bulk $CaCO_3$ as function of pH.

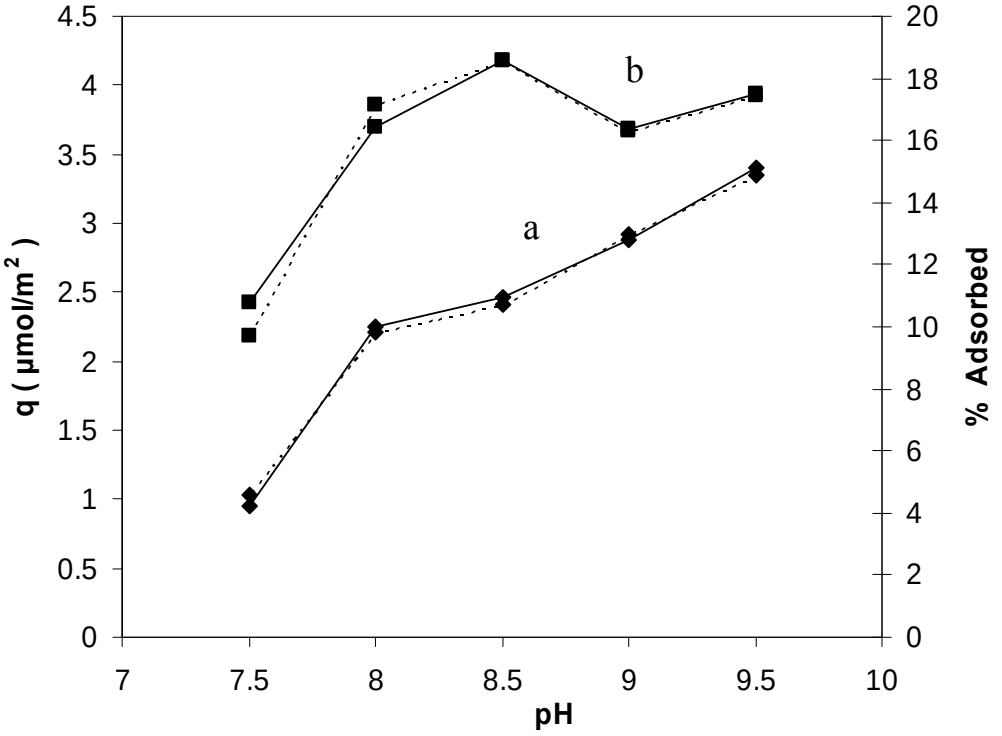


**Figure 5.16** **a)** Adsorption of As(V) **b)** As(III) on nano (*in situ* deposition method) $CaCO_3$ as function of pH.

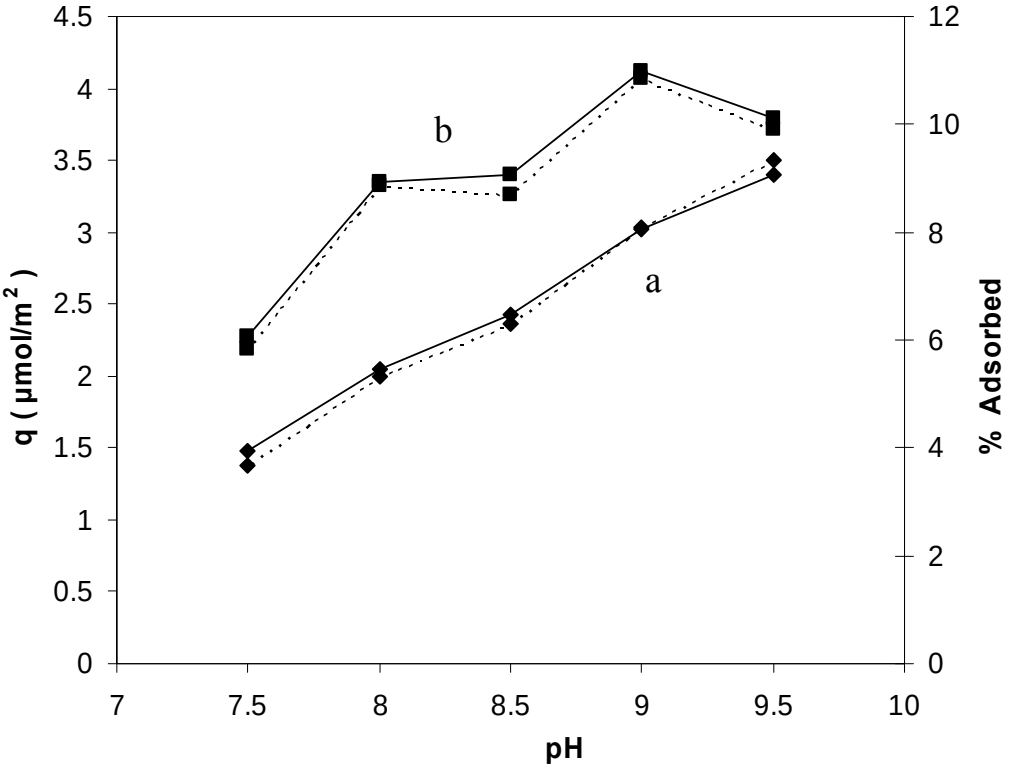


**Figure 5.17** **a)** Adsorption of As(V) **b)** As(III) on nano (interfacial method) $CaCO_3$ as function of pH.

Adsorption of arsenite on nano $CaCO_3$ by percent uptake is twice that of arsenite adsorbed onto the bulk $CaCO_3$. Also, the amount of arsenite sorbed on nano $CaCO_3$ produced by PEG-based *in situ* deposition is greater than the arsenate sorption on the interfacially-produced nano $CaCO_3$.

### 5.2.3. Electrophoretic mobility:

Zero EM indicates that there is no net movement of charged particle in response to an applied electric field which is the condition for point of zero charge (PZC) (Parks and De Bruyn, 1962). Anion or cation sorption on minerals depends on the mineral surface charge and the solution pH. Anion sorption is favored when the pH of the solution is below the PZC of the mineral surface whereas pH above the PZC favors cation sorption. The PZC of 1g/L bulk $CaCO_3$ solution in 0.01M $NaNO_3$ occurred at pH 8.87 whereas for nano $CaCO_3$ obtained using different methods it was found to be at pH values 8.30 and 7.92 respectively. (See table 5.5)

Nano $CaCO_3$ from method 1and 2 spiked with 500 μM arsenate solution exhibited PZC at pH 5.60 and 6.57, whereas spiking with the same concentration of arsenite resulted in PZC at 5.85 and 6.64 respectively. On the other hand, spiking of 500 μM arsenate solution on bulk $CaCO_3$ resulted in PZC at pH 7.55 and spiking similar arsenite concentration yielded PZC at pH 7.67. Adsorption of arsenic resulted in reduction of PZC by as much as 2.70 pH units for arsenate and slightly less reduction in the case of arsenite for nano $CaCO_3$. However, in the case of bulk $CaCO_3$ reduction, there was a reduction of PZC by 1.32 pH units for arsenate and 1.20 units for arsenite.

Adsorption of anionic arsenic species resulting in shifts in PZC to lower pH values are an indication of inner-sphere complex formation (Goldberg and Johnston, 2001). According to Table 5.4, As(V), ΔPZC descends in the order 2.70, 1.35 and 1.32 due to the interaction with nano (in situ deposition method), nano (interfacial method) and bulk $CaCO_3$ respectively. For As(III), ΔPZC descends in the order 2.45, 1.28 and 1.20 due to the interaction with nano (*in situ* deposition), nano (interfacial method) and bulk $CaCO_3$ respectively. From these experimental data, it can be inferred that both arsenate and arsenite interact more strongly with nano (*in situ* deposition method), than with nano (interfacial method) and have weakest reactivity with bulk $CaCO_3$. Such experimental observation also supports a hypothesis that as particles become smaller, their interactions with arsenic oxyanions becomes stronger, and hence the lower the PZC. This was the underlying motivation for my research to synthesize the $CaCO_3$ particles in nanometer size. Based on the PZC result, it is also evident that the nano-sized $CaCO_3$ synthesized by Method 1 is different in reactivity from that synthesized following Method 2. This PZC observation is also consistent with the particle size analysis, since average particle size is <120 nm and <200 nm for nano 1 and nano 2 respectively (see Figure 5.1). The arsenite and arsenate forms stronger inner-sphere complexes with nano $CaCO_3$ compared to bulk $CaCO_3$, and stronger with nano 1(calcite/aragonite mixture) than nano 2 (calcite/vaterite mixture).

**Table 5.5** Variation in the PZC value of $CaCO_3$ after spiking with 500 µM Arsenic

| **$CaCO_3$** | **Arsenic** | **PZC** | **∆PZC** |
|---|---|---|---|
| Bulk | 0 µM | 8.87 | _____ |
| | As (V) | 7.55 | 1.32 |
| | As (III) | 7.67 | 1.20 |
| Nano (*in situ* deposition method ) | 0 µM | 8.30 | _____ |
| | As (V) | 5.60 | 2.70 |
| | As (III) | 5.85 | 2.45 |
| Nano (interfacial method ) | 0 µM | 7.92 | _____ |
| | As (V) | 6.57 | 1.35 |
| | As (III) | 6.64 | 1.28 |

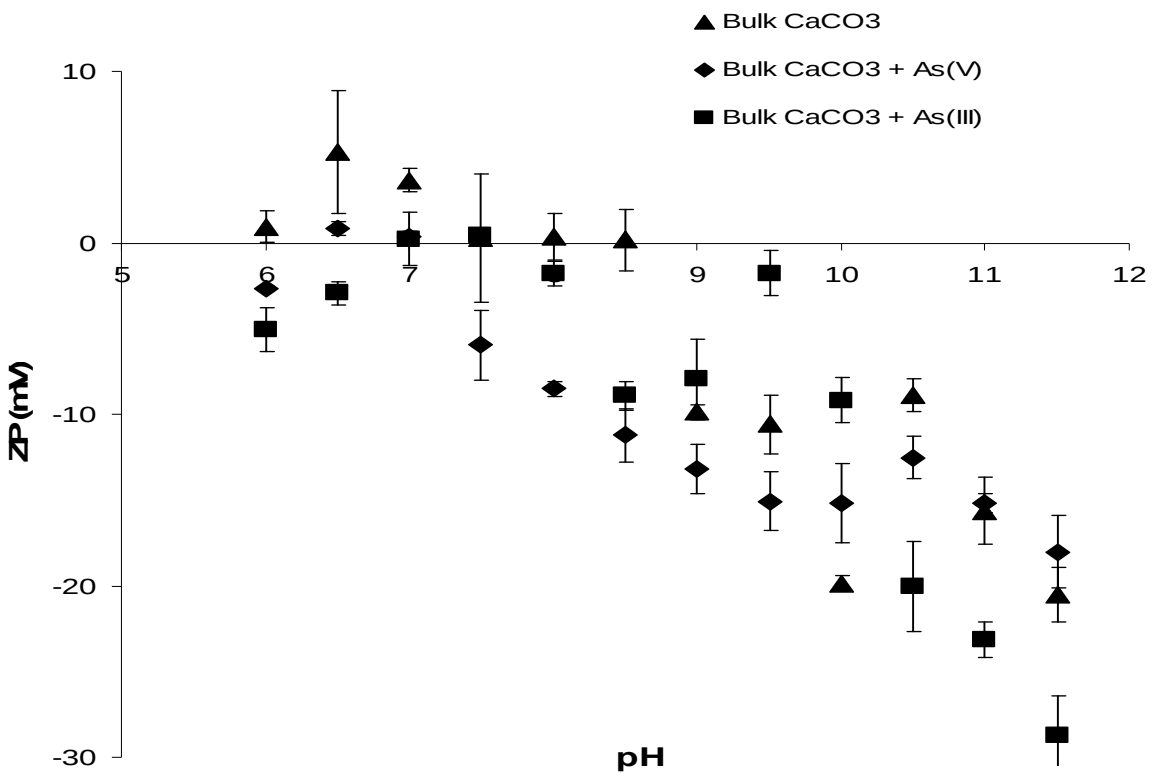


**Figure 5.18** Zeta potential values at different pH for bulk $CaCO_3$/As system.

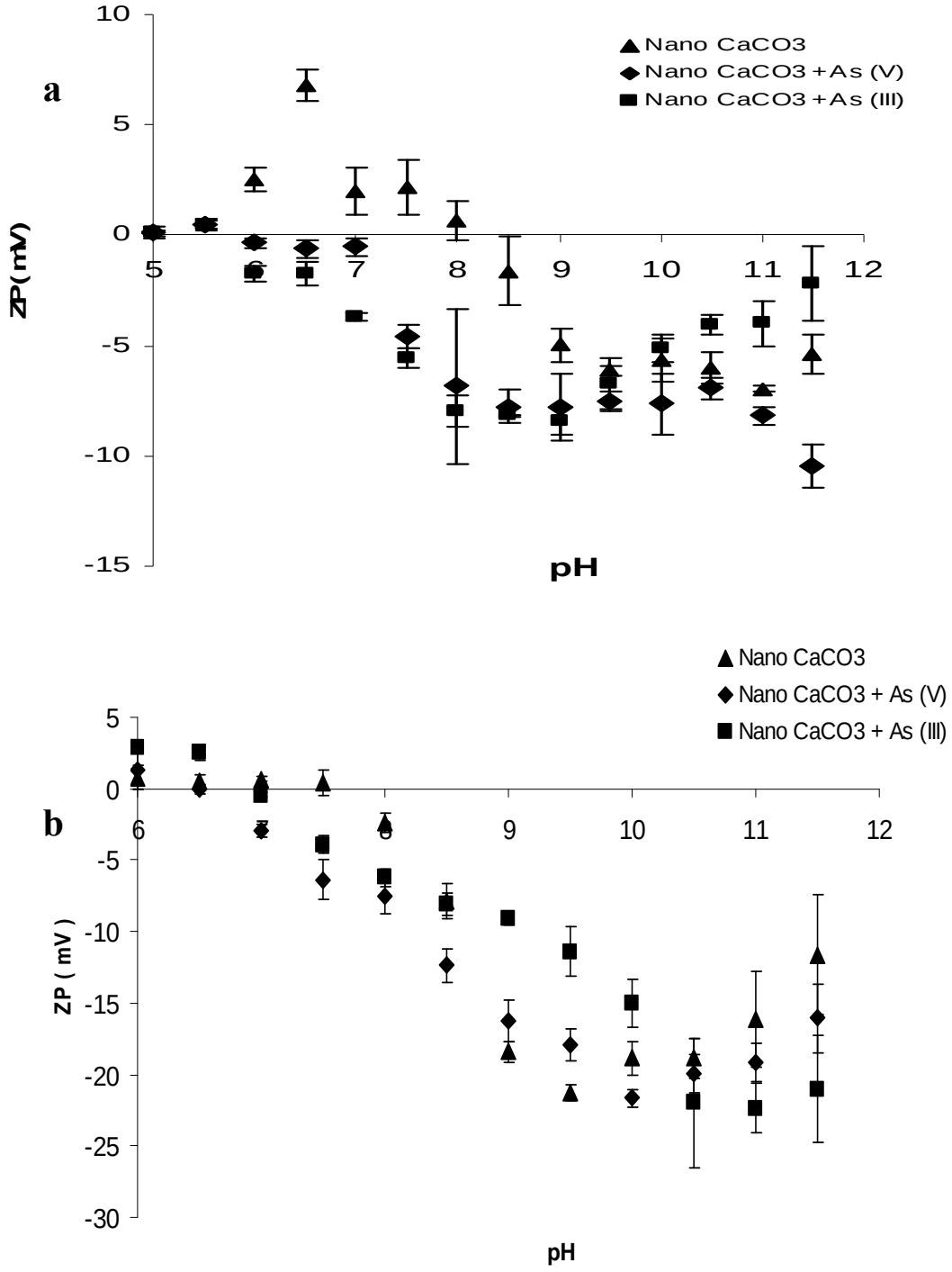


**Figure 5.19** Zeta potential values at different pH for **a)** nano $CaCO_3$ (*in situ* deposition method)/As system and **b)** nano $CaCO_3$ (interfacial method)/As system.

### 5.2.4. Kinetic Experiments:

Understanding the kinetics of As adsorption is important for predicting the fate of As and its dynamic interaction with soil and groundwater sorbents. This type of experiment can also provide insight into the mechanisms of adsorption of As on calcium carbonate. Several research groups reported that the adsorption of arsenate on hydrous iron oxides is rapid, initially followed by a slow stage. Fuller *et al.* (1993) and Raven *et al.* (1998) reported that the reaction kinetics of arsenate/arsenite with ferrihydrite follow a parabolic diffusion model. In this study, adsorption kinetics of As(V) and As(III) (at either 290 or 550 μM) on $CaCO_3$ were investigated at pH 9.5 in the presence of 0.01 M $NaNO_3$ solution ( Fig. 5.20-5.23).

The results of the kinetic uptake experiments show that there is a rapid sorption of As(V) and As(III) taking place within the first 2 hours of interaction. This initial step of rapid sorption is followed by slow uptake which continues up to 48 hrs of reaction, and then attains a steady state. This biphasic adsorption is consistent with that observed for arsenate and arsenite on metal oxides, and is fairly common for inorganic sorption on mineral surfaces in general. The fast initial uptake step has commonly been interpreted as chemisorption to readily available surface sites, while the slow rate of approach to equilibrium would classically be interpreted as evidence that diffusion-controlled mass transfer of As to less accessible internal sites may be the rate limiting step at longer times.

In accordance with the above explanation, a first order kinetics model was used to describe the initial fast reaction (t=0-2hrs) while the slow reaction kinetics in the time period (t=2-48hrs) was fitted with a parabolic diffusion equation. (See Figure 5.24-5.31) Based on the fitting shown in the figures below first order and the parabolic diffusion model based parameter were calculated and have been reported in the following tables 5.6 and 5.7.

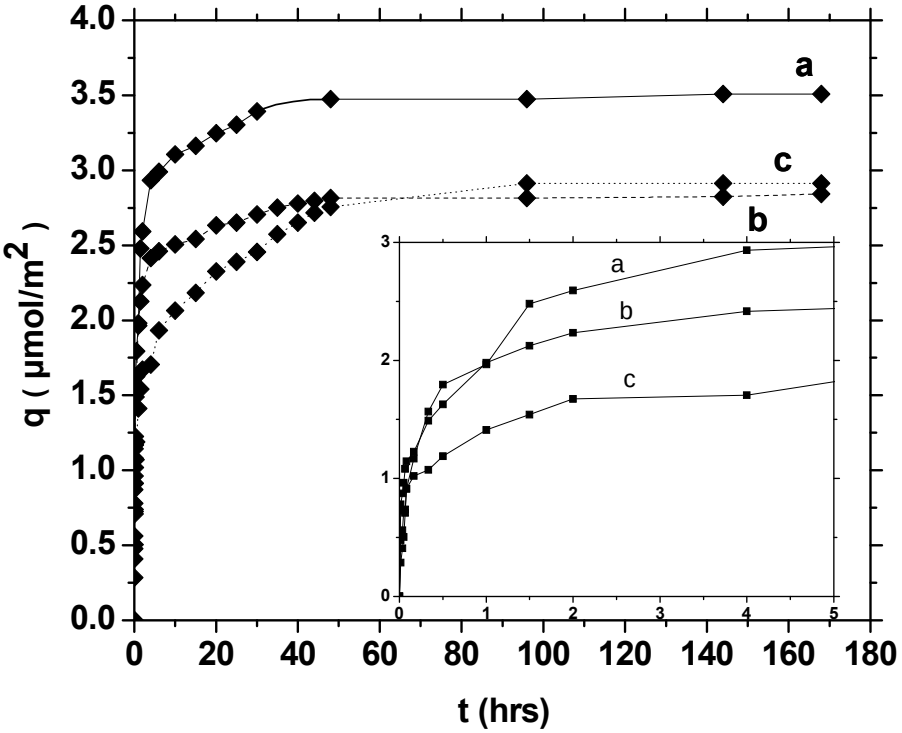


**Figure 5.20** Kinetics of 290 µM As(V) adsorption with **a)** Bulk **b)** Nano (*in situ* deposition method) and **c)** Nano (interfacial method) $CaCO_3$ at pH 9.5. The first five hours of the reaction is inset for clarity.

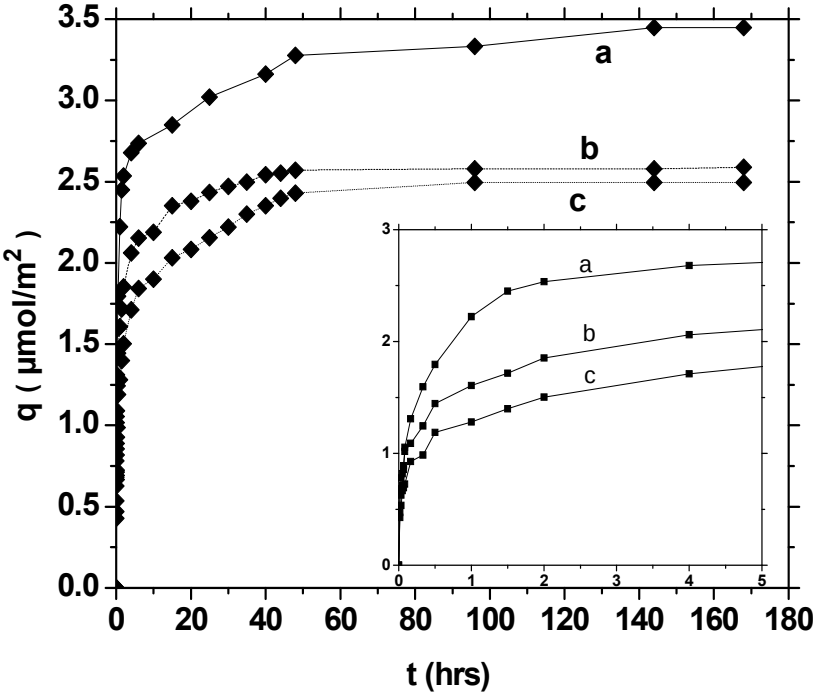


**Figure 5.21** Kinetics of 550 µM As(V) adsorption with **a)** Bulk **b)** Nano (*in situ* deposition method) and **c)** Nano (interfacial method) $CaCO_3$ at pH 9.5. The first five hours of the reaction is inset for clarity.

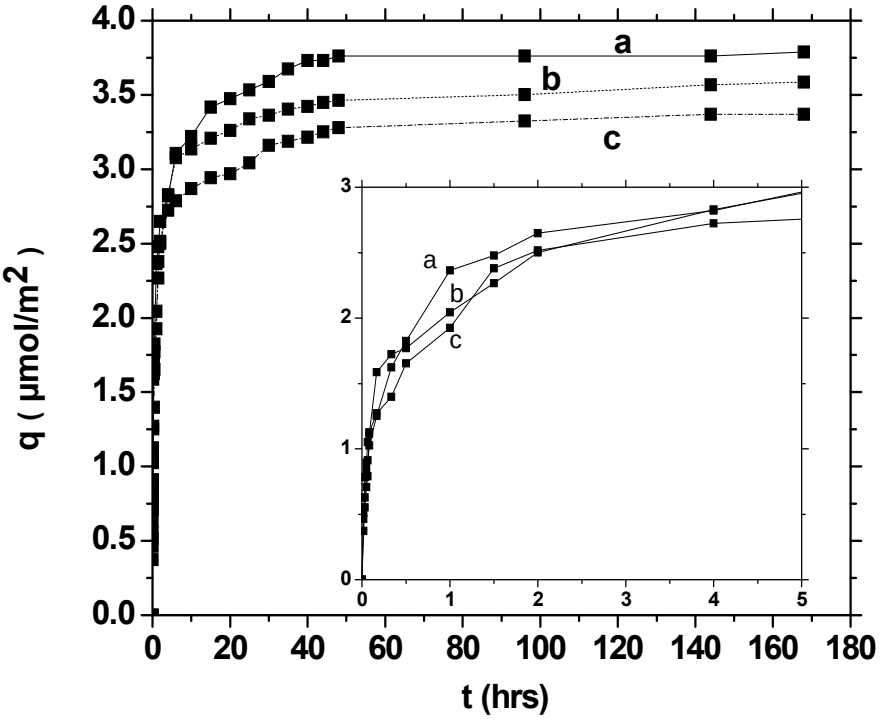


**Figure 5.22** Kinetics of 290 µM As(III) adsorption with **a)** Bulk **b)** Nano (*in situ* deposition method) and **c)** Nano (interfacial method) $CaCO_3$ at pH 9.5. The first five hours of the reaction is inset for clarity.

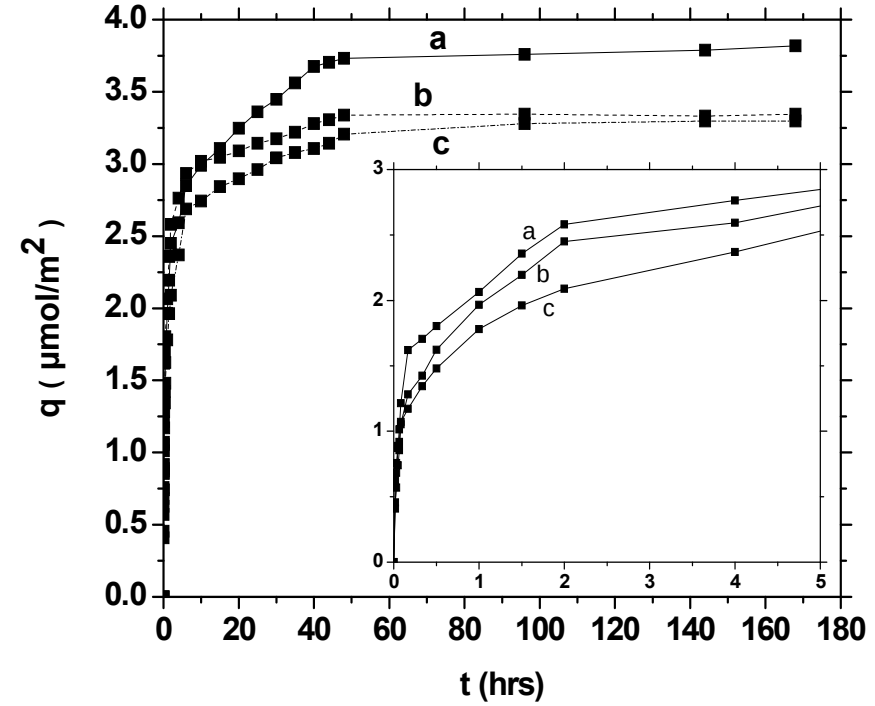


**Figure 5.23** Kinetics of 550 µM As(III) adsorption with **a)** Bulk **b)** Nano (*in situ* deposition method) and **c)** Nano (interfacial method) $CaCO_3$ at pH 9.5. The first five hours of the reaction is inset for clarity.

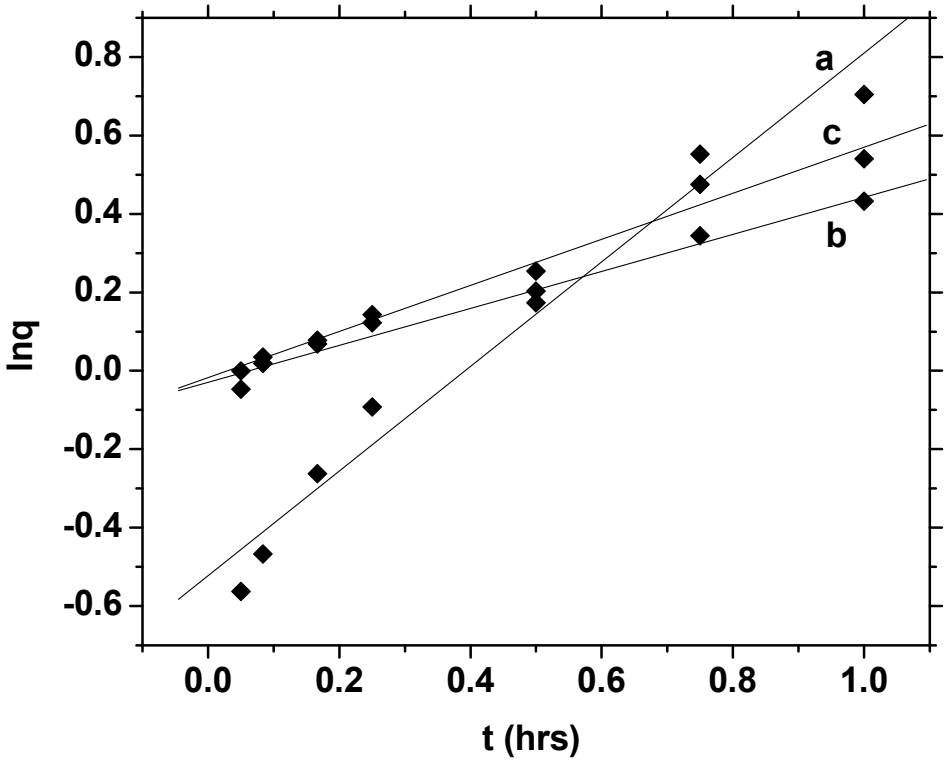


**Figure 5.24** First order fit for 290 μM As(V) on **a)** bulk **b)** Nano (*in situ* deposition method) and **c)** Nano (interfacial method) $CaCO_3$.

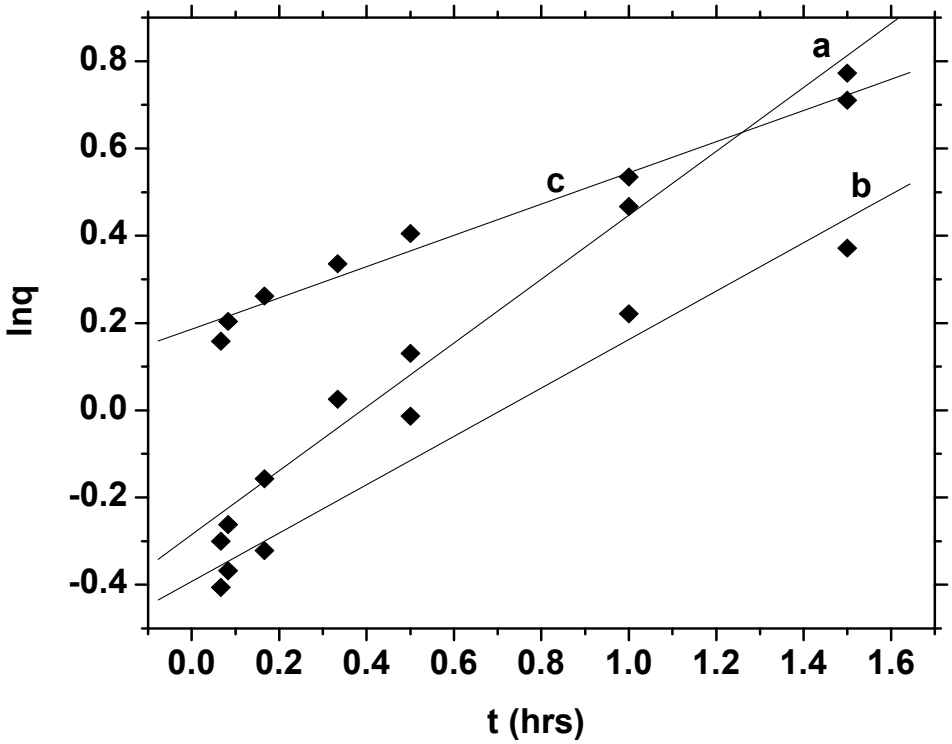


**Figure 5.25** First order fit for 550 μM As(V) on **a)** bulk **b)** Nano (*in situ* deposition method) and **c)** Nano (interfacial method) $CaCO_3$.

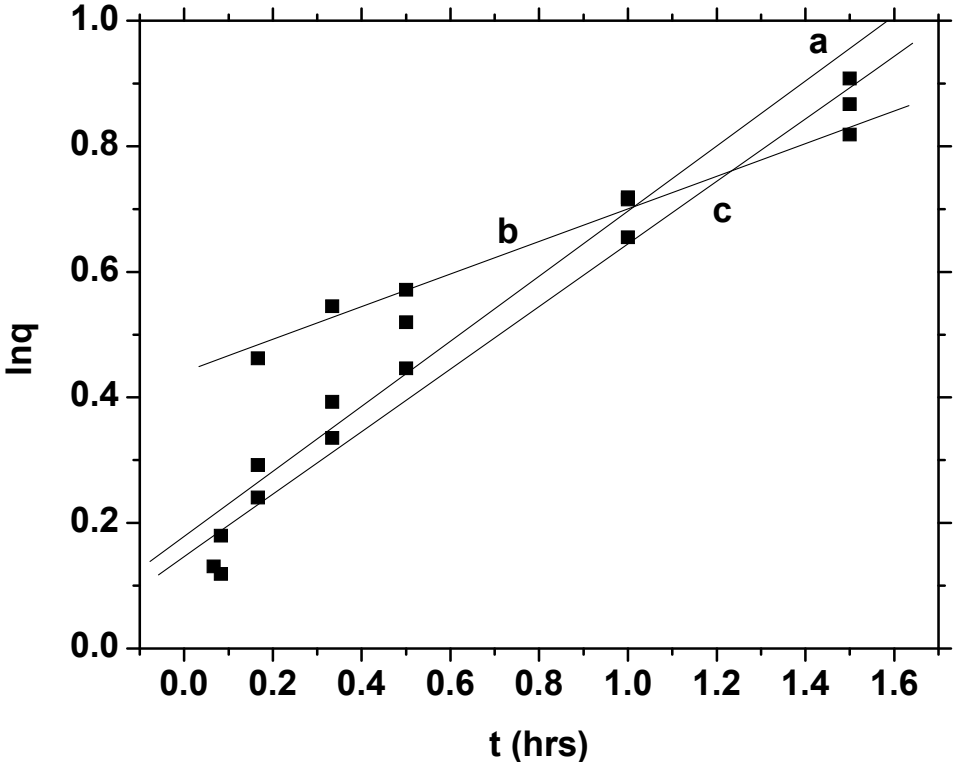


**Figure 5.26** First order fit for 290 µM As(III) on **a)** bulk **b)** Nano (*in situ* deposition method) and **c)** Nano (interfacial method) $CaCO_3$.

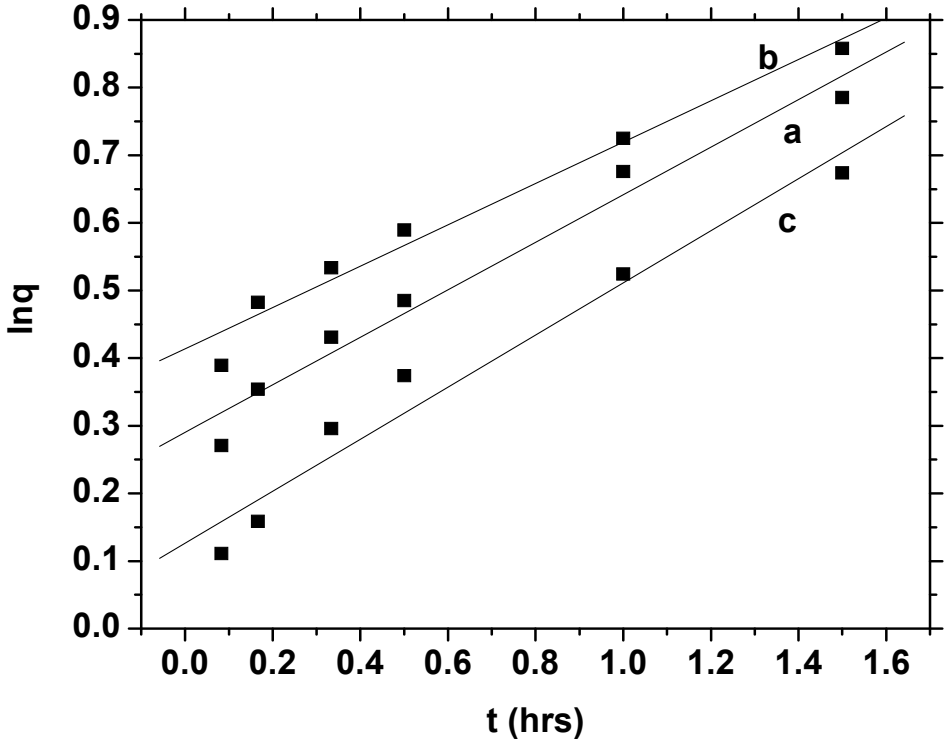


**Figure 5.27** First order fit for 550 µM As(III) on a) bulk b) Nano (*in situ* deposition method) and c) Nano (interfacial method) $CaCO_3$

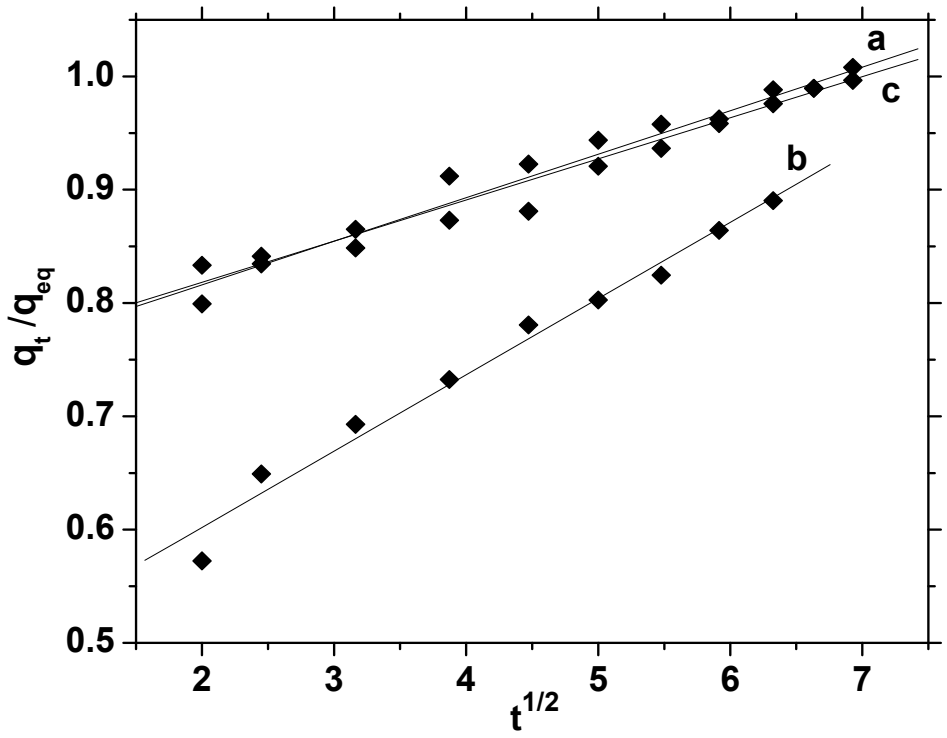


**Figure 5.28** Fit for parabolic diffusion model of 290 µM As(V) on **a)** bulk **b)** Nano (*in situ* deposition method) and **c)** Nano (interfacial method) $CaCO_3$.

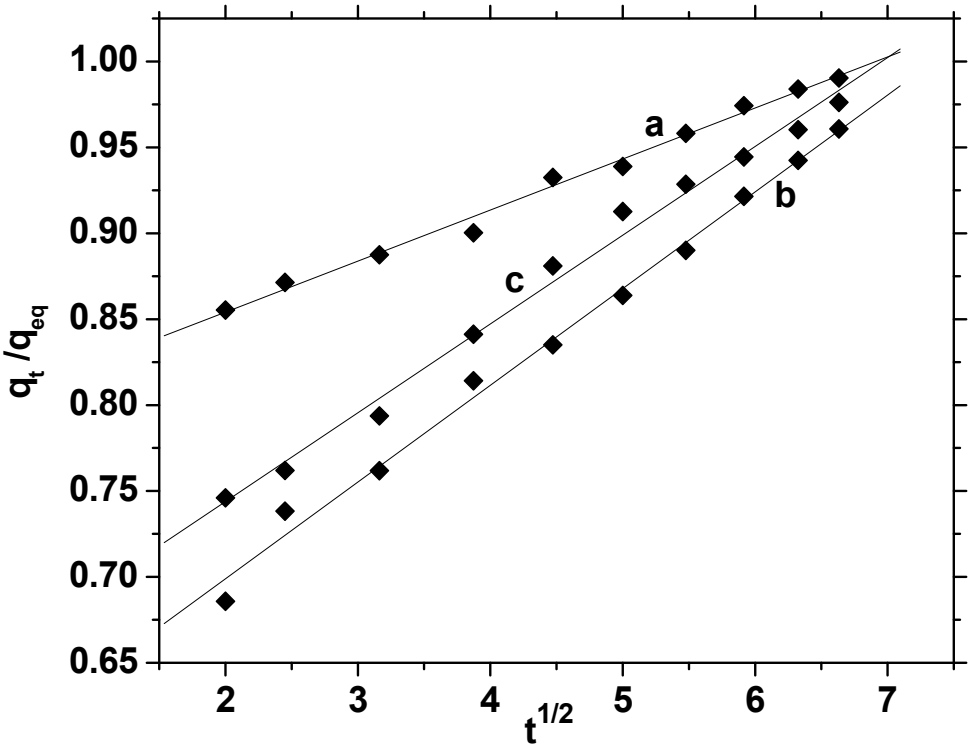


**Figure 5.29** Fit for parabolic diffusion model of 550 µM As(V) on a) bulk b) Nano (*in situ* deposition method) and c) Nano (interfacial method) $CaCO_3$.

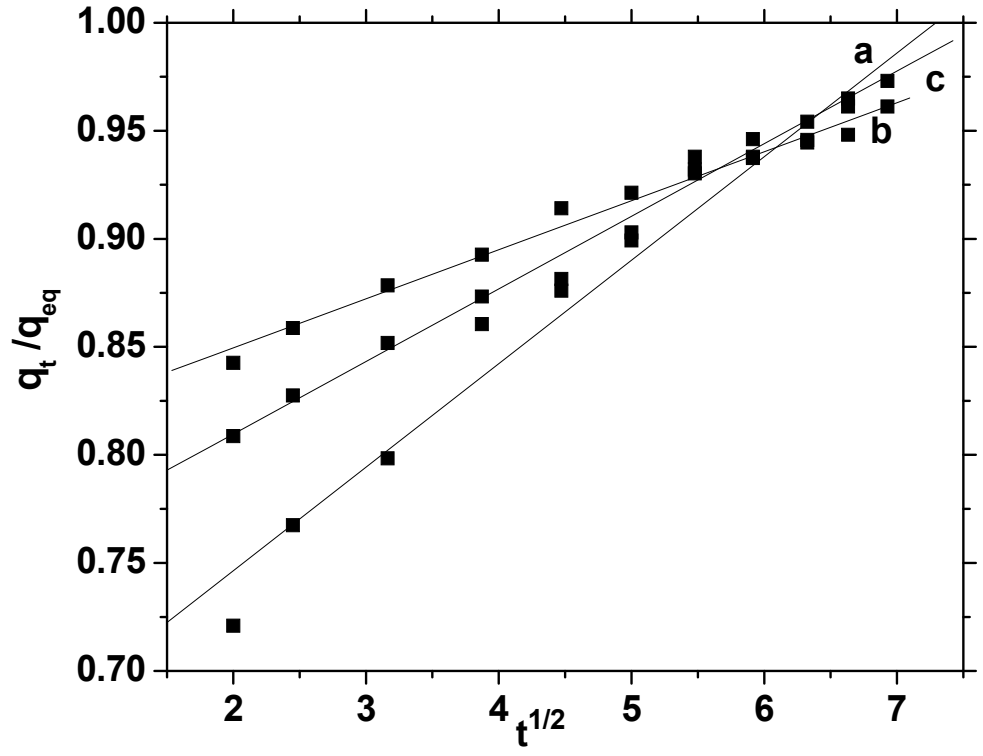


**Figure 5.30** Fit for parabolic diffusion model of 290 μM As(III) on **a)** bulk **b)** Nano (*in situ* deposition method) and **c)** Nano (interfacial method) $CaCO_3$.

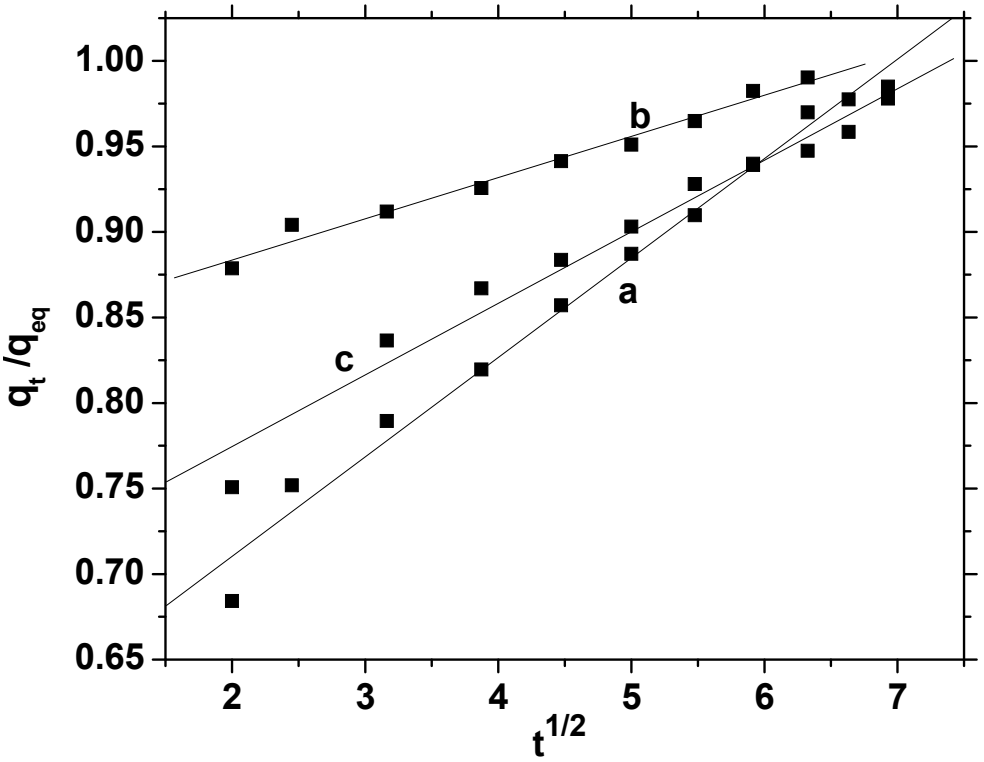


**Figure 5.31** Fit for parabolic diffusion model of 550 μM As(III) on **a)** bulk **b)** Nano (*in situ* deposition method) and **c)** Nano (interfacial method) $CaCO_3$.

**Table 5.6** First order model based parameters for different concentrations of As(V) and As(III) adsorption on bulk and nano $CaCO_3$ at pH 9.5.

| As | | Bulk $CaCO_3$ | | Nano $CaCO_3$ | | | |
|---|---|---|---|---|---|---|---|
| | | | | From Method 1 | | From Method 2 | |
| | | $R^2$ | -k | $R^2$ | -k | $R^2$ | -k |
| As(V) | 290 μM | 0.97 | 1.33 | 0.96 | 0.32 | 0.99 | 0.49 |
| | 550 μM | 0.98 | 0.73 | 0.96 | 0.55 | 0.97 | 0.36 |
| As(III) | 290 μM | 0.96 | 0.52 | 0.99 | 0.26 | 0.98 | 0.48 |
| | 550 μM | 0.97 | 0.35 | 0.97 | 0.31 | 0.96 | 0.39 |

**Table 5.7** Parabolic model based parameters for different concentrations of As(V) and As(III) adsorption on bulk and nano $CaCO_3$ at pH 9.5.

| As | | Bulk $CaCO_3$ | | Nano $CaCO_3$ | | | |
|---|---|---|---|---|---|---|---|
| | | | | From Method 1 | | From Method 2 | |
| | | $R^2$ | $R_D$ | $R^2$ | $R_D$ | $R^2$ | $R_D$ |
| As(V) | 290 μM | 0.99 | 0.041 | 0.98 | 0.067 | 0.97 | 0.039 |
| | 550 μM | 0.99 | 0.051 | 0.99 | 0.056 | 0.99 | 0.029 |
| As(III) | 290 μM | 0.98 | 0.048 | 0.99 | 0.024 | 0.99 | 0.034 |
| | 550 μM | 0.99 | 0.058 | 0.99 | 0.026 | 0.97 | 0.042 |

Since first order reaction kinetics does not describe the data over the period of 168 hours, the above modeling may not be the only explanation for the observed reactivity. To evaluate this, the Elovich equation was fitted to describe the reaction kinetics during the whole course of reaction time. Adsorption behaviour that fits Elovich model is typical for metal ions with strong binding interaction with the targeted sorption site because adsorbents with specific binding sites are most effective for binding when the sites are largely unoccupied. As the number of sites becomes occupied, the binding affinity of the adsorbate decreases.

The Elovich equation (Chen and Clayton, 1980) is as follows:

$dq/dt = \alpha \exp(-\beta q)$ ……( 5.2.3)

The parameter α and β are constant and are inversely proportional to the rate constant. Since, $dq/dt \rightarrow \alpha$ as $q \rightarrow 0$ the constant α can be regarded as initial rate, i.e., a rapid adsorption not governed by the exponential law (Low, 1960).When q = 0 at t = 0 the equation becomes

$q = (1/\beta) \ln (1 + \alpha\beta t)$ …….(5.2.4)

Assuming $\alpha\beta t >> 1$, the Elovich equation simplifies to

$q = 1/\beta \ln (\alpha\beta) + (1/\beta) \ln t$ ……. (5.2.5)

For this model, data will be linear for a plot of q vs ln(t) with slope of (1/β) and intercept of (1/β) ln (αβ) if the results follow an Elovich equation. The value of β decreases with rate constant and is a function of particle size and diffusion.

For our experiments, the results generally fitted well with the Elovich equation. (See Figure 5.32-5.35). Elovich fitting of kinetic data for arsenic adsorption has previously been reported by other research groups as well (Zhang and Stanforth, 2005; Fendorf *et al.*, 1997; Grossl *et al.*, 1997; Sun and Doner, 1996; Zhao and Stanforth, 2002; Chen and Clayton, 1980; Chen *et al.*, 1980).

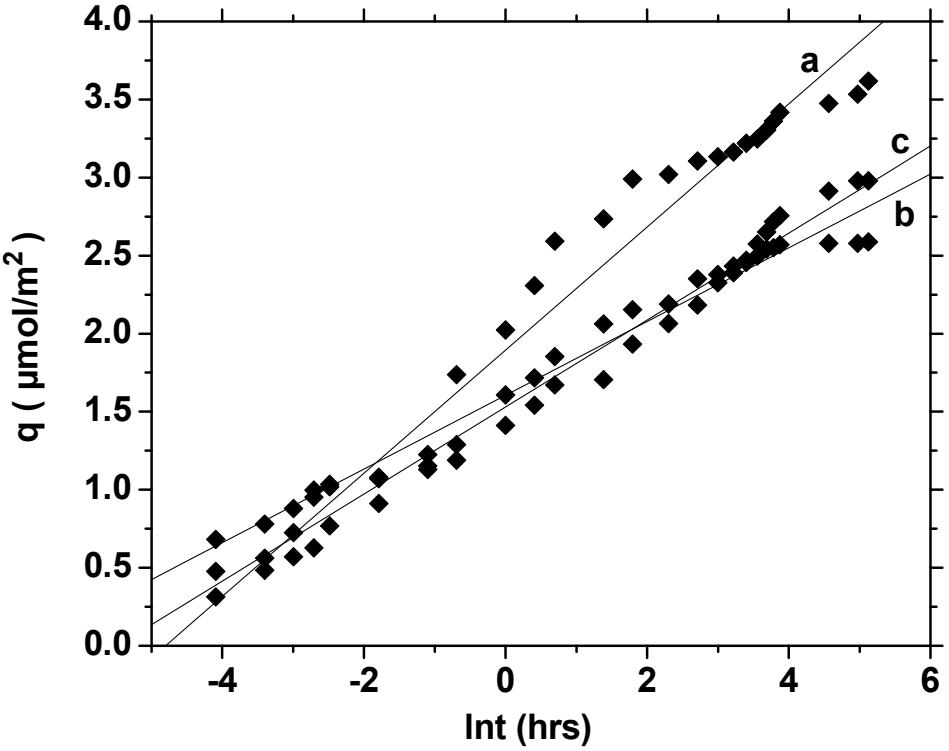


**Figure 5.32** Elovich fit for 290 µM As(V) on **a)** bulk **b)** Nano (*in situ* deposition method) and **c)** Nano (interfacial method) $CaCO_3$ at pH 9.5.

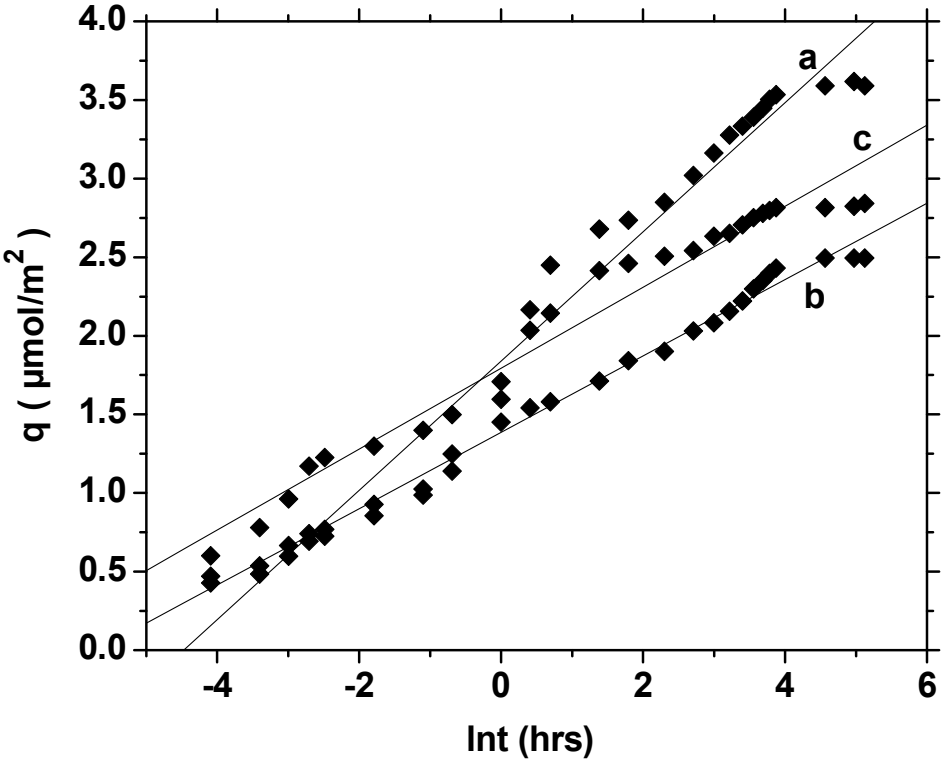


**Figure 5.33** Elovich fit for 550 µM As(V) on **a)** bulk **b)** Nano (*in situ* deposition method) and **c)** Nano (interfacial method) $CaCO_3$ at pH 9.5.

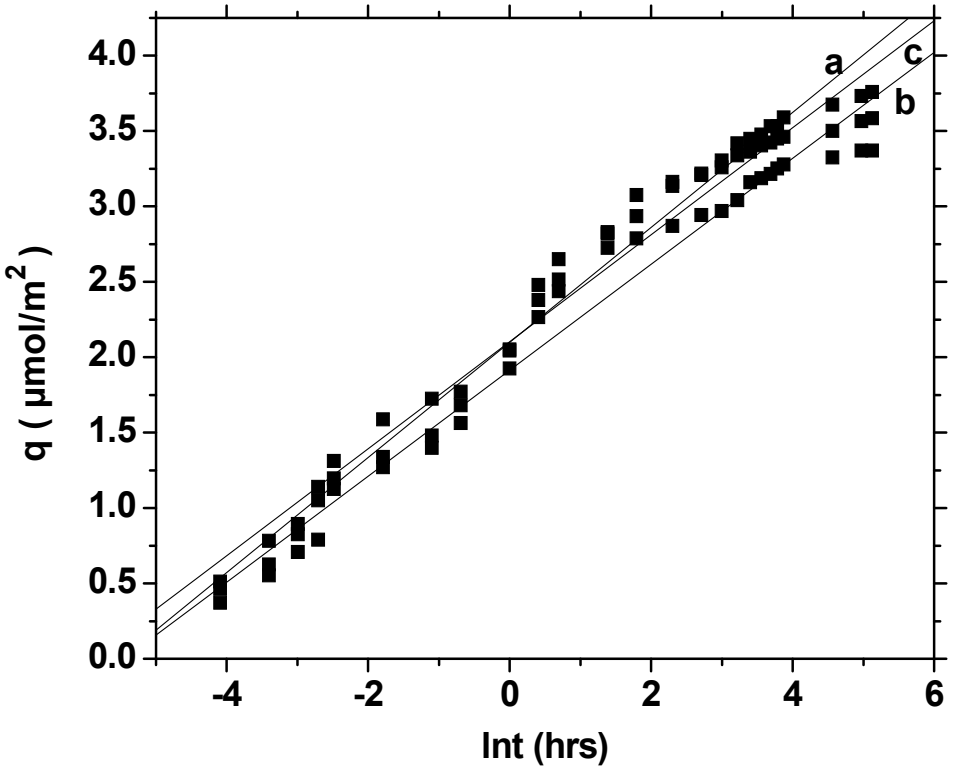


**Figure 5.34** Elovich fit for 290 µM As(III) on **a)** bulk **b)** Nano (*in situ* deposition method) and **c)** Nano (interfacial method) $CaCO_3$ at pH 9.5.

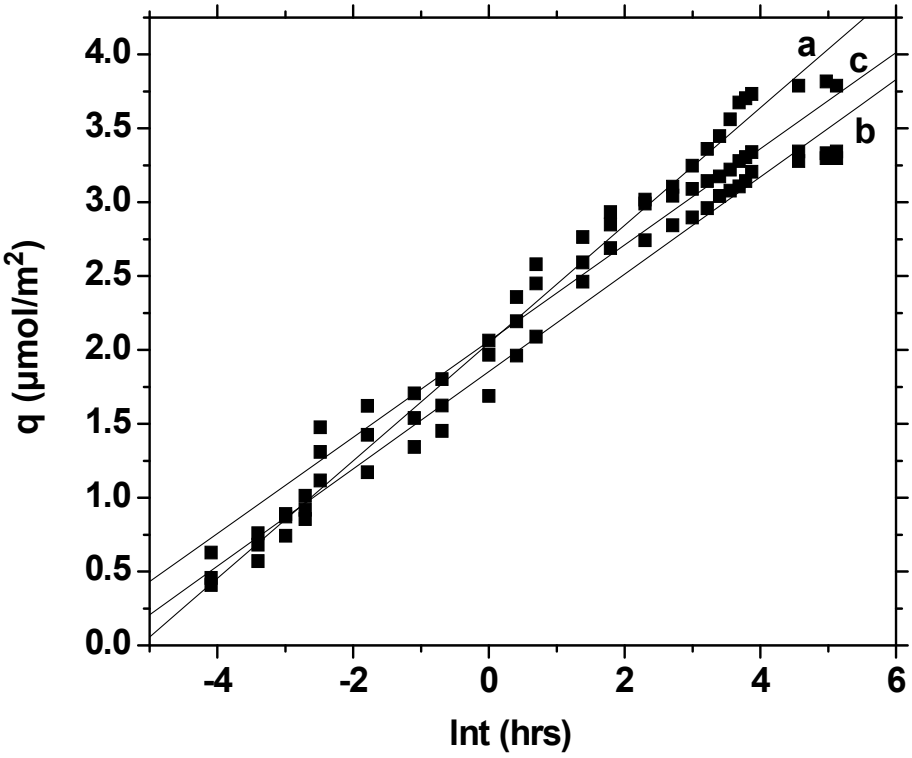


**Figure 5.35** Elovich fit for 550 µM As(III) on **a)** bulk **b)** Nano (*in situ* deposition method) and **c)** Nano (interfacial method) $CaCO_3$ at pH 9.5.

Based on the fitting shown in the above figures Elovich model based parameters were calculated and have been reported in the following Table 5.8. The calculated values of β (Table 5.8) shows that the product of α and β are much greater than 1. This indicates that the assumption of $\alpha\beta t >> 1$ is valid and its use to derive equation 5.2.5 seems justified.

With a decrease in As(V) and As(III) concentrations from 550 to 290 μM, the value of β decreases for both bulk and nano $CaCO_3$.The decrease in concentration allows more rapid diffusion of As in $CaCO_3$, hence, rate increases (since β decreases).With the increase in particle size of $CaCO_3$, i.e., nano (*in situ* deposition) < nano (interfacial) < bulk the value of β also decreases. This means that the rate of diffusion for bulk $CaCO_3$ is higher compared to that of nano $CaCO_3$ (*in situ* deposition and interfacial method) as the rate constant is inversely proportional to β. From the values of β, (See Table 5.8) it can be inferred that the observed rate of diffusion increases with increase in particle size and increase in As(V) and As(III) concentration. This implies that stronger inner sphere complexes result with the increase in As(III) concentration from 290 to 550 μM and As(III) forms stronger inner-sphere complexes with nano $CaCO_3$ compared to bulk $CaCO_3$. Also, the inner sphere complexes formed by As(III) is stronger compared to As(V) with $CaCO_3$. This interpretation of the results is also in agreement with the findings from EM experiment.

**Table 5.8** Elovich equation based parameters for different concentrations of As(V) and As(III) adsorption on i) bulk and ii) nano $CaCO_3$ at pH 9.5.

| As | | Bulk $CaCO_3$ | | | Nano $CaCO_3$ | | | | | |
|---|---|---|---|---|---|---|---|---|---|---|
| | | | | | From Method 1 | | | From Method 2 | | |
| | | $R^2$ | β | 1/βln(αβ) | $R^2$ | β | 1/βln(αβ) | $R^2$ | β | 1/βln(αβ) |
| As(V) | 290 μM | 0.96 | 2.33 | 1.91 | 0.98 | 3.85 | 1.53 | 0.98 | 3.57 | 1.61 |
| | 550 μM | 0.97 | 2.43 | 1.83 | 0.99 | 4.16 | 1.39 | 0.97 | 4.00 | 1.79 |
| As(III) | 290 μM | 0.98 | 2.56 | 2.09 | 0.98 | 2.86 | 2.10 | 0.97 | 2.86 | 1.91 |
| | 550 μM | 0.99 | 2.63 | 2.05 | 0.96 | 3.13 | 2.07 | 0.99 | 2.94 | 1.84 |

## 6.0 OVERALL CONCLUSIONS

In the first part of this project, laboratory synthesized $CaCO_3$ (bulk and nano) was synthesized and then characterized. The external surface area of the bulk $CaCO_3$ was 4.68 $m^2/g$, versus 20.41 $m^2/g$ and 14.59 $m^2/g$ for nano $CaCO_3$ synthesized using *in situ* deposition and interfacial methods, respectively. The size of the bulk $CaCO_3$ particles were in the range from 0.3-100 μm, with an average particle size of 19.9 μm. In the case of nano $CaCO_3$ (*in situ* deposition method), majority of the particles were less than 100 nm and less than 200 nm for nano $CaCO_3$ (interfacial method).XRD, FT-IR and FT-Raman spectroscopy was used to characterize the $CaCO_3$ samples. The results show bulk $CaCO_3$ to be composed of only thermodynamically stable calcite. PEG based nano $CaCO_3$ was found to be mixture of calcite and aragonite and results on surfactant based nano $CaCO_3$ indicates a mixture of calcite and vaterite. Additionally, the characteristic FTIR absorption peaks of PEG and Tween 80 were not observed in our $CaCO_3$ samples indicating the absence of their contamination in the nano $CaCO_3$ samples.

With respect to the effect of $CaCO_3$ size on adsorption isotherms, both As(III) and As(V) had larger $q_{max}$ values (which was normalized for surface area) for nano-sized particles which means nano-sized particles have slightly higher affinity for As oxyanions than does the bulk calcite. From the pH envelope experiments, it can be concluded that As(III) adsorption is higher than As(V) adsorption on $CaCO_3$ over the range of 7.5-9.5. The reduction in the As(V) adsorption compared to that of As(III) at high pH values (>pH 8) is likely due to electrostatic repulsion of the negatively charged As(V) species by the negatively charged surface above its PZC. Electrophoretic mobility experiments revealed greater shifts in PZC in the case of arsenate and arsenite adsorption on nano $CaCO_3$ than on bulk $CaCO_3$, implying that arsenite and arsenate form stronger inner-sphere complexes with our nano-materials. For all kinetics experiments, an initial period of rapid sorption (t = 0-2 hrs) due to adsorption to readily available surface sites is followed by slow uptake which continues up to 48 hrs of reaction and then attains equilibrium. This slow continued reaction indicates that diffusion-controlled mass transfer of As to additional less accessible sites located in the internal porosity of $CaCO_3$may be the rate limiting step for longer reaction periods. Data was fit reasonably

well with either a combination of First order model and parabolic diffusion equation or with the Elovich equation. From the Elovich fit it can be inferred that the rate of surface diffusion increases with i) particle size and ii) As(V) and As(III) concentration.

Finally, it should be noted that the PEG based nano $CaCO_3$ prepared by an *in-situ* deposition technique contains a mixture of aragonite and calcite in proportions similar to that observed in bioreactors that were developed in a companion project (J.Arnold thesis) to study As sorption on ureolytically-generated $CaCO_3$. This suggests that the *in situ* deposition method produces mineral products that are reasonable simulation of ureolytically synthesized biogenic $CaCO_3$. Hence, nano $CaCO_3$ synthesized in this method represents an inexpensive, rapid, and reproducible proxy for the study of adsorption of contaminants on biogenic $CaCO_3$. The result presents a novel and facile route towards inorganic synthesis of minerals representative of biological systems. Hence, nano $CaCO_3$ synthesized from the in-situ technique can be used as proxy for the biogenic $CaCO_3$ to mimic real conditions.

## 7.0 FUTURE WORK

Synthesis of nano-sized $CaCO_3$ by varying parameters in the *in situ* deposition should be performed. For example, it is possible to perform the synthesis with other polymer instead of only PEG. Tri block co-polymer (Kato *et al*., 2002) could be used in presence of other additives to control the size of the polymorphs. Changing the pH of the system will also affect the polymorphs, shapes, and particle sizes of the $CaCO_3$ products. The effects of performing synthesis in a nitrogen environment should also be investigated.

The adsorption kinetics of As(III) and As(V) on synthetic $CaCO_3$ at pH 9.5 was studied in this project, but adsorption at different pH values (7.5-10) would be useful as well. Depending on the acidity, the sorption profile of As will vary. Carrying out the kinetic study on a wide range of pH will make our results more widely applicable to environmental scientists.

Thermodynamic adsorption of arsenic oxyanions on the synthesized $CaCO_3$ polymorphs should also be performed at different temperature. If experiments were carried out on bulk and nanosized $CaCO_3$ at (for example) 15°C, 25°C, 35°C and 45°C, it would allow us to determine the isosteric heat of adsorption. The isosteric heat of adsorption of component $i$ ($q_i$, cal/mol) is defined as the negative of the differential change in total enthalpy ($H^\circ$, cal/g) for a differential change in the surface excess of component $i$ ($n_i^m$) at constant system temperature ($T$)and constant values of surface excesses of other components $\left(n_{j\neq i}^m\right)$ of the closed system (Sircar *et al.*, 1999).

$$q_i = -\left[\frac{\delta H^\circ}{\delta n_i^m}\right]_{T,n_{j\neq i}^m} \qquad \ldots\ldots\ldots\ldots (7.1)$$

From the value of the isosteric heat of adsorption, one could obtain information on whether adsorption is physical or chemical (Romo *et al*., 2004). Also, thermodynamic adsorption of arsenic on the synthesized $CaCO_3$ polymorph at different temperatures (15-45°C) could be performed with different pH values (7.5-10) to analyze the effect of temperature on the adsorption of arsenic oxyanions at different pH.

It would also be very useful to perform adsorption and kinetic experiments on biogenic $CaCO_3$ cultured by ureolytic enzymes. This will enable us to compare the adsorption more directly and determine how the reactivity of arsenic oxyanions with biogenic $CaCO_3$ differs with that of the synthetic ones.

Desorption studies at longer time frames could be investigated to provide better estimates of the stability constant of the As-$CaCO_3$ complex. From the value of the stability constant, a better estimate of the long-term feasibility of $CaCO_3$ as a sorbent for arsenic removal could be evaluated. Similarly, spectroscopic investigation of sorption mechanisms, i.e., mode of bonding of arsenic oxyanions with $CaCO_3$ can be performed by EXAFS available at the Canadian Light Source (CLS).

## REFERENCES


Acharyya, S. K. 2002. Arsenic contamination in groundwater affecting major parts of southern West Bengal and parts of western Chhattisgarh: Source and mobilization process. Curr. Sci. 82: 740-744.

Acharyya S.K., P. Chakraborty, S. Lahiri, B.C. Raymahashay, S. Guha, and A. Bhowmik. 1999. Arsenic poisoning in the Ganges delta. Nature. 401: 545.

Adamson, A.W. 1990. Physical chemistry of surfaces, fifth ed. Wiley-Interscience, New York.

Adriano, D.C. 2001. Trace elements in terrestrial environments: biogeochemistry, bioavailability and risks of metals, p. 219-261. ed. Springer-Verlag, New York.

Ahmed, K.M., P. Bhattacharyya, M.A. Hasan, S.H. Akhter, S.M.M. Alam, M.A.H. Bhuyian, M.B. Imam, A. A. Khan, and O. Sracek. 2004. Arsenic enrichment in groundwater of the alluvial aquifers in Bangladesh: an overview. Appl.Geochem. 19:181-200.

Aizenberg, J. 2004. Crystallization in patterns: A bio-inspired approach. Adv. Mater. 16: 1295.

Aizenberg, J., J. Hanson, T. F. Koetzle, S. Weiner, and L. Addadi. 1997. Control of macromolecule distribution within synthetic and biogenic single crystals. J. Am. Chem.Soc. 119: 881.

Akai, J., K. Izumi, H. Fukuhara, H. Masuda, S. Nakano, T. Yoshimura, H. Ohfuji, H.M. Anawar, and K. Akai. 2004. Mineralogical and geomicrobiological investigations on groundwater arsenic enrichment in Bangladesh. Appl. Geochem. 19: 215-230.

Alam, M.G.M., G. Allinson, F. Stagnitti, A. Tanaka, and M. Westbrooke. 2002. Arsenic contamination in Bangladesh ground water: a major environmental and social Disaster. Int. J. Environ. Health Res.12: 236-253.

Alexandros, V.G., E. J. Elzinga, and R.J. Reeeder. 2007 Arsenate uptake by calcite: Macroscopic and spectroscopic characterization of adsorption and incorporation Mechanisms. Geochim. Cosmochim. Acta. 71: 4172-4187.

Anawar, H.M., J. Akai, K. Komaki, H. Terao, T. Yoshioka, T. Ishizuka, S. Safiullah, and K. Kato. 2003.Geochemical occurrence of arsenic in groundwater of Bangladesh: sources and mobilization processes. J. Geochem. Explor. 77: 109-131.

Anawar, H.M., J. Akai, K.M.G. Mostofa, S. Safiullah, and S.M. Tereq. 2002. Arsenic poisoning in groundwater: Health risk and geochemical sources in Bangladesh. Environ. Int. 27:597-604.

Andersen, S., G. Rasmussen, P. Snilsberg C.E Amundsen, and T.Westby. 1996. Assessing toxicity and mobilization of impregnation salts at a contaminated site. Fresenius. J. Anal. Chem. 354: 676-680.

Anderson, M.A., J.F. Ferguson, and J. Gavis. 1976. Arsenate adsorption on amorphous aluminium hydroxide. J. Colloid Interface Sci. 54:391-399.

Appelo, C.A.J., Van der Weiden, C. Tournassat, and L. Charlet. 2002. Surface complexation of ferrous iron and carbonate on ferrihydrite and the mobilization of arsenic. Environ. Sci. Technol. 36: 3096-3103.

Arai, Y., E.J. Elzinga, and D.L. Sparks. 2001. X-ray absorption spectroscopic investigation of arsenite and arsenate adsorption at the aluminum oxide-water interface. J. Colloid Interface Sci. 235:80-88.

Arnold, J. 2007. Ureolytic $CaCO_3$ precipitation for immobilization of arsenic in an aquifer system. M.Sc. thesis, University of Saskatchewan, Saskatoon, Sask.

Balasoiu, C.F., G.J. Zagury, and L. Deschˆenes. 2001. Partitioning and speciation of chromium, copper, and arsenic in CCA-contaminated soils: influence of soil composition. Sci. Total Environ. 280: 239-255.

Berg, M., H.C. Tran, T.C. Nguyen, H.V. Pham, R. Schertenleib, and W. Giger. 2001. Arsenic contamination of groundwater and drinking water in Vietnam: a human health Threat. Environ. Sci. Technol. 35: 2621-2626.

Bhattacharya P., M. Claesson, J. Bundschuh, O. Sracek, J. Fagerberg, and G. Jacks. 2006b. Distribution and mobility of arsenic in the Rio Dulce alluvial aquifers in Santiago del Estero Province, Argentina. Sci Total Environ. 358: 97-120.

Bothe, J.V., and P. Brown. 1999. The stabilities of calcium arsenates at 23±1ºC. J. Hazard Mat. 69:197-207.

Bottcher, A.L., and P. J. Wyllie. 1968. Calcite-Aragonite transition measured in system $CaO$-$CO_2$-$H_2O$. J. Geol. 76: 314.

Bose, P., and A. Sharma. 2002. Role of iron in controlling speciation and mobilization of arsenic in subsurface environment. Water Res. 36: 4916-4926.

Brar, N.S., and H.H. Schloesin. 1979. Effects of pressure, temperature and grain size on the kinetics of the calcite-aragonite transformation. Can. J. Earth Sci.16:1402-1418.

Brar, N.S., and H.H. Schloesin. 1981. Nucleation and growth of aragonite in a calcite single crystal. Phase Trans.1:299-323.

Brunauer, S., P.H. Emmett, and E. Teller. 1938. Adsorption of gases in multimolecular layers. J. Am. Chem. Soc. 60:309.

Budd, D.A. 1988. Aragonite-to-calcite transformation during fresh water diagenesis of carbonates: Insights from pore-water chemistry. Geol. Soc. Am. Bull.100:1260-1270.

Chakraborty, D., and S.K. Bhatia. 1996. Formation and aggregation of Polymorphs in Continuous Precipitation. 2. Kinetics of $CaCO_3$ Precipitation. Ind. Eng. Chem. Res. 35: 1995-2006.

Chen, S.H., and W.R. Clayton. 1980. Application of Elovich equation to the kinetics of phosphate release and sorption in soils. Soil Sci. Soc. Am. J. 44: 265-268.

Chen, S.H., W.R. Clayton, and G.H. McClellan. 1980. Kinetics of dissolution of phosphate rocks in soils. Soil Sci. Soc. Am. J. 1980, 44: 260-264.

Cheng, L., P. Fenter, N.C. Sturchio, Z. Zhong, and M.J. Bedzyk. 1999. X-ray standing wave study of arsenite incorporation at the calcite surface. Geochim. Cosmochim. Acta 63: 3153-3157.

Cicerone, D.S., A.E. Regazzoni, and M.A. Blesa. 1992. Electrokinetic properties of the calcite water interface in the presence of magnesium and organic matter. J. Colloid Interface Sci. 154: 423-433.

Colfen, H. 2003. Precipitation of carbonates: recent progress in controlled production of complex shapes. Curr. Opin. Colloid Interface Sci. 8: 23.

Cooper, P.A. 1994. Leaching of CCA: Is it a problem? In: Environmental considerations in the manufacture, use and disposal of preservative-treated wood. Madison, Wisconsin. Forest Products Society. 45-57.

Couture, L. 1947. Etude des specters de vibrations de monocristaux ioniques. Ann. Phys Ser. 12:5-94.

Cullen, W. R., and K. J. Reimer. 1989. Arsenic speciation in the environment. Chem. Rev. 89:713-764.

Davis, J.A., and D.B. Kent. 1990. Surface complexation modeling in aqueous geochemistry", Rev. mineral. 23:177-260.

Deng, S.G., J.M. Cao, J. Feng, J. Guo, B. Q. Fang, M.B. Zheng, and J. Tao. 2005. A Bio-inspired approach to the synthesis of $CaCO_3$ spherical assemblies in a soluble ternary-additive system. J. Phys. Chem. B. 109: 11473.

De Villiers, J.P.R. 1971. Crystal structure of aragonite, strontianite and witherite. Am. Mineralogist 56: 758-767.

Dhar, R.K., B.K. Biswas, G. Samanta, B.K. Mandal, D. Chakraborti, S. Roy, A. Jafar, A. Islam, G. Ara, S. Kabir, A.W. Khan, S.K. Ahmed, and S.A. Hadi. 1997. Groundwater arsenic calamity in Bangladesh. Curr. Sci. 73: 48-59.

Dickinson, S. R., and K.M. McGrath. 2004 Aqueous precipitation of calcium carbonate modified by hydroxyl-containing compounds. Cryst. Growth. Des. 4:1411.

Dobran, S., and G.J. Zagury. 2006. Arsenic speciation and mobilization in CCA-contaminated soils: Influence of organic matter content. Sci. Total Environ. 364: 239-250.

Donners, J.J.M., B.R. Heywood, E.W. Meijer, J.M. Nolte, and N.M. Sommerdijk. 2002. Control over calcium carbonate phase formation by dendrimer/surfactant templates. Chem. Eur. J. 8:2562-2567.

Driehaus, W., R. Seith, and M. Jekel. 1995. Oxidation of arsenate (III) with manganese oxides in water treatment: Water Res.29:297-305.

Dujardin, E., and S. Mann. 2002. Advanced materials progress report on bio-inspired materials chemistry. Adv. Mater. 14: 775.

Dzombak, D.A., and F.M.M. Morel. 1990. Surface Complexation Modeling: Hydrous Ferric Oxide. Wiley, New York.

Elzinga, E.J., R.J. Reeder, S.H. Withers, R.E. Peale, R.A. Mason, K.M. Beck, and W.P. Hess. 2002. EXAFS study of rare-earth element coordination in calcite. Geochim.Cosmochim. Acta. 66: 2875-2885.

Farmer, V.C. 1974. The Infrared Spectra of Minerals, p. 227-284, *In* V. C. Farmer, ed. Mineralogical Society Monograph 4. Mineralogical Society, London, England.

Fazal, M.A., T. Kawachi, and E. Ichion. 2001a. Validity of the latest research findings on causes of groundwater Arsenic contamination in Bangladesh. Water Int. 26: 380-389.

Fendorf, S., M.J. Eick, P.R. Grossl, and D.L. Sparks. 1997. Arsenate and chromate retention mechanisms on goethite.1. Surface structure. Environ. Sci. Technol.31:315.

Ferguson, J.F., and J. Gavis. 1972. A review of the arsenic cycle in natural waters. Water Res. 6: 1259-1274.

Foster, A.L. 2003. Spectroscopic investigations of arsenic species in solid phases, p. 27-66, *In* A. H. Welch and K. G. Stollenwerk, eds. Arsenic in Ground Water: Geochemistry and Occurrence. Kluwer Academic Publishers, Boston.

Foxall, T., G.C. Peterson, H.M. Rendall, and A.L. Smith. 1979. Charge determination at calcium salt/aqueous solution interface. *J. Chem. Soc. Faraday Trans.* 75: 1034-39

Frost, R.R., and R.A. Griffin. 1977. Effect of pH on adsorption of arsenic and selenium from landfill leachate by clay minerals. Soil Sci. Soc. Am. J. 41: 53-57.

Fuerstenau, D.W., J. Pradip, and R. Herrera-Urbina. 1992. The surface chemistry of bastnaesite, barite and calcite in aqueous carbonate solutions. Colloids Surf. 68: 95-102.

Fujita, Y., F.G. Ferris, R.D. Lawson, F.S. Colwell, and R.W. Smith. 2000. Calcium carbonate precipitation by ureolytic subsurface bacteria. Geomicrobiol. J. 17: 305-318.

Fujita, Y., G.D. Redden, J.C. Ingram, M.M. Cortez, F.G. Ferris, and R.W. Smith. 2004. Strontium incorporation into calcite generated by bacterial ureolysis. Geochim. Cosmochim. Acta 68:3261-3270.

Fuller, C.C., and J.A. Davis. 1989. Influence of coupling of sorption and photosynthetic processes on trace element cycles in natural waters. Nature 340: 52-54.

Fuller, C. C., J. A. Davis, and G. A. Waychunas. 1993. Surface-chemistry of ferrihydrite. 2. Kinetics of arsenate adsorption and coprecipitation. Geochim. Cosmochim. Acta 57: 2271-2282.

Gabrielli, C., R. Jaouhari, S. Joiret, and G. Maurin. 2000. *In situ* Raman Spectroscopy applied to electrochemical scaling. Determination of the structure of vaterite. J. Raman Spectrosc. 31: 497-501.

Gammage, R.B., and D.R. Glasson. 1976. The effect of grinding on the polymorphs of calcium carbonate. J. Colloid Interface Sci. 55: 396-401.

Goldberg, S., and R.A. Glaubig. 1988. Anion sorption on a calcareous, montmorillonitic soil-arsenic. Soil Sci. Soc. Am. J. 52: 1297-1399.

Goldberg, S., and C.T. Johnston. 2001. Mechanisms of arsenic adsorption on amorphous oxides evaluated using macroscopic measurements, vibrational spectroscopy, and surface complexation modeling. J. Colloid Interface Sci. 234:204-216.

Gotliv, B., L. Addadi, and S.Weiner. 2003. Mollusk shell acidic proteins: in search of individual functions. Chem. Bio Chem. 4:52.

Griffith, W. P. 1969. Raman spectroscopy of minerals. Nature 224: 264.

Grossl, P.R., M. Eick, D.L. Sparks, S. Goldberg, and C.C. Ainsworth. 1997. Arsenate and chromate retention mechanisms on goethite. 2. Kinetic evaluation using a pressure-jump relaxation technique. Environ. Sci. Technol. 31:321.

Grosz, A.E., J.N. Grossman, R. Garret, P. Friske, D.B. Smith, A.G. Darnley, and E. Vowinkel. 2004. A preliminary geochemical map for arsenic in surficial materials of Canada and the United States. Appl. Geochem. 19: 257-260.

Hammes, F., A. Seka, S. de Knijf, and W. Verstraete. 2003. A novel approach to calcium removal from calcium-rich industrial wastewater. Water Res. 37:699-704.

Han,Y., and J. Aizenberg. 2003. Effect of magnesium ions on oriented growth of calcite on carboxylic acid functionalized self-assembled monolayer. J. Am. Chem. Soc. 125: 4032.

Harvey, C.F., C.H. Swartz, A.B.M. Badruzzaman, N. Keon-Blute, W. Yu, M. A. Ali, J. Jay, R. Beckie, V. Niedan, D. Brabander, P.M. Oates, K.N. Ashfaque, S. Islam, H.F. Hemond, and M.F. Ahmed. 2002. Arsenic mobility and groundwater extraction in Bangladesh. Science 298: 1602-1606.

Hem, J.D. 1985. Study and interpretation of the chemical characteristics of natural water (3rd ed.): U.S. Geological Survey Water-Supply Paper 2254, 263 p.

Hingston, F.J., A.M. Posner, and J.P. Quirk. 1972. Anion adsorption by goethite and gibbsite: 1. The role of the proton in determining adsorption envelopes. J. Soil Sci. 23:177-192.

Horneman, A., A. van Geen, D.V. Kent, P.E. Mathe, Y. Zheng, R.K. Dhar, S. O'Connell, M.A. Hoque, Z. Aziz, M. Shamsudduha, A.A. Seddique, and K.M. Ahmed. 2004. Decoupling of As and Fe release to Bangladesh groundwater under reducing conditions. Part I: evidence from sediment profile. Geochim. Cosmochim. Acta. 68: 3459-3473.

Hossain, M.F. 2006. Arsenic contamination in Bangladesh–An overview. Agricult. Ecosys. Environ. 113: 1-16.

Huang, C.K., and P.F. Kerr. 1960. Infrared study of the carbonate minerals. Am. Mineral. 43:311.

Hug, S., L. Canonica, M. Wegelin, D. Gechter, and U. Gunten. 2001. Solar oxidation and removal of arsenic at circum neutral pH in iron containing waters: Environ. . Sci. Technol. 37: 5050-5056.

Jain, A., and R.H. Loeppert. 2000. Effect of competing anions on the adsorption of arsenate and arsenite by ferrihydrite. J. Enviro. Qual. 29: 1422-1430.

Jain, A., P.R. Klaus, and R.H. Loeppert. 1999. Arsenite and arsenate adsorption on ferrihydrite: Surface charge reduction and net $OH^-$ release stoichiometry. Environ. Sci. Technol. 33:1179-1184.

James Jr, V. B., and W.B. Paul. 1999. Arsenic Immobilization by Calcium Arsenate Formation. Environ. Sci. Technol. 33: 3806-3811.

Jamieson, J. C. 1953. Phase equilibrium in the system calcite-aragonite. J. Chem. Phys. 21: 1385-1390.

Jarbi, E. M.B. Carr, R.P. Hausinger, and P.A. Karplus. 1995. The crystal structure of urease from Klebsiella aerogenes. Sci. 268: 998-1004.

Johnaness, W., and D. Puhan. 1971. Calcite-Aragonite transition reinvestigated. Contrib. Mineral. Petrol. 31: 28.

Kabata-Pendias, A., and D.C. Adriano. 1995. Trace metals. *In*: Soil amendments and environmental quality. Rechcigl, J. E. (Ed.). CRC press. Boca Raton. USA. pp. 139-167.

Kahmi, S.R. 1963. On the structure of vaterite, $CaCO_3$. Acta Cryst. 16: 770-772.

Karim, M. 2000. Arsenic in ground water and health problems in Bangladesh. Wat. Res. 34: 304-310.

Kato, T. 2000. Polymer/calcium carbonate layered thin-film composites. Adv. Mater. 12:1543.

Kato, T., A. Sugawara, and N. Hosoda. 2002. Calcium carbonate - organic hybrid Materials. Adv. Mater.14: 869.

Kontoyannis, C.G., and N.V. Vagenas. 2001. Calcium carbonate phase analysis using XRD and FT-Raman spectroscopy. Analyst. 125: 251-255.

Langmuir, D. 1971. The geochemistry of some carbonate groundwaters in central Pennsylvannia. Geochim. Cosmochim. Acta 35:1023-1045.

Lin, Z., and R.W. Puls. 2000. Adsorption, desorption and oxidation of arsenic affected by clay minerals and aging process. Environ. Geol. 39: 753-759.

Low, M.J.D. 1960. Kinetics of chemisorption of gases on solids. Chem. Rev. 60:267-312.

Maeda, S., Ohki, A., Saikoji, S., and K. Naka. 1992. Iron (III) hydroxide-loaded coral limestone as an adsorbent for arsenic (III) and arsenic (V). Sep. Sci. Technol. 27: 681-689.

Mallick, S., and N.R. Rajagopal. 1996. Groundwater development in the arsenic-affected alluvial belt of West Bengal–Some Questions. Curr. Sci. 70: 956-958.

Mandal, B.K., T.R. Chowdhury, G. Samanta, D. Mukherjee, C.R. Chanda, K.C. Saha, and D. Chakraborti. 1998. Impact of safe water for drinking on five families for 2 years in West Bengal, India. Sci. Total Environ. 218: 185-201.

Manning, B. A., and S. Goldberg. 1996a. Modeling arsenate competitive adsorption on kaolinite, montmorillonite and illite. Clays Clay Miner. 44:609-623.

Manning, B. A., and S. Goldberg. 1996b. Modeling competitive adsorption of arsenate with phosphate and molybdate on oxide minerals. Soil Sci. Soc. Am. J. 60:121-131.

Manning, B.A., and S. Goldberg. 1997a. Adsorption and stability of arsenic(III) at the clay mineral-water interface. Environ. Sci. Technol. 31:2005-2011.

Manning, B.A., and S. Goldberg. 1997b. Arsenic(III) and arsenic(V) adsorption on three California soils. Soil Sci. 162: 886-895.

Manning, B.A. and D.A. Martens. 1997. Speciation of arsenic (III) and arsenic (V) in sediment extracts by high performance liquid chromatography-hydride generation atomic absorption spectrophotmetry. Environ. Sci. Technol. 31: 171-177.

Mansur, H.S., R.L. Orefice, and A.P. Alexandra. 2004. Characterization of poly (vinyl alcohol)/poly (ethylene glycol) hydrogels and PVA-derived hybrids by small-angle X-ray scattering and FTIR spectroscopy. Polymer 45:193-202.

Mariner, P.E., F.J. Holzmer, R.E. Jackson, H.W. Meinardus, and F.G. Wolf. 1996. Effects of high pH on arsenic mobility in a shallow sandy aquifer and on aquifer permeability along the adjacent shoreline, Commencement Bay Superfund site, Tacoma, Washington. Environ. Sci. Technol. 24: 102-107.

Masscheleyn, P.H., R.D. Delaune, and W.H. Patrick. 1991. Effect of redox potential and pH on arsenic speciation and solubility in contaminated soil. Environ. Sci. Technol. 25: 1414-1419.

Matschullat, J. 2000. Arsenic in the geosphere – a review. Sci. Total Environ. 249 (1-3): 297-312.

MacDonald, G.J.F. 1956. Experimental determination of calcite-aragonite equilibrium relations at elevated temperatures and pressures. Am. Mineral. 41: 744-756.

McKenzie, R.M. 1981. The surface charge on manganese oxides. Aus. J. Soil. Res. 19: 41-50.

Mishra, S., H. Sonawane, and R.P. Singh. 2004. Studies on characterization of nano $CaCO_3$ prepared by the *in situ* deposition technique and its application in PP-nano $CaCO_3$ Composites. J. Polym. Sci. 43:107-113.

Mitchell, A.C, and F.G. Ferris. 2006. Effect of strontium contaminants upon the size and solubility of calcite crystals precipitated by the bacterial hydrolysis of urea. Environ. Sci. Technol. 40:1008-1014.

Mori, Y., T. Enomae, and I. Akira. 2005. A preparation of spherical calcium carbonate and application to paper".NIP21, Final Program and Proceedings of the International Conference on Digital Printing Technologies, 21st, Baltimore, MD, United States, Sept. 18-23, 457-460.

Moulin, P., and H. Roques. 2003. Zeta potential measurement of calcium carbonate. J. Colloid Interface Sci. 261:115-126.

Myneni, S.C.B., S.J. Traina, T.J. Logan, and G.A. Waychunas. 1997. Oxyanion behavior in alkaline environments: sorption and desorption of arsenate in ettringite. Environ. Sci. Technol. 31:1761-1768.

Nancollas, G.H., and K. Swada. 1982. Formation of scales of calcium carbonate polymorphs: the influence of magnesium ion and inhibitors. J. Petroleum Techn. 34: 645-652.

Navrotsky, A. 2004. Energetic clues to pathways to biomineralization: precursors, clusters and nanoparticles. Proc Natl Acad Sci USA. 101: 12096-12101.

Nickson, R.T., J.M. McArthur, W.G. Burges, K.M. Ahmed, P. Ravenscroft, and M. Rahman. 1998. Arsenic poisoning of ground water. Nature 395:338.

Nickson, R.T., J. McArthur, W. Burgess, P. Ravenscroft, W.G. Burgess, and K.M. Ahmed. 2000. Mechanism of As release to groundwater Bangladesh and West Bengal. Appl. Geochem.15: 403-413.

Ng, J.C., J. Wang, and A. Shraim. 2003. A global health problem caused by arsenic from natural sources. Chemosphere 52:1353-1359.

Nordstrom, D.K., and D.G. Archer. 2003. Arsenic thermodynamic data and environmental geochemistry, p. 1-26, *In* A. H. Welch and K. G. Stollenwerk, eds. Arsenic in Ground Water: Geochemistry and Occurrence. Kluwer Academic Publishers, Boston.

Nriagu, J. O. 1990. Global metal pollution. Environment. 32: 28-33.

Ohki, A., K. Nakayachigo, K. Naka, and S. Maeda. 1996. Adsorption of inorganic and organic arsenic compounds by aluminum-loaded coral limestone. Appl. Organomet. Chem. 10: 747-52.

Oscarson, D.W., P.M. Huang, W.K. Liaw, and U.T. Hammer. 1983. Kinetics of oxidation of arsenite by various manganese dioxides. Soil Sci. Soc. Am. J. 47: 644-648.

Panstar-Kallio, M., and P.K.G. Manninen. 1997. Speciation of mobile arsenic in soil samples as a function of pH. Sci. Total Environ. 204: 193-200.

Parga, J.R., D.L. Cocke, J.L. Valenzuela, J.A. Gomes, M. Kesmez, G. Irwin, H. Moreno and M. Weir. 2005. Arsenic removal via electro coagulation from heavy metal contaminated groundwater in La Comarca Lagunera Mexico. J. Hazard. Mat. B124: 247-254.

Parks, G.A., and P.L. De Bruyn. 1962. The zero point of charge of oxides. J. Phy. Chem. 66: 967-973.

Pathak, A., A.B. Panda, A. Tarafdar, and P.J. Pramanik. 2003. Studies on nano $CaCO_3$ prepared by the *in situ* deposition technique and its application in PP-nano composites. Indian Chem. Soc. 80: 289.

Patrick, W. H, Jr., Gambell, R.P., and Faulkner, S.P. 1996. Redox measurements of soils. In " Methods of soil analysis: Part23- Chemical Methods"(D.L. Sparks, Ed.) Soil Sci. Soc. Am. Book ser. 5, pp. 1255-1273. Soil Sci. Am. Madison,W.I.

Peric, J., M. Vucak, R. Krstulovib, Lj. BreEevib, and D. Kralj. 1996. Phase transformation of calcium carbonate polymorphs. Thermochim. Acta. 277: 175-186.

Plant, J.A., D.G. Kinniburgh, P.L. Smedley, F.M. Fordyce, and B.A. Klinck. 2004. Arsenic and Selenium, p. 17-66, *In* B. S. Lollar, ed. Environmental Geochemistry, Vol. 9. Elsevier Science.

Plummer, L.N. 1977. Defining reactions and mass transfer in part of the Floridian aquifer. Water Res. 13: 801-812.

Pongratz, R. 1998. Arsenic speciation in environmental samples of contaminated soil. Sci. Total Environ. 224:133-140.

Rasul, S.B., A.K.M. Munir, Z.A. Hossain, A.H. Khan, M. Alauddin, and A. Hussam. 2002. Electrochemical measurement and speciation of inorganic arsenic in groundwater of Bangladesh. Talanta. 58: 33-43.

Raven, K. P., A. Jain, and R. H. Loeppert. 1998. Arsenite and arsenate adsorption on ferrihydrite: Kinetics, equilibrium, and adsorption envelopes. Environ. Sci. Technol. 32:344-349.

Ravenscroft, P., W.G. Burgess, K.M. Ahmed, M. Burren, and J. Perrin. 2004. Arsenic in groundwater of the Bengal Basin, Bangladesh: Distribution, field relations, and hydrogeological setting. J. Hydrogeol.13: 727-751.

Rodriguez, R., J.A. Ramos, and A. Armienta. 2004. Groundwater arsenic variations: the role of local geology and rainfall Appl. Geochem. 19: 245-250.

Romo, A., F.J. Penas, and J.R. Isasi. 2004. Sorption of dibenzofuran derivatives from β- cyclodextrin polymers: an isosteric heat approach. J. Colloid Interface Sci. 279: 55-60.

Ross, R.G., G.J. Cuello, X. Turrillas, A.F. Martinez, and L. Charlet. 2006. Arsenite sorption and Co-precipitation with calcite. Chem. Geol. 233: 328-336.

Rouff, A.A., E.J. Elzinga, and R.J. Reeder. 2004. X-ray absorption spectroscopic evidence for the formation of Pb(II) inner-sphere adsorption complexes and precipitates at the calcite-water interface. Environ. Sci. Technol. 38:1700-1707.

Roy, P., and A. Saha. 2002. Metabolism and toxicity of arsenic: A human carcinogen. Curr. Sci. 82: 38-45.

Sadiq, M.1990. Arsenic chemistry in marine environments: A comparison between theoretical and field observations. Mar chem. 31: 285-297.

Sadiq, M. 1997. Arsenic chemistry in soils: an overview of thermodynamic predictions and field observations. Water Air Soil Pollut. 93: 117-136.

Sancha, A.M., and M.L. Castro. 2001. Arsenic in Latin America: occurrence, exposure, health effects and remediation. In: Chapell, W.R., Abernathy, C.O., Calderon, R.L. (Eds.), Arsenic Exposure and Health Effects IV. Elsevier, Amsterdam, pp. 87–96.

Santo, M., and S.Matsuda. 1969. Structure of vaterite and infrared spectra. Zeits. Krist. 129: 405-410.

Saunders, J.A., M.A. Pritchett, and R.B. Cook. 1997. Geochemistry of biogenic pyrite and ferromanganese coatings from a small watershed: A bacterial connection? Geomicrobiol. J. 14:203-217.

Sengupta Mrinal, K. 2003. Groundwater arsenic contamination in the Ganga-Padma-Meghna-Brahmaputra plain of India and Bangladesh. Arch. Environ. Health. 58:701-702.

Shriver, D.F., P. Atkins, and C.H. Langford. 1994. Inorganic Chemistry, p. 137-138, Second ed. W. H. Freeman and Company, New York.

Siffert, B., and P. Fimbel. 1984. Parameters affecting the sign and the magnitude of the electrokinetic potential of calcite. Colloids Surf. 11: 377-389.

Simmons, G., and P. Bell. 1963. Calcite-aragonite equilibrium. Science 139: 1197-1198

Sircar, S., R. Mohr, C. Ristic, and M.B. Rao. 1999. Isosteric heat of adsorption: Theory and experiment. J. Phys. Chem. B. 103: 6539-6546.

Small, R., L. Warren, E. Roden, and F.G. Ferrris. 1998. Sorption of strontium by bacteria, Fe(III) oxide, and bacteria-Fe(III)oxide composites. Environ. Sci. Technol.32:2331-37.

Smedley, P.L., and D.G. Kinniburgh. 2002. A review of the source, behaviour and distribution of arsenic in natural waters. Appl. Geochem. 17: 517-568.

Smith P.G., I. Koch, and R.A. Gordon. 2005. X-ray Absorption Near-Edge Structure Analysis of arsenic species for application to biological environmental samples. Environ. Sci. Technol. 39: 248-254.

Smith, E., R. Naidu, and A.M. Alston. 1998a. Arsenic in the soil environment: a review. Advances in Agronomy 64: 149-195.

Somasundaran, P., and G.E. Agar. 1967. Zero point of charge of calcite. *J. Colloid Interface Sci.* 24: 433.

Sposito, G., and S. Goldberg. 1984. A chemical-model of phosphate adsorption by soils. 1. Reference oxide minerals. Soil Sci. Soc. Am. J. 48: 772-778.

Stilwell, D.E, and K.D. Gorny. 1997. Contamination of soil with copper, chromium, and arsenic under decks built from pressure treated wood. Bull Environ. Contam. Toxicol. 58: 22-29.

Stipp, S.L.S. 1999. Toward a conceptual model of the calcite surface: Hydration , hydrolysis, and surface potential. Geochim. Cosmochim. Acta. 63:3121-3131.

Stock-Fischer, S., J.K. Galiant, and S.S. Bang. 1999. Microbiological precipitation of $CaCO_3$. Soil Biol. BioChem. 31: 1563-1571.

Stollenwark, K.G. 2003. Geochemical Processes Controlling Transport of Arsenic in Groundwater: A Review of Adsorption, p. 67-100, *In* A. H. Welch and K.G Stollenwerk, eds. Arsenic in Ground Water: Geochemistry and Occurrence. Kluwer Academic Publishers, Boston.

Stronach S.A., N.L. Walker, D.E. Macphee, and F.P. Glasser. 1997. Reactions between cement and As(III) oxide: The system $CaO$-$SiO_2$-$As_2O_3$-$H_2O$ at 25°C. Waste Management.17: 9-13.

Sugawara, A., T. Ishii, and T. Kato. 2003. Self-organized calcium carbonate with regular surface-relief structures. Angew. Chem. Int. Ed. 42: 5299.

Sun, X., and H. Doner. 1998. Adsorption and oxidation of arsenite on goethite. Soil Sci. 163: 278-287.

Turpeinen, R., M. Panstar-Kallio, M. Häggblom, T. Kairesalo. 1999. Influence of microbes on the mobilization, toxicity and biomethylation of arsenic in soil. Sci. Total Environ. 236: 173-180.

Turpeinen, R., M. Pantsar-Kallio, and T. Kairsalo. 2002. Role of microbes in controlling the speciation of arsenic and production of arsines in contaminated soils. Sci. Total Environ. 285:133-145.

Van Everdingen, R.O. 1968. The influence of the South Saskatchewan reservoir on the local groundwater regime - A prognosis. M44-65-39, Ottawa.

Vaughan, D.J. 2006. Arsenic. Elements 2: 71-75.

Vecht, A., and T.G. Ireland. 2000. The role of vaterite and aragonite in the formation of pseudo-biogenic carbonates structures: implications for Martian exobiology. Geochim.Cosmochim. Acta 64: 2719-2725.

Vodovic, N. 2001. Electrokinetic behaviour of calcite-the relationship with other calcite Properties. Chem. Geol. 177: 241-248.

Warren, L.A., and F.G. Ferris. 1998. Continuum between sorption and precipitation of Fe (III) on microbial surfaces. Environ. Sci. Technol.32: 2331-2337.

Warren, L.A., P.A. Maurice, and F.G. Ferris. 2001. Microbially mediated calcium carbonate precipitation: Implications for interpreting calcite precipitation and for solid –phase capture of inorganic contaminants. Geomicrobiol. J. 18:93-115.

Waychunas, G.A., B.A. Rea, C.C. Fuller, and J.A. Davis. 1993. Surface chemistry of ferrihydrite: part 1. EXAFS studies of the geometry of co-precipitated and adsorbed arsenate. Geochim. Cosmochim. Acta. 57: 2251-2269.

Welch, A.H., M.S. Lico, and J.L. Hughes.1988. Arsenic in groundwater of the western United States. Ground Water, 26, 333-347.

White, W.B. 1997. Thermodynamic equilibrium, kinetics, activation barriers, and reaction mechanisms for chemical reactions in Karst terrains. Environ. Geol. 30: 46-58.

Williams, M. 1997. Mining-related Arsenic Hazards: Thailand Case-study. Summary Report. Brit. Geol. Surv. Tech. Rep., WC/97/49.

Williams, M., F. Fordyce, A. Paijitprapapon, and P. Charoenchaisri. 1996. Arsenic contamination in surface drainage and groundwater in part of the southeast Asian tin belt, Nakhon Si Thammarat Province, southern Thailand. Environ. Geol. 27, 16–33.

Wray, J.L. and F. Daniel. 1957. Precipitation of Calcite and Aragonite. J. Am. Chem. Soc.79: 2031-2058.

Xu, X., J.T. Han, and K.Cho. 2004. Formation of amorphous calcium carbonate thin films and their role in Biomineralization. Chem. Mater. 16: 1740-1746.

Yan, X.P., R. Kerrich, and J.M. Hendry. 2000. Distribution of arsenic (III), arsenic (V) and total inorganic arsenic in pore waters from a thick till and clay-rich aquitard sequence, Saskatchewan, Canada. Geochim. Cosmochim. Acta 62: 2637-2648.

Zagury, G.J., and P. Pouschat. 2005. Comments on "Arsenic on the hands of children after playing in playgrounds. Environ Health Perspect. 113:A2.

Zagury G.J., R. Samson and L. Deschesnes. 2003. Occurrence of metals in soil and groundwater near chromated copper arsenate-treated utility poles. J. Environ. Qual. 32: 507-514.

Zhang, J., and R. Stanforth. 2005. Slow Adsorption Reaction between Arsenic Species and Goethite (γ-FeOOH): Diffusion or Heterogeneous Surface Reaction Control. Langmuir 21: 2895-2901.

Zhang, X., H. Yin, X. Cheng, H. Hu, W. Yu, and A.Wang. 2006. Effect of various polyoxyethylene sorbitan monooils (tweens) and sodium doceyl sulphate on reflux synthesis of Copper nano particles. Mater. Res. Bull. 41: 2045-2046.

Zhao, H.S., and R. Stanforth. 2002. Competitive adsorption of phosphate and arsenate on Goethite. Environ. Sci. Technol. 35: 4753.